Hi-Res Environmental Data for Enhanced UDW Operations Safety Final Contract Report

RPSEA Document No. 11121.5801.01.FINAL

Hi-Res Environmental Data for Enhanced UDW Operations Safety

RPSEA Project No. 11121-5801-01

October 3, 2016

Grant A. Stuart
Project Manager
Fugro
6100 Hillcroft
Houston, TX 77081

LEGAL NOTICE

This report was prepared by *FUGRO GLOBAL ENVIRONMENTAL AND OCEAN SCIENCES, INC.* as an account of work sponsored by the Research Partnership to Secure Energy for America, RPSEA. Neither RPSEA, members of RPSEA, the National Energy Technology Laboratory, the U.S. Department of Energy, nor any person acting on behalf of any of the entities:

a. MAKES ANY WARRANTY OR REPRESENTATION, EXPRESS OR IMPLIED WITH RESPECT TO ACCURACY, COMPLETENESS, OR USEFULNESS OF THE INFORMATION CONTAINED IN THIS DOCUMENT, OR THAT THE USE OF ANY INFORMATION, APPARATUS, METHOD, OR PROCESS DISCLOSED IN THIS DOCUMENT MAY NOT INFRINGE PRIVATELY OWNED RIGHTS, OR

b. ASSUMES ANY LIABILITY WITH RESPECT TO THE USE OF, OR FOR ANY AND ALL DAMAGES RESULTING FROM THE USE OF, ANY INFORMATION, APPARATUS, METHOD, OR PROCESS DISCLOSED IN THIS DOCUMENT.

THIS IS AN INTERIM REPORT. THEREFORE, ANY DATA, CALCULATIONS, OR CONCLUSIONS REPORTED HEREIN SHOULD BE TREATED AS PRELIMINARY.

REFERENCE TO TRADE NAMES OR SPECIFIC COMMERCIAL PRODUCTS, COMMODITIES, OR SERVICES IN THIS REPORT DOES NOT REPRESENT OR CONSTIITUTE AND ENDORSEMENT, RECOMMENDATION, OR FAVORING BY RPSEA OR ITS CONTRACTORS OF THE SPECIFIC COMMERCIAL PRODUCT, COMMODITY, OR SERVICE.

ABSTRACT

This Final Contract Report for 11121-5801-01 combines three interim contract deliverables:

- Deliverable 7 - Final Report Bottom Current Measurements and Modeling (Task 5)
- Deliverable 15 - Final Report Real-Time Measurement of Surface Currents (Task 8)
- Deliverable 18 - Final Remote Ocean Current Imaging System Commercialization Report (Task 9)

These three final reports combine to serve as the summary final report for the defined effort as specified in RPSEA subcontract 11121-5801-01. It is noted here that Task 6, "Currents During a Joint Tropical Revolving Storm-Loop Current or Loop Current Eddy Event", was not completed during the time period allotted for this subcontract as no candidate events presented during the three field seasons.

SIGNATURE AND DATE STAMP

FUGRO GLOBAL
ENVIRONMENTAL AND
OCEAN SCIENCES, INC.

By: _____
(Signature)

Name: **Grant A. Stuart**

Title: **Project Manager**

Date: **3 October 2016**

THIS PAGE INTENTIONALLY LEFT BLANK

CONTENTS

1. EXECUTIVE SUMMARY

2. FINAL REPORT: BOTTOM CURRENT MEASUREMENTS AND MODELING (TASK 5)

3. FINAL REPORT: CURRENTS DURING A JOINT TRS-LC OR LCE EVENT (TASK 6)

4. FINAL REPORT: REAL-TIME MEASUREMENT OF SURFACE CURRENTS (TASK 8)

5. REMOTE OCEAN CURRENT IMAGING SYSTEM COMMERCIALIZATION REPORT (TASK 9)

0	Final	Various Authors	Grant Stuart Systems Manager	Rob Smith Managing Director	3 October 2016
Rev	**Description**	**Prepared**	**Checked**	**Approved**	**Date**

1. EXECUTIVE SUMMARY

This Final Contract Report for 11121-5801-01 combines three interim contract deliverables:

- Deliverable 7 - Final Report Bottom Current Measurements and Modeling (Task 5)
- Deliverable 15 - Final Report Real-Time Measurement of Surface Currents (Task 8)
- Deliverable 18 - Final Remote Ocean Current Imaging System Commercialization Report (Task 9)

These three final reports combine to serve as the summary final report for the defined effort as specified in RPSEA subcontract 11121-5801-01. It is noted here that Task 6, "Currents During a Joint Tropical Revolving Storm-Loop Current or Loop Current Eddy Event", was not completed during the time period allotted for this subcontract as no candidate events presented during the three field seasons.

Task 5 quantified relatively strong near-bottom currents in an area of complex bathymetry; however, there was little evidence that these relatively strong currents were amplified by reflections of energy due to inertial forcing at the surface. There was evidence that the strong loop current condition at the surface influenced the currents measured at the seabed. Three near-bottom current measurement moorings were deployed in 1,100 - 1,400m of water for one year. The location is an area of the Gulf of Mexico with complex bathymetry. A hi-res 3-D numerical model simulated the currents in the region during the data collection period. The results of Task 5 highlight the complexity of near-bottom currents and their variability within the outer continental shelf area of the northwestern Gulf of Mexico. It is difficult to capture this variability over a region of even only a few kilometers in size with direct current observations. Thus, high-resolution numerical simulations should be considered, at least to complement moored observations, for projects in such regions. Additionally, for projects with large spatial footprints such as pipelines, it is especially important to consider the variability of characteristics of bottom currents throughout the region.

As pointed out above, Task 6 was not completed during the time period allotted for this subcontract as no candidate events presented during the three field seasons.

The objective of Task 8 was to develop, design, engineer, and test a technique to monitor surface current velocities in real-time over a range of at least 300 km per day. Existing research on ROCIS (Remote Ocean Current Imaging System), conducted by Areté and Fugro, was developed further during this program, moving ROCIS from a prototype system to a real-time service. From February to June 2015, the ROCIS prototype was deployed commercially in the Gulf of Mexico for a total of 137 flights. This not only proved its capability, but also provided a unique and unprecedented view of the Loop Current and its evolution during that time period. Looking forward, ROCIS is well suited for operational missions to support offshore oil and gas operations, assist with emergency oil spills, and support search and rescue, where timely knowledge of surface currents is crucial.

Task 9 produced a commercialization plan for the Remote Ocean Current Imaging System (ROCIS). The third report in this document outlines the overall strategy the prime subcontractor, Fugro, together with technology partner, Areté Associates, are developing to bring an operational ROCIS survey service to the market. It reviews the market opportunities and develops a business execution plan. The goal to have a field-ready package and operational service available following completion of this task was met.

2. FINAL REPORT: BOTTOM CURRENT MEASUREMENTS AND MODELING (TASK 5)

Bottom Current Measurements and Modeling – Final Report

RPSEA Document No. 11121.5801.01.Final1

Hi-Res Environmental Data for Enhanced UDW Operations Safety

RPSEA Project No. 11121-5801-01

September 30, 2016

Steven Morey, Dmitry Dukhovskoy, & Eric Chassignet
Task 6 Principal Investigators
Florida State University Center for Ocean – Atmospheric Prediction Studies
2000 Levy Avenue, Building A, Suite 292
Tallahassee, FL 32306-2741

LEGAL NOTICE

This report was prepared by *FUGRO GLOBAL ENVIRONMENTAL AND OCEAN SCIENCES, INC.* as an account of work sponsored by the Research Partnership to Secure Energy for America, RPSEA. Neither RPSEA, members of RPSEA, the National Energy Technology Laboratory, the U.S. Department of Energy, nor any person acting on behalf of any of the entities:

a. MAKES ANY WARRANTY OR REPRESENTATION, EXPRESS OR IMPLIED WITH RESPECT TO ACCURACY, COMPLETENESS, OR USEFULNESS OF THE INFORMATION CONTAINED IN THIS DOCUMENT, OR THAT THE USE OF ANY INFORMATION, APPARATUS, METHOD, OR PROCESS DISCLOSED IN THIS DOCUMENT MAY NOT INFRINGE PRIVATELY OWNED RIGHTS, OR

b. ASSUMES ANY LIABILITY WITH RESPECT TO THE USE OF, OR FOR ANY AND ALL DAMAGES RESULTING FROM THE USE OF, ANY INFORMATION, APPARATUS, METHOD, OR PROCESS DISCLOSED IN THIS DOCUMENT.

THIS IS AN INTERIM REPORT. THEREFORE, ANY DATA, CALCULATIONS, OR CONCLUSIONS REPORTED HEREIN SHOULD BE TREATED AS PRELIMINARY.

REFERENCE TO TRADE NAMES OR SPECIFIC COMMERCIAL PRODUCTS, COMMODITIES, OR SERVICES IN THIS REPORT DOES NOT REPRESENT OR CONSTIITUTE AND ENDORSEMENT, RECOMMENDATION, OR FAVORING BY RPSEA OR ITS CONTRACTORS OF THE SPECIFIC COMMERCIAL PRODUCT, COMMODITY, OR SERVICE.

ABSTRACT

This Final Report for Task 5 presents the results of the ocean current mooring measurement program and subsequent numerical model simulations. The objective of Task 5 was to identify and quantify relatively strong near-bottom currents, amplified by reflections of energy due to inertial forcing at the surface. Three near-bottom current measurement moorings were deployed in 1,100 - 1,400m of water for one year. The deployment location was an area of the Gulf of Mexico with complex bathymetry. A high-resolution 3-D numerical model was used to simulate the currents in the region during the data collection period. The research aim was to enhance the accuracy of metocean design criteria and fatigue assessment of UDW subsea seabed infrastructure.

The results of Task 5 highlight the complexity of near-bottom currents and their variability within the outer continental shelf area of the northwestern Gulf of Mexico that is characterized by numerous bathymetric features such as salt domes, pinnacles, canyons and basins with length scales of roughly 10km. It is difficult to capture this variability over a region of even only a few kilometers in size with direct current observations. Thus, high-resolution numerical simulations should be considered, at least to complement moored observations, for projects in such regions. Additionally, for projects with large spatial footprints such as pipelines, it is especially important to consider the variability of characteristics of bottom currents throughout the region.

SIGNATURE AND DATE STAMP

FUGRO GLOBAL ENVIRONMENTAL AND OCEAN SCIENCES, INC.

By: _____
(Signature)

Name: **Grant A. Stuart**

Title: **Project Manager**

Date: 30 September 2016

THIS PAGE INTENTIONALLY LEFT BLANK

CONTENTS

		Page
1.	**EXECUTIVE SUMMARY**	**1**
2.	**EXPERIMENTAL METHODS**	**2**
2.1	Location	2
2.2	Moorings	3
2.3	Numerical Simulation	5
3.	**RESULTS AND DISCUSSION**	**10**
3.1	Wind and Upper Ocean Circulation Regimes	10
3.2	Observed Near-Bottom Currents	12
3.3	Modeled Near-Bottom Currents	20
3.4	Spectral Characteristics of Measured and Modeled Currents	23
3.5	Analysis of Strong Near-Bottom Currents	31
3.6	Spatial Variability of Near-Bottom Currents	35
4.	**IMPACT TO PRODUCERS**	**39**
5.	**CONCLUSION**	**39**
6.	**RECOMMENDATIONS**	**40**
7.	**REFERENCES**	**41**

1	Final	Steven Morey Task 6 PI - FSU	Grant Stuart Systems Manager	Grant Stuart Systems Manager	30 September 2016
0	Draft version	Steven Morey Task 6 PI - FSU	Grant Stuart Systems Manager	Grant Stuart Systems Manager	29 August 2016
Rev	**Description**	**Prepared**	**Checked**	**Approved**	**Date**

TABLES

Page

Table 2.1 Mooring locations and configurations for the three deployments. 3

FIGURES

Figure 2.1 Bathymetry of the study area, with target mooring locations, depths, and spacing indicated. The location of the study area is shown by the small rectangle on the map of the Gulf of Mexico. Actual mooring locations and depths are shown in Table 2.1. 2

Figure 2.2 Schematics of the different ADCP mooring configurations used for the three deployment time periods. 4

Figure 2.3 Percent of ADCP data record passing quality control checks plotted against height above the seafloor for each deployment of moorings S1, S2, and S3. Deployment 1 is shown in red, deployment 2 in green, and deployment 3 in blue. 5

Figure 2.4 Map of the model domain and bathymetry. Outside of the white box is the relaxation zone for nesting where the model grid is stretched (model grid spacing is 250m inside the white box). Bathymetry contours are drawn every 50m, with thicker contour lines drawn each 200m and bold contours drawn along the 1000m and 2000m isobaths. The S1, S2, and S3 mooring locations are shown by the small blue diamonds and the 42370 (Holstein) mooring location is shown by the pink diamond. The location of the model domain is shown by the small rectangle on the map of the Gulf of Mexico. 6

Figure 2.5 Top Left: Vertical grid for the NCOM simulation shown along the latitude of the mooring line (27.375°N). Every fifth vertical grid interface is drawn in red. The S1, S2, and S3 mooring locations are indicated with the red + symbols. An expanded view for depths greater than 800m is shown in the bottom left panel. Right: The vertical grid spacing versus depth plotted for the lower water column at the S2 mooring location. 7

Figure 3.1 Wind vector time series (north up) from NAVGEM 10m winds at 90.5W, 30N. The vector color indicates the speed (m/s), which is also plotted by the black line. The scale for the vector speed and speed time series is shown as the *y*-axis, and the dates along the *x*-axis are shown as month/year. 10

Figure 3.2 SSH (anomaly) maps from the Gulf of Mexico HYCOM Nowcast/Forecast system, with the nested model region shown by the pink rectangle. Note that the SSH within the nested model is very close to the HYCOM SSH due to model adjustment to the relaxed temperature and salinity fields. The small inset shows the SSH from the entire Gulf of Mexico with the region shown by the expanded view indicated by the black rectangle. Daily SSH fields from the full 1-year study time period can be seen in Animation 5.1. 11

Figure 3.3 Mean vectors and standard deviation ellipses for the velocity vector time series at measured at 38mab by the ADCPs at mooring locations S1-S3 and 42370. The tails of the vectors are at the mooring locations. The semi-major and semi-minor axes indicate the standard deviation of the velocity principal components (directions of greatest and least variability). 13

Figure 3.4 38mab velocity time series from S1, S2, S3, and 42370 ADCP observations. Vectors are colored based on magnitude (cm/s), and magnitude is also indicated by the black time series. North is toward the top of the plots. The time periods indicated by the black rectangles (parts of December 2014 and March 2015) are those selected for later analysis below. 15

Figure 3.5 Profile of mean vectors for each ADCP bin from the third mooring deployment time period. The mean is computed over the portion of the observational record that had good data retrievals at all heights. A vertical line projects the mean vector of the topmost bin to the bottom for comparison with the other vectors. 17

Figure 3.6 Top: Velocity projected onto the major principal axis computed over the time period 1-28 Feb 2015 at S2 at 39mab (blue) and 13mab (red). Bottom: Velocity projected onto the major principal axis computed over the time period 15 Nov – 15 Dec 2014 at S1 at 36mab (blue) and 18mab (red). 19

Figure 3.7 Mean vectors and standard deviation ellipses for the velocity vector time series simulated by the NCOM at 38mab at mooring locations S1-S3 and 42370. The tails of the vectors are at the mooring locations. The semi-major and semi-minor axes indicate the standard deviation of the velocity principal components (directions of greatest and least variability). 20

Figure 3.8 38mab velocity time series simulated by the NCOM at the S1, S2, S3, and 42370 mooring locations. Vectors are colored based on magnitude (cm/s), and magnitude is also indicated by the black time series. North is toward the top of the plots. The time periods indicated by the black rectangles (parts of December 2014 and March 2015) are those selected for later analysis below. 22

Figure 3.9 Normalized wavelet power spectra for the 38mab principal component velocity time series measured by the ADCPs. The color indicates the power normalized by the total variance. The horizontal axis is time (month/year) and the vertical axis is period (wavelet scale). The shaded regions in the upper corners indicate contamination by the record end points yielding less than 90% confidence. 24

Figure 3.10 Normalized wavelet power spectra for the 38mab principal component velocity time series simulated by the NCOM at the mooring locations. The color indicates the power normalized by the total variance. The horizontal axis is time (month/year) and the vertical axis is period (wavelet scale). The shaded regions in the upper corners indicate contamination by the record end points yielding less than 90% confidence. 25

Figure 3.11 Rotary power spectra for the 38mab velocity time series measured by the ADCPs. The red curves (S-) indicate clockwise rotating currents and the blue curves (S+) indicate the power associated with anticlockwise rotating currents. The black line/green dot indicates 95% confidence interval. 27

Figure 3.12 Rotary power spectra for the 38mab velocity time series simulated by the NCOM. The red curves (S-) indicate clockwise rotating currents and the blue curves (S+) indicate the power associated with anticlockwise rotating currents. The black line/green dot indicates 95% confidence interval. 28

Figure 3.13 Left: Depth profile (m) of negative rotary power spectral density at the near-inertial peak for velocity simulated by NCOM at the four mooring locations. Right: Rotary coefficient computed from the near-inertial peak rotary power spectra density versus depth. Rotary coefficients computed from the ADCP measurements at 38mab are shown by the colored x symbols. 30

Figure 3.14 Same as Figure 2.5.13, but with the addition of a profile simulated at a deep water site (27.07°N, 90.17°W, 2308m) (pink curves). 31

Figure 3.15 Top: Sea surface height from the HYCOM Nowcast/Forecast System on 27 February, 2015. The region in the large image is shown by the black rectangle in the small inset showing the entire Gulf

region. Bottom Left: 30mab velocity vectors and speed (cm/s, colors) from the NCOM simulation on 27 February, 2015. Bottom right: Horizontal velocity shown by colors for a section crossing through the mooring array (27.375°N, white line in bottom left panel). Hue indicates direction and the color intensity indicates speed, as shown on the color bar. Mooring locations are shown by the red dots on the bottom left panel, and black dotted lines extending from the bottom in the bottom right panel. The bottom two panels are animated in Animation 5.2. 33

Figure 3.16 Top: Sea surface height from the HYCOM Nowcast/Forecast System on 2 December, 2014. The region in the large image is shown by the black rectangle in the small inset showing the entire Gulf region. Bottom Left: 30mab velocity vectors and speed (cm/s, colors) from the NCOM simulation on 2 December, 2014. Bottom right: Horizontal velocity shown by colors for a section crossing through the mooring array (27.375°N, white line in bottom left panel). Hue indicates direction and the color intensity indicates speed, as shown on the color bar. Mooring locations are shown by the red dots on the bottom left panel, and black dotted lines extending from the bottom in the bottom right panel. The bottom two panels are animated in Animation 5.3. 34

Figure 3.17 Mean velocity (speed in m/s indicated by colors) from the NCOM simulation at 1050m depth (top) and 30mab (bottom). The locations of the moorings are shown by the red dots. 36

Figure 3.18 Mean eddy kinetic energy (cm2/s2) from the NCOM simulation at 1050m depth (left) and 30mab (right). EKE is computed here as the mean of the magnitude of the horizontal velocity anomalies from the mean over the entire simulation. The locations of the moorings are shown by the red dots. 37

Figure 3.19 Probability of the instantaneous speed at 30mab exceeding 20 cm/s (left) and 30 cm/s (right) computed from the NCOM. The locations of the moorings are shown by the red dots. 38

ABBREVIATIONS

BSEE	Bureau of Safety and Environmental Enforcement
BOEM	Bureau of Ocean Energy Management
COAPS	Center for Ocean-Atmospheric Prediction Studies
cph	cycles per hour
DAC	Data Acquisition Computer
FSU	Florida State University
GB	Gigabytes
GEOS	Global Environmental and Ocean Sciences Inc
GoM	Gulf of Mexico
Hi-Res	High Resolution
HSEQ	Health, Safety, Environment, and Quality
JSA	Job Safety Analyses
LC	Loop Current
LCE	Loop Current Eddy
m, mbsl, mab	meters, meters below sea level, meters above bed
NCOM	Navy Coastal Ocean Model
NMEA	National Marine Electronics Association
NOAA	National Oceanic and Atmospheric Administration
NM	nautical mile
OCS	Outer Continental Shelf
PI	Principal Investigator
PM	Project Manager
QA	Quality Assurance
QC	Quality Control
RPSEA	Research Partnership to Secure Energy for America
TR	Technical Reviewer
UDW	Ultra Deep Water

1. EXECUTIVE SUMMARY

Ocean currents can pose significant challenges to safe oil and gas operations in the Gulf of Mexico (GoM). Examples include both short term operational concerns as the Loop Current (LC) or a Loop Current Eddy (LCE) that increase current speeds in an area or longer term effects of riser or platform fatigue due to current generated vibrations. Considerable work to understand and forecast ocean currents in the GoM has been undertaken by both industry (CASE/EJIP, DeepStar®, RPSEA, API and individual operators) and the Government (BSEE, BOEM). Studies have focused on the impacts of the LC/LCEs as well as the impact of Tropical Revolving Storms (TRS) and stronger winter storms. While the general climatology and broad circulation of the GoM is understood, questions remain.

Task 5 of this project used ADCPs to focus on high resolution measurement, analysis, and modeling of near-bottom currents in areas of complex local bathymetry. There is a lack of measured data relating to near-bottom deep water currents in depths from the seabed to 100msb. The limited data that has been collected and analyzed have shown that strong reflections of inertial energy can occur, resulting in intensification of currents. With increased deep water subsea tiebacks and pipelines, such features need to be quantified for use in pipeline and flow line design and fatigue assessments.

Task 5 quantified relatively strong near-bottom currents in an area of complex bathymetry; however, there was little evidence that these relatively strong currents were amplified by reflections of energy due to inertial forcing at the surface. There was evidence that the strong loop current condition at the surface influenced the currents measured at the seabed. Three near-bottom current measurement moorings were deployed in 1,100 - 1,400m of water for one year. The location is an area of the Gulf of Mexico with complex bathymetry. A hi-res 3-D numerical model simulated the currents in the region during the data collection period.

The results of Task 5 highlight the complexity of near-bottom currents and their variability within the outer continental shelf area of the northwestern Gulf of Mexico that is characterized by numerous bathymetric features such as salt domes, pinnacles, canyons and basins with length scales of roughly 10km. It is difficult to capture this variability over a region of even only a few kilometers in size with direct current observations. Thus, high-resolution numerical simulations should be considered, at least to complement moored observations, for projects in such regions. Additionally, for projects with large spatial footprints such as pipelines, it is especially important to consider the variability of characteristics of bottom currents throughout the region.

2. EXPERIMENTAL METHODS

2.1 Location

The overall goal of Task 5 was to characterize near-bottom currents and their variability in the vicinity of complex bathymetry, particularly in response to energetic forcing, with moored Acoustic Doppler Current Profilers (ADCP) and a high-resolution numerical model. The region selected for this study is a pinnacle-like salt dome and basin feature to the north of the Holstein development in Block GC 645 (Figure 2.1). This site is characteristically similar to much of the Central Slope and Mississippi-Alabama Domes regions of the outer continental shelf.

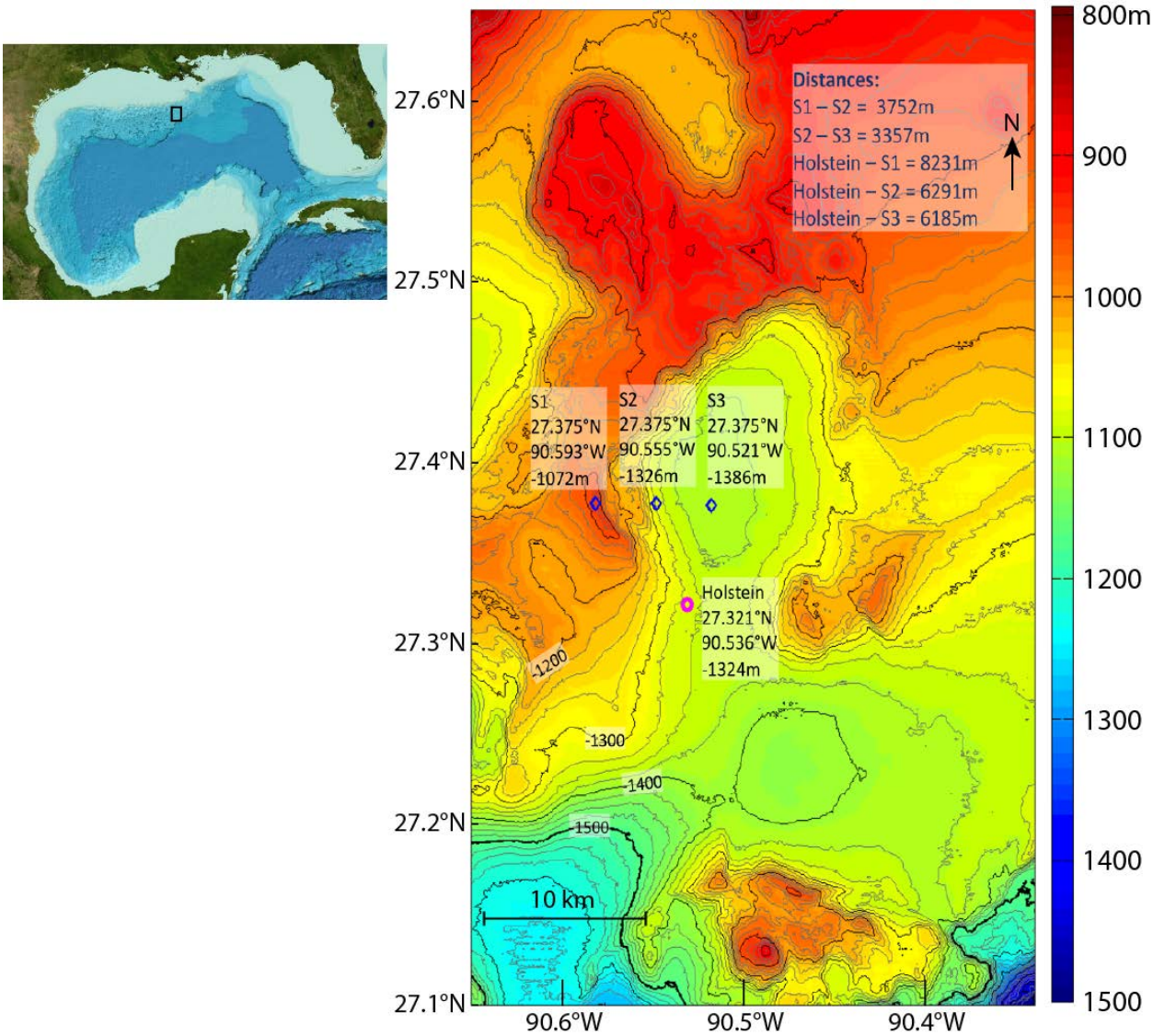

Figure 2.1 Bathymetry of the study area, with target mooring locations, depths, and spacing indicated. The location of the study area is shown by the small rectangle on the map of the Gulf of Mexico. Actual mooring locations and depths are shown in Table 2.1.

2.2 Moorings

Near-bottom ADCP moorings were placed in three locations along a transect spanning from the peak of the pinnacle at the west end (planned depth of 1072m) to the center of the basin at the east end (1386m). The middle mooring was placed along the same isobath as the existing mooring at the Holstein development (1326m) (Figure 2.1, Table 2.1). The naming convention of the moorings is S1, S2 and S3 from west (shallowest) to east (deepest), respectively, and the mooring at Holstein is referred to by its National Data Buoy Center designation 42370. Spacing of moorings along the transect, which was located approximately 6km north of the Holstein mooring, was 3.7km between S1 and S2, and 3.4km between S2 and S3.

The three moorings S1 - S3 were deployed between 26 May 2014 and 21 May 2015, and serviced during two visits at four-month intervals. Each mooring was instrumented with a 300 kHZ RDI Workhorse ADCP configured to record a 120-ping ensemble every 20 minutes with 45 cells at 2m intervals. The maximum range with this configuration is from 3.44 to 91.44m from the ADCP. The moorings for the first deployment were constructed with an expendable anchor, dual acoustic releases, plasma rope, and a downward looking ADCP situated approximately 70m above the seabed with appropriate buoyancy and an Argos beacon (Figure 2.2). Upon recovery during the first service visit, it was found that the rate of good data return fell off at approximately 30m from the ADCP (Figure 2.3). In order to better sample the velocity near the seabed, the ADCP was lowered to approximately 50mab for the second deployment. For the final deployment, the ADCPs were turned to be upward-looking and placed on short moorings so that good measurements were obtained beginning 10 - 12mab. This study also analyzed data from the Holstein mooring (42370), which consists of an upward-looking 150 kHz Long Ranger ADCP with 20m cell size.

Table 2.1 Mooring locations and configurations for the three deployments.

	Start Date	End Date	Actual Latitude	Actual Longitude	Actual Depth	ADCP Depth
Deployment 1 – Downward-Looking ADCP						
S1	5/26/2014	10/2/2014	27.375°N	90.592°W	1078m	1009m
S2	5/26/2014	10/2/2014	27.375°N	90.555°W	1314m	1246m
S3	5/26/2014	10/2/2014	27.375°N	90.522°W	1382m	1309m
Deployment 2 – Downward-Looking ADCP						
S1	10/3/2014	1/22/2015	27.375°N	90.593°W	1086m	1039m
S2	10/3/2014	1/22/2015	27.375°N	90.555°W	1326m	1271m
S3	10/3/2014	1/22/2015	27.375°N	90.521°W	1391m	1341m
Deployment 3 – Upward-Looking ADCP						
S1	1/22/2015	5/21/2015	27.375°N	90.593°W	1086m	1082m
S2	1/23/2015	5/21/2015	27.375°N	90.555°W	1327m	1323m
S3	1/23/2015	5/21/2015	27.375°N	90.593°W	1391m	1387m

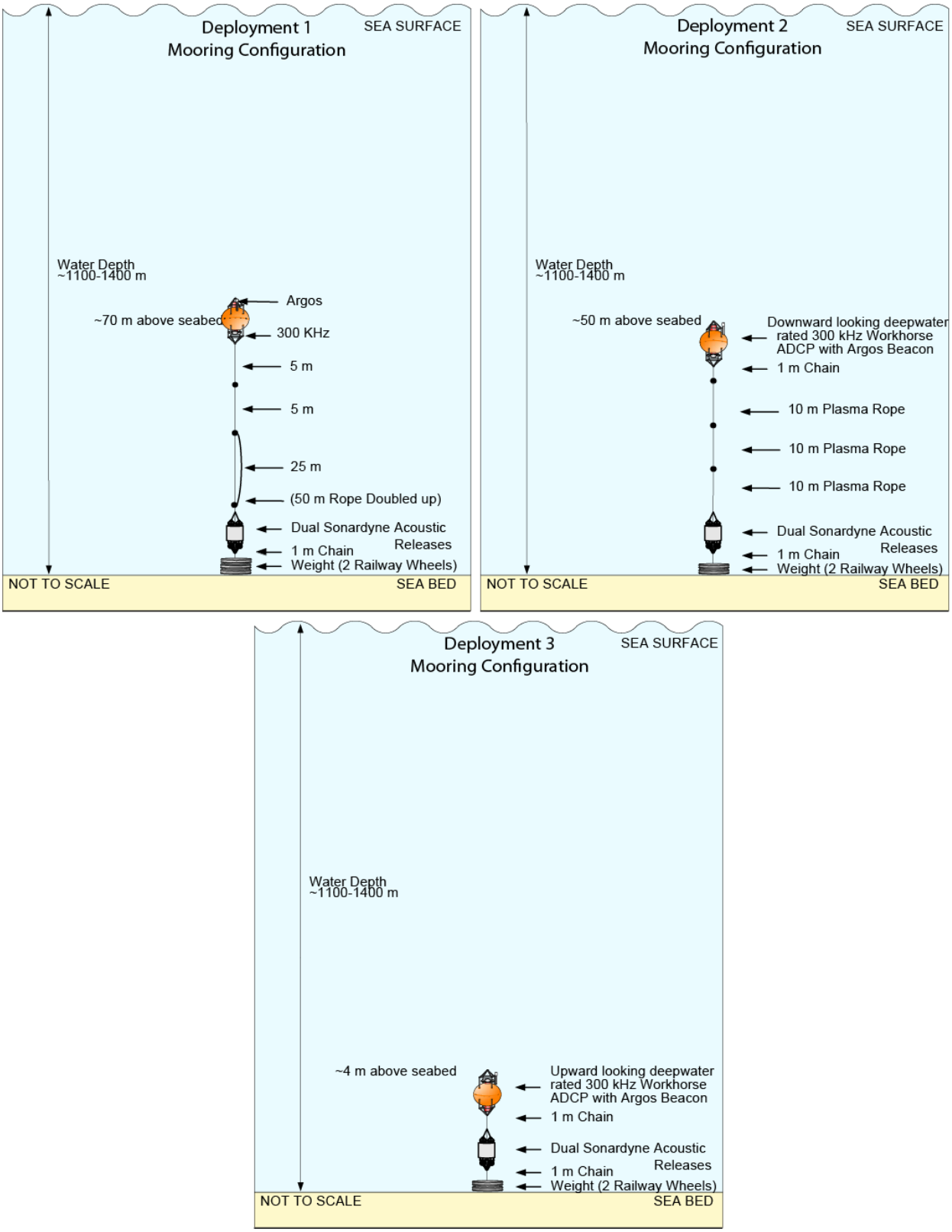

Figure 2.2 Schematics of the different ADCP mooring configurations used for the three deployment time periods.

ADCP data from moorings S1-S3 underwent standard quality control (QC) procedures. The data records were truncated to eliminate erroneous values during deployment and recovery, and magnetic declination corrections were applied if necessary. Global filters were applied at all bins and time steps where less than 80% of good ensemble pings were reported by the ADCP. Data were flagged where error velocity exceeded ±0.1 m/s. Data from bins where sea bed echo or other interference was observed were removed. Finally, the records were inspected to manually remove obviously invalid data.

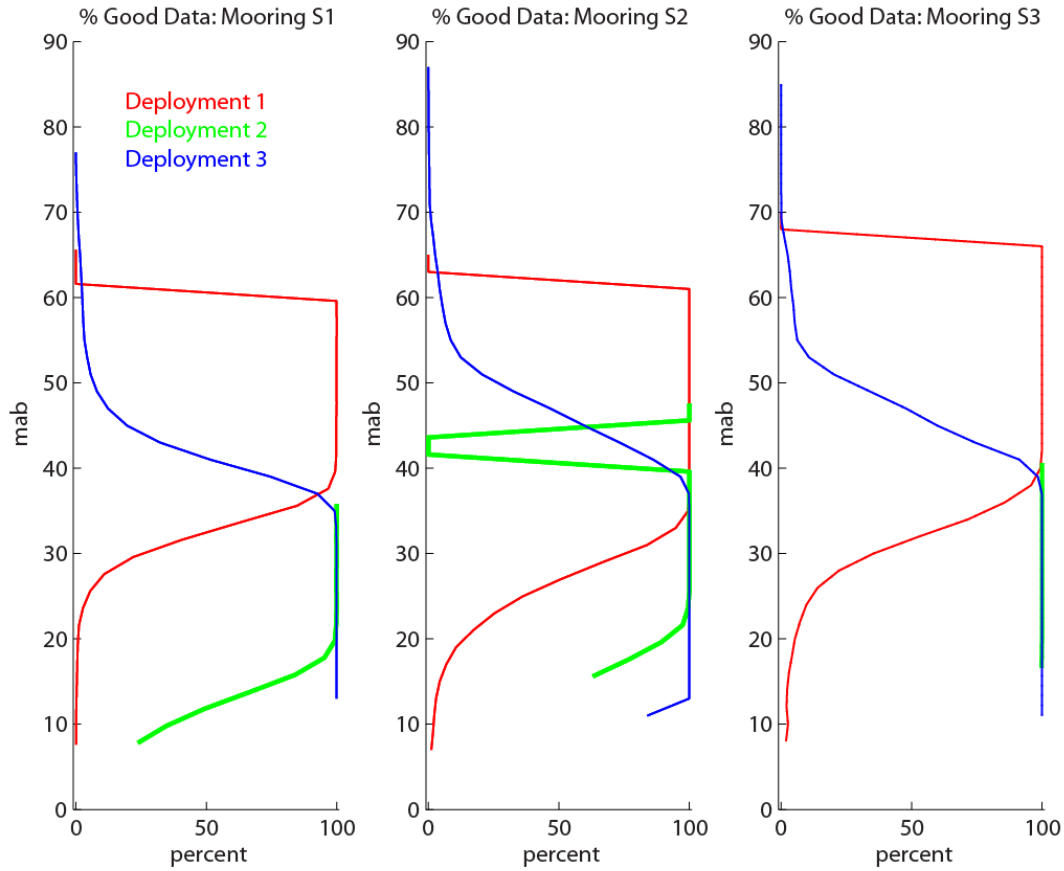

Figure 2.3 Percent of ADCP data record passing quality control checks plotted against height above the seafloor for each deployment of moorings S1, S2, and S3. Deployment 1 is shown in red, deployment 2 in green, and deployment 3 in blue.

2.3 Numerical Simulation

The Navy Coastal Ocean Model (NCOM) with the Vanishing Quasi-Sigma (VQS) vertical coordinate system (Dukhovskoy et al., 2009) was used to conduct a hindcast of the time period of the mooring deployments. NCOM is a three-dimensional primitive equation ocean model with the hydrostatic and Boussinesq approximations. Though originally designed with a hybrid geopotential level vertical grid with terrain following (sigma) vertical grid above a specified depth to facilitate application in both deep and shallow waters (Martin, 2000), extension to a generalized vertical coordinate permitted the implementation of the VQS. The VQS vertical grid system is partially terrain-following, but allows vertical grid surfaces to vanish as the water depth becomes shallower, resulting in generally smaller slopes of the vertical grid surfaces

than the traditional sigma grid. This trait permits application over steep slopes with reduced numerical errors in calculation of horizontal gradients that can lead to spurious velocities. This issue typically requires models with terrain-following coordinates to use a substantially smoothed topography, which is not ideal for application in this study. Dukhovskoy et al. (2009) showed that over steep bathymetry of the northwestern Gulf of Mexico, the VQS vertical coordinate reduced the magnitude of spurious velocities found when using the sigma coordinates to approximately one-third, and greatly reduced the area impacted by the spurious velocities.

The portion of model domain analyzed for this study spans 91.045°W to 90.027°W and 26.887°N to 27.755°N, a 100.5km x 96.5km region centered at the location of the Holstein mooring (90.536°W, 27.321°N) with 250m grid spacing. Outside of this region, the model domain has a buffer region 47 grid cells in width added around the boundaries with grid spacing in the direction normal to the boundary stretched at a ratio of 1.03 to a maximum of 1km at the model boundary. The resulting total grid dimensions of the model are 496 x 480, with limits of 86.768°W to 91.307°W, and 26.654°N to 27.986°N (Figure 2.4).

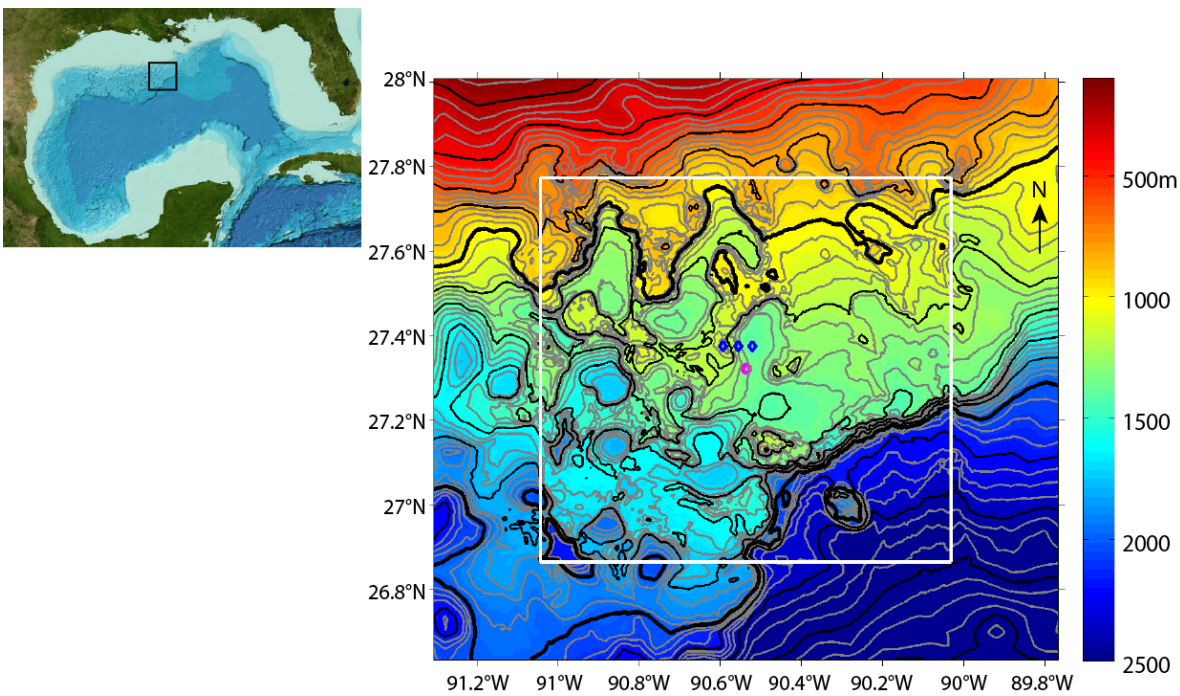

Figure 2.4 Map of the model domain and bathymetry. Outside of the white box is the relaxation zone for nesting where the model grid is stretched (model grid spacing is 250m inside the white box). Bathymetry contours are drawn every 50m, with thicker contour lines drawn each 200m and bold contours drawn along the 1000m and 2000m isobaths. The S1, S2, and S3 mooring locations are shown by the small blue diamonds and the 42370 (Holstein) mooring location is shown by the pink diamond. The location of the model domain is shown by the small rectangle on the map of the Gulf of Mexico.

The VQS vertical grid for this simulation is configured with 100 grid cells with compressed spacing near the surface and bottom. Maximum grid spacing at the surface is 2.5 m, and thicknesses of the bottommost grid cells range from 2.5m to approximately 3m (Figure 2.5). As these vertical layers vanish with depth, 82

layers remain active at the location of the S3 mooring (model depth of 1386m), and 76 layers are active at the S1 mooring location (model depth of 1079m).

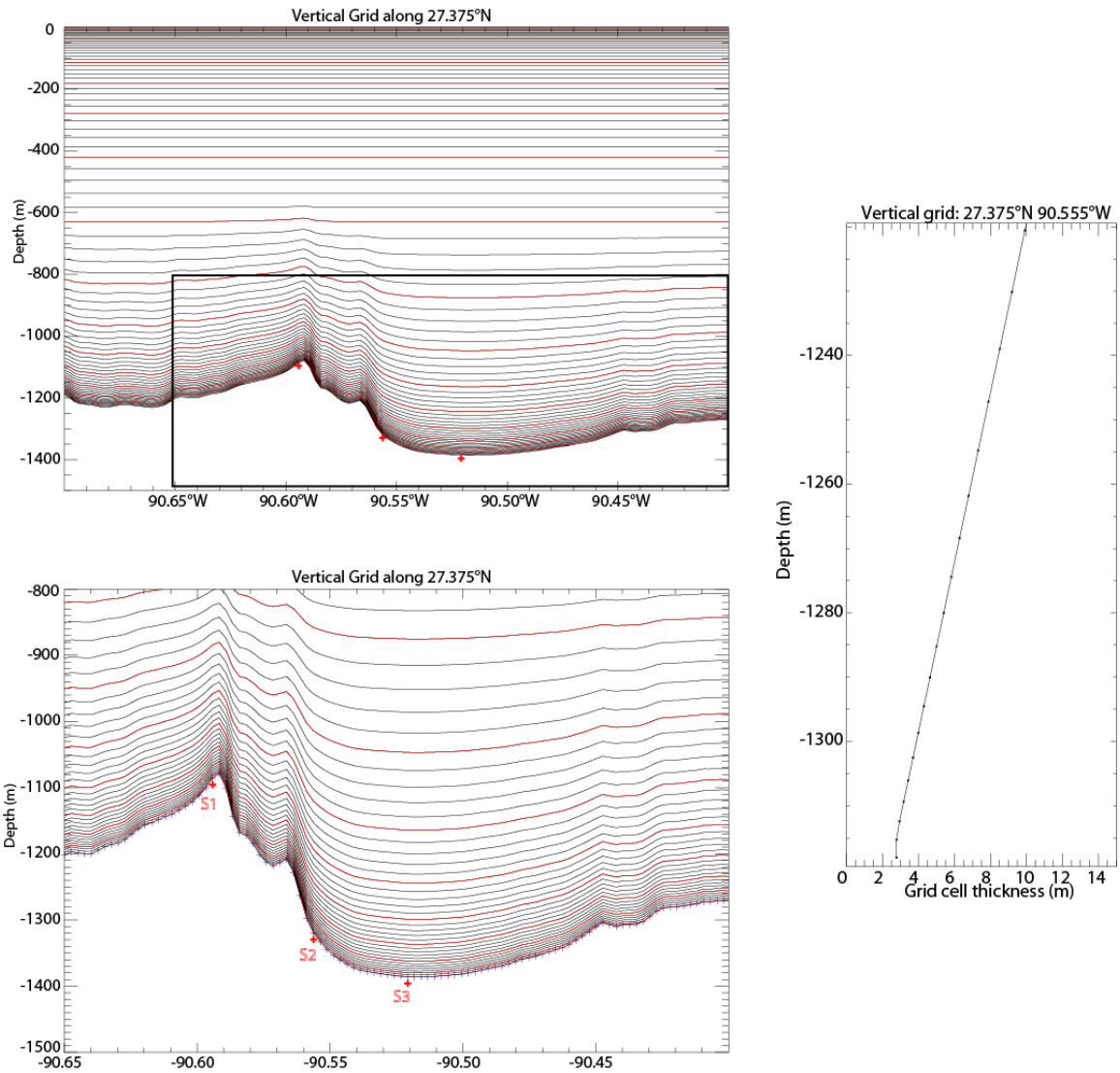

Figure 2.5 Top Left: Vertical grid for the NCOM simulation shown along the latitude of the mooring line (27.375°N). Every fifth vertical grid interface is drawn in red. The S1, S2, and S3 mooring locations are indicated with the red + symbols. An expanded view for depths greater than 800m is shown in the bottom left panel. Right: The vertical grid spacing versus depth plotted for the lower water column at the S2 mooring location.

The bathymetry for the model is derived from the National Geophysical Data Center (NGDC) 3 arcsec (approximately 90m) resolution central Gulf of Mexico coastal relief data set. A 25-point box filter is applied to this data set, resulting in a smoothing of bathymetric variations with length scales less than about 450m (or roughly twice the model grid spacing). The smoothed bathymetry is interpolated to the model horizontal grid. Over the buffer region of stretched grid spacing near the boundaries, the model bathymetry is blended to the bathymetry of the Gulf of Mexico 1/25° HYCOM (HYbrid Coordinate Ocean Model) Nowcast/Forecast System described in the following paragraph. The resulting model bathymetry and high horizontal resolution

allow accurate representation of the complex bathymetry in the region, as evidenced by the good agreement between reported mooring locations and depths and nearest model grid cell centers (differences between 60m and 93m) and model seafloor depths (differences between 0m and 12m).

The NCOM simulation is run as a hindcast for the time period 22 April 2014 to 22 May 2015, nested within the Gulf of Mexico 1/25° HYCOM Nowcast/Forecast System Experiment 32.5 (GoM HYCOM; www.hycom.org) using a nesting procedure similar to that used by Morey et al. (2013). This HYCOM modeling system is run daily by the US Naval Research Laboratory, producing data assimilative analysis fields and forecast fields. The analysis fields comprise a hindcast data set, assimilating satellite altimeter observations as well as available in situ observations using the Navy Coupled Ocean Data Assimilation (NCODA) system (Cummings and Smedstad, 2013). The model is forced by NAVGEM (Navy Global Environmental Model) 0.5a atmospheric forcing and tides.

Hourly hindcast fields of velocity, temperature, salinity and sea surface height from the GoM HYCOM hindcast are interpolated to the NCOM model grid. Near the boundary, the NCOM prognostic variables are relaxed toward these interpolated values using an incremental updating procedure (Newtonian relaxation). The relaxation time scale increases monotonically from 15 minutes at the boundaries to greater than 9000 hours at the interior of the 47 cell relaxation zone. The relaxation time scale is increased near the seafloor to reduce impacts of inconsistencies between the NCOM bathymetry and the GoM HYCOM bathymetry on the near-bottom currents over this zone. Over the interior of the domain, the temperature and salinity fields of the NCOM simulation are relaxed to the interpolated GoM HYCOM fields with a time scale that increases from 86 hours at the surface to greater than 30 days depth. At these subthermocline depths, the anomalies of the GoM HYCOM temperature and salinity fields are also damped toward climatology. This has the effect of constraining the geostrophically balanced mesoscale circulation features (eddies) in the NCOM to the data assimilating GoM HYCOM fields while allowing the deeper subthermocline circulation to evolve with the NCOM's high resolution bathymetry in response to the upper ocean and lateral forcing.

The NCOM hindcast is forced by wind stress derived from the National Center for Environmental Prediction (NCEP) North American Mesoscale (NAM) weather model. Hourly 10m NAM winds ($\mathbf{u_{10}}$) are interpolated to the NCOM grid and converted to stresses using the Large and Pond (1982) wind speed dependent drag coefficient as

$$\boldsymbol{\tau} = \rho_A C_D |\mathbf{u_{10}}| \mathbf{u_{10}} \tag{1}$$

where ρ_A is the air density (1.2 kg/m^3). The drag coefficient is computed as

$$C_D = 10^{-3} V^{-1} (2.7 + .142V + .0764V^2) \tag{2}$$

capped at wind speeds greater than 27 m/s by

$$\mathrm{V}=\min(27\ m\ s^{-1}, |\mathbf{u_{10}}|) \tag{3}$$

No thermal forcing is prescribed since the model assimilates the HYCOM temperature field rather aggressively (time scale of about three-and-a-half days) at depths in the surface mixed layer. No additional forcing by local tidal potential is used in this simulation, but the tidal forcing coming from the strong relaxation (15 minute time scale) to the HYCOM velocity and sea surface height fields at the boundary force a very good tidal response over this relatively small domain, as determined by tidal harmonic analysis of the model and observed velocity time series. Fields of all model prognostic variables are saved at hourly intervals for analysis.

3. RESULTS AND DISCUSSION

3.1 Wind and Upper Ocean Circulation Regimes

During the study period, no tropical disturbances directly impacted the region. As determined from inspection of the NAVGEM 10m wind time series at 90.5°W, 27.5°N, winds were typically light and dominantly southerly (northward) and southeasterly during the summer months of 2014 (Figure 2.5.1). During the fall and winter months, more energetic synoptic weather patterns influenced the wind variability, with cold front passages causing periods of intensified southerly winds rotating around to strong northerly winds at quasi-regular intervals. Cessation of the strong cold front passages occurred during March, 2015, when the wind regime shifted back to nearly persistent moderate southerly and southeasterly winds. Maximum wind speeds during this year-long study remained below 20 m/s.

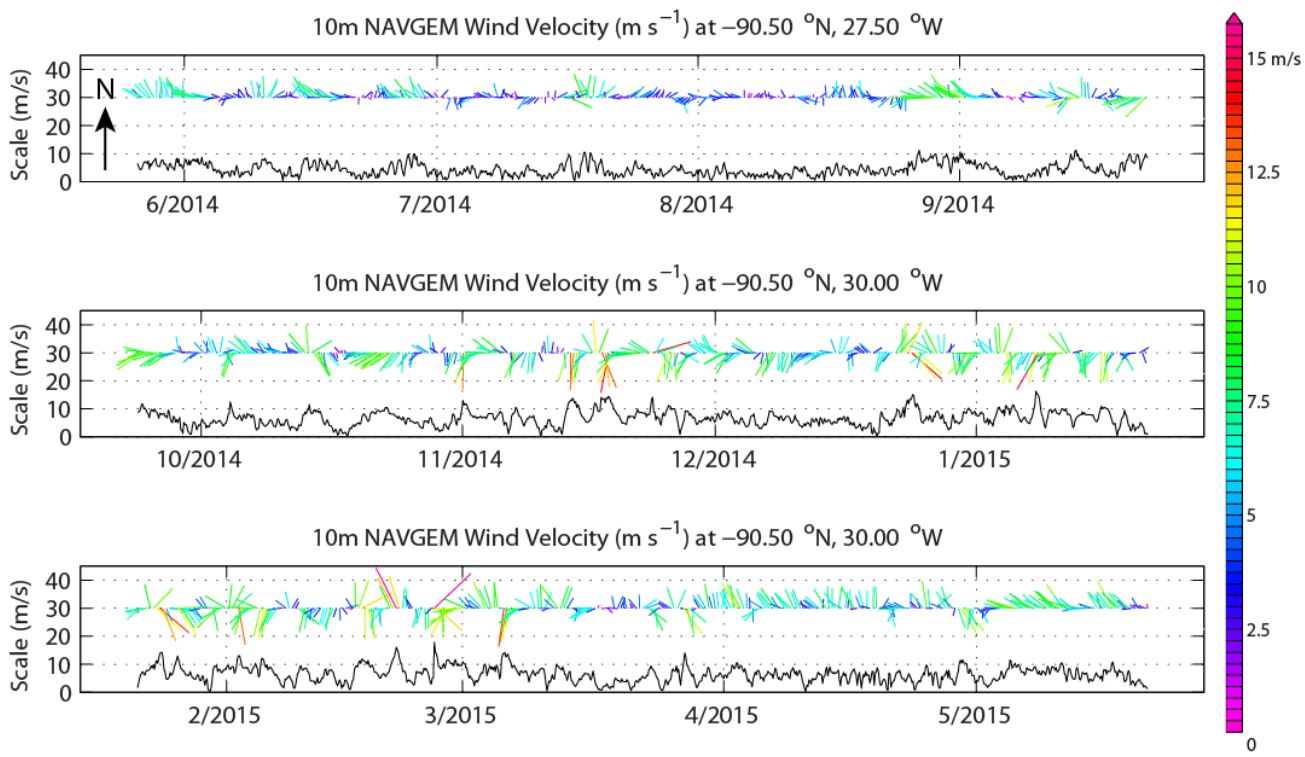

Figure 3.1 Wind vector time series (north up) from NAVGEM 10m winds at 90.5W, 30N. The vector color indicates the speed (m/s), which is also plotted by the black line. The scale for the vector speed and speed time series is shown as the *y*-axis, and the dates along the *x*-axis are shown as month/year.

Though no strong tropical disturbances passed through the region allowing for observations of their impact on near-bottom currents, the region was impacted by an anomalously extended Loop Current and several eddies during much of the year-long study. The Loop Current extended far to the northwest during the late summer of 2014, even reaching as far west as the mooring array in October following the remerging of a briefly detached eddy (Figure 3.2; Animation 5.1). The Loop Current eventually shed a small anticyclonic ring, named “Lazarus” by Horizon Marine, Inc. (www.horizonmarine.com/loop-current-eddies.html), which

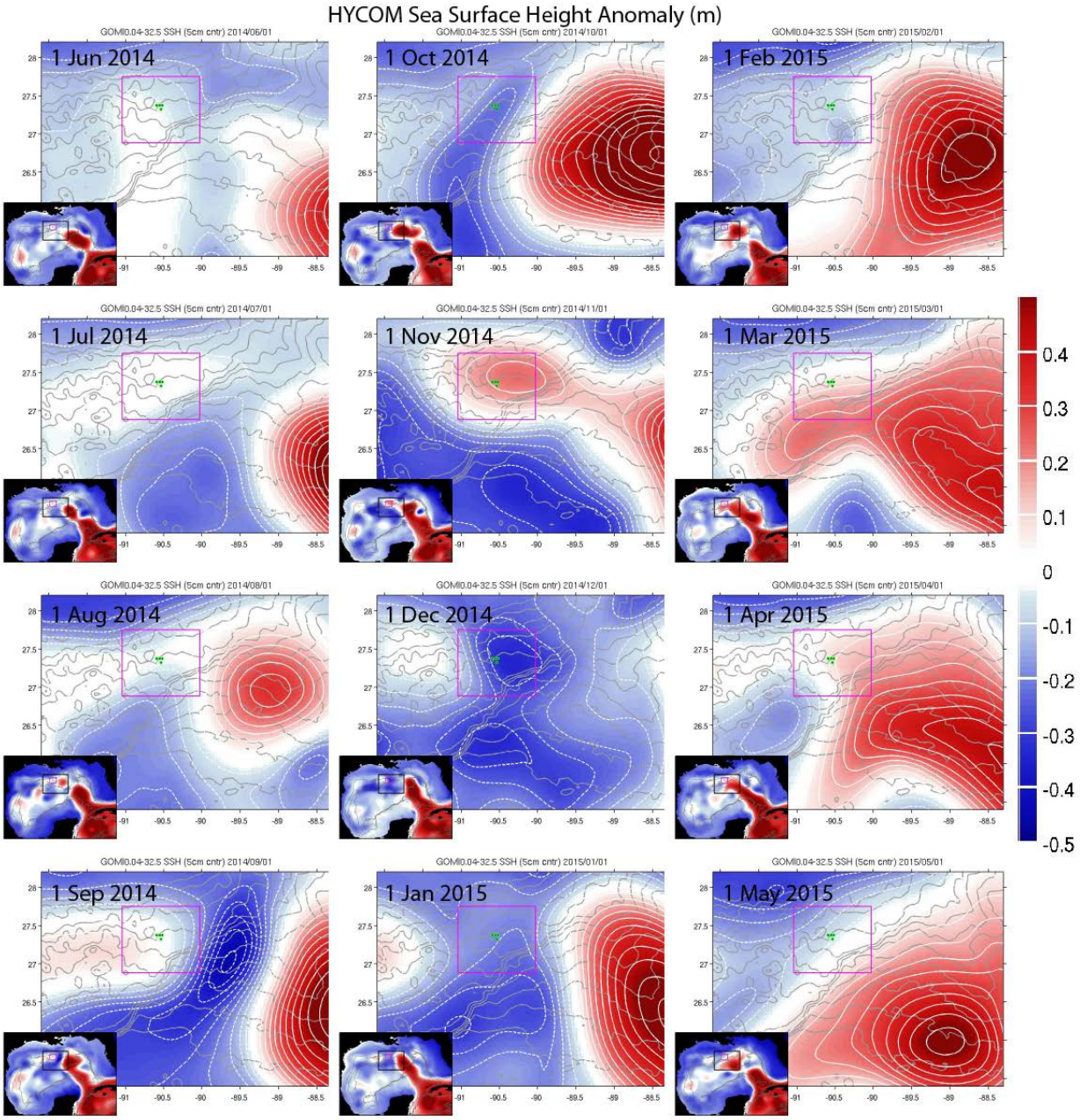

Figure 3.2 SSH (anomaly) maps from the Gulf of Mexico HYCOM Nowcast/Forecast system, with the nested model region shown by the pink rectangle. Note that the SSH within the nested model is very close to the HYCOM SSH due to model adjustment to the relaxed temperature and salinity fields. The small inset shows the SSH from the entire Gulf of Mexico with the region shown by the expanded view indicated by the black rectangle. Daily SSH fields from the full 1-year study time period can be seen in Animation 5.1.

migrated westward directly over the mooring array in November. The Loop Current remained elongated to the northwest before detaching a large eddy (Eddy "Michael") in January 2015. This eddy remained in the region and subsequently remerged with the Loop Current. At the end of the observational period in May, 2015, a large eddy ("Nautilus") detached from the Loop Current over the study area. Associated with these anticyclonic features were also numerous small cyclones.

Dukhovskoy et al. (2015) showed that the Loop Current has a low probability of extending as far west as the study region. Analysis of Loop Current position determined from CCAR (Colorado Center for Astrodynamic Research) gridded altimetry (Leben, 2005) from 1993 through 2010 reveals that the likelihood of the western edge of the Loop Current extending westward past 90°W on any given day is 5.7%, and only 3.3% of the time does it extend past 90.5°W. Thus, this study occurred during a year of anomalous Loop Current forcing on the region offering several opportunities to examine the influence of strong upper ocean currents on the near-bottom dynamics over the complex bathymetry.

3.2 Observed Near-Bottom Currents

The three different mooring configurations used during the field component of this study resulted in inhomogeneous sampling of the deep water column (Figure 2.3). However, currents at 38mab were consistently well sampled throughout year-long observational record. Thus, a nearly continuous year-long record of currents at 38mab is available for analysis, and the second and third deployments provide information about the vertical structure of the current profile down to approximately 10 - 12mab.

Mean vectors from the 38mab velocity time series show a generally southward flow at all mooring locations except S1, which has a nearly zero mean velocity (0.7 cm/s toward the northeast) (Figure 3.3). Ellipses drawn at the heads of the vectors indicate the standard deviation of the current variability in all directions, based on the standard deviations along the major and minor principal component axes. The relative size of the mean current vector relative to the size of the ellipse indicates the relative persistence of the current in the mean direction. That is, the mean vector at S2 is longer than the semi-major axis indicating that current reversals from the southward direction occur infrequently. The eccentricity of the S2 standard deviation ellipse also indicates that the current primarily varies in the direction of the major principal axis (dominantly north-south variability from the mean), which is largely along the local topographic slope. The currents at 42370 (Holstein) also have variability primarily oriented along the topographic slope. At the top of the pinnacle, the currents at S1 have nearly isotropic variability, shown by the nearly circular standard deviation ellipse, and variability at S3 is similar except it is superimposed on a stronger southeastward mean flow. These traits suggest a largely southward mean flow extending from the center of the basin (S3) to the western rim of the basin, intensified along the steep bathymetry, with the currents at the shallower S1 mooring location on top of the pinnacle displaying distinctly different characteristics.

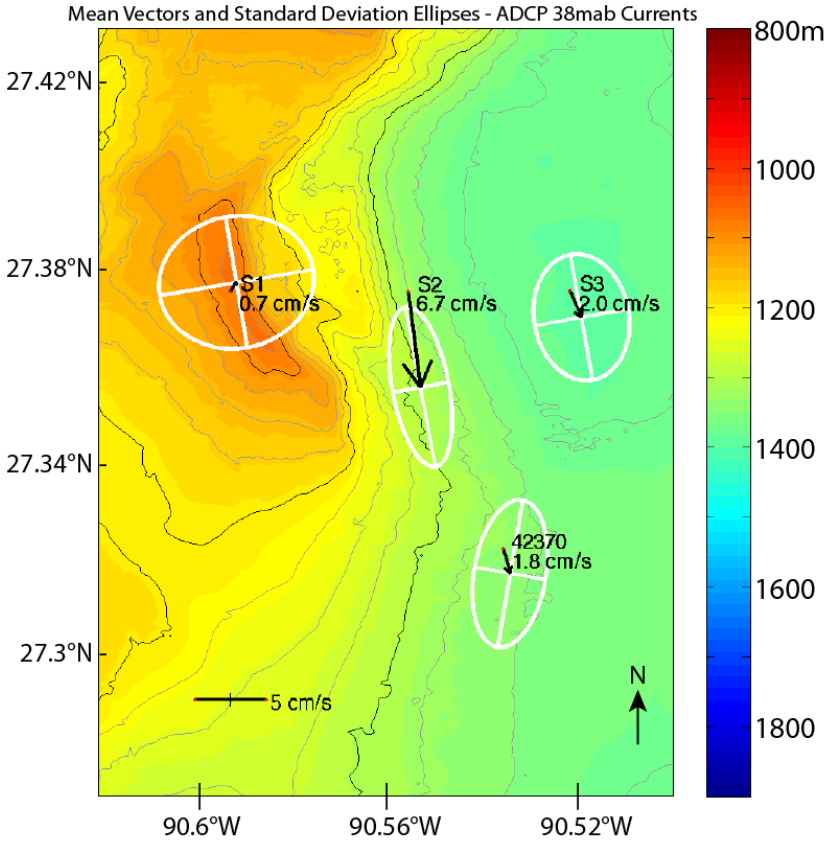

Figure 3.3 Mean vectors and standard deviation ellipses for the velocity vector time series at measured at 38mab by the ADCPs at mooring locations S1-S3 and 42370. The tails of the vectors are at the mooring locations. The semi-major and semi-minor axes indicate the standard deviation of the velocity principal components (directions of greatest and least variability).

The time series of the 38mab velocity from S1 - S3, as well as from 42370 (Figure 3.4), show the variability of the currents at the four locations and reveal several episodes of energetic currents. As anticipated from the mean vectors and standard deviation ellipses, currents at S1 fluctuate in all directions. There appears to be substantial quasi-inertial variability that at times has peak amplitudes exceeding 20 cm/s (for example, early December 2014 and late January 2015). Currents during these time periods of enhanced energy tend to be somewhat more persistently oriented in a particular direction, though that direction varies between energetic episodes (westward during the peak in late September 2014, southwestward during the early December 2014 and late January 2015 episodes, and southeastward during an energetic episode in late February 2015). The lack of strong topographic steering atop this pinnacle-like feature likely allows for the isotropic variability in the near-bottom velocity.

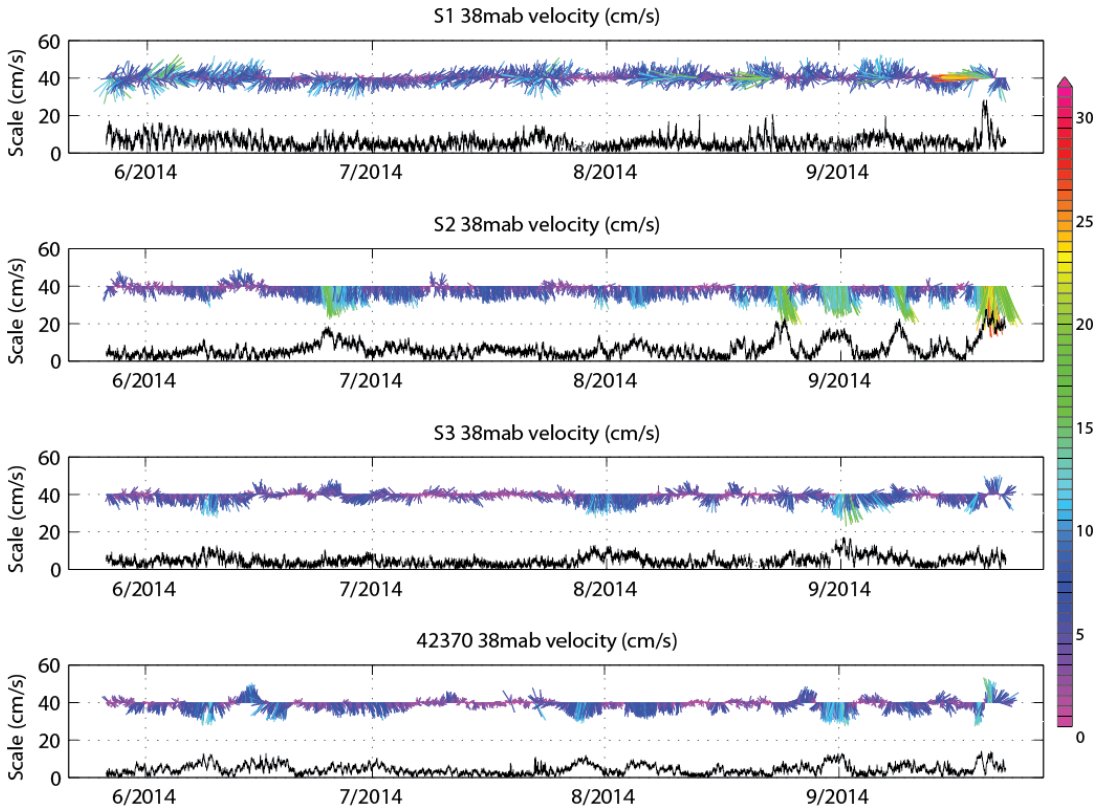
S1 38mab velocity (cm/s)
S2 38mab velocity (cm/s)
S3 38mab velocity (cm/s)
42370 38mab velocity (cm/s)
Scale (cm/s)
0
20
40
60
6/2014
7/2014
8/2014
9/2014
0
5
10
15
20
25
30

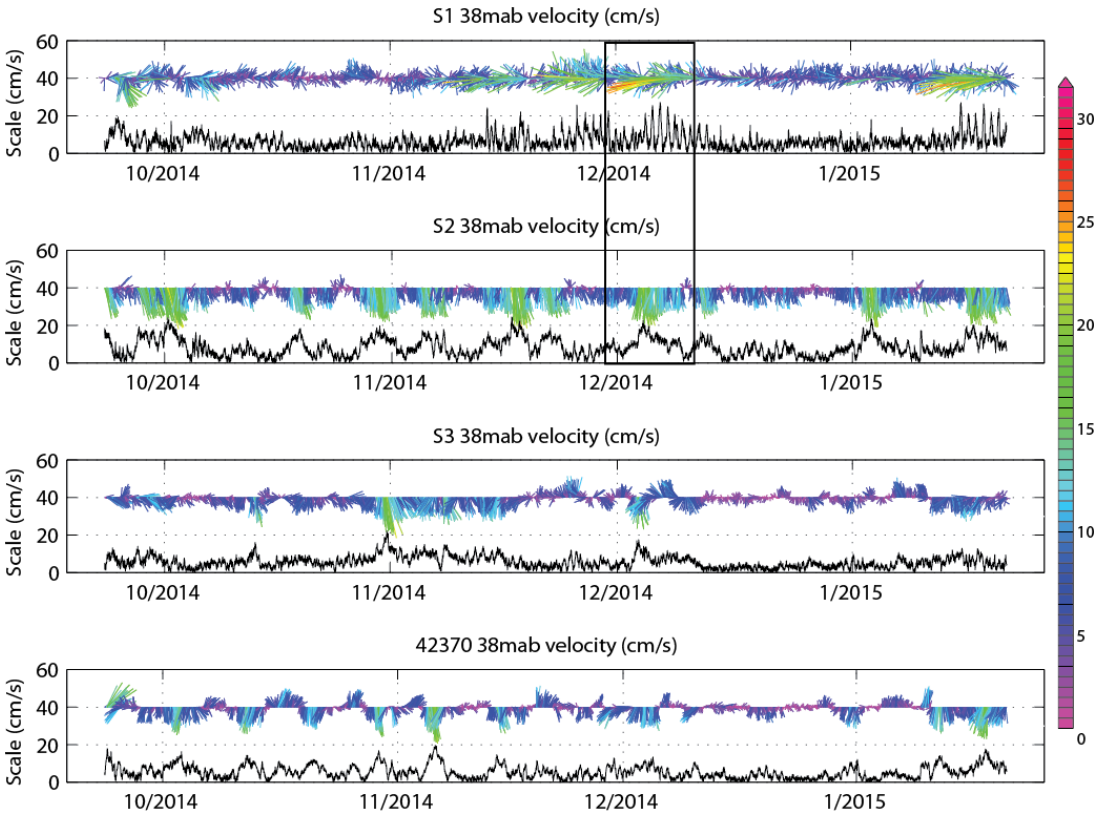
S1 38mab velocity (cm/s)
S2 38mab velocity (cm/s)
S3 38mab velocity (cm/s)
42370 38mab velocity (cm/s)
Scale (cm/s)
0
20
40
60
10/2014
11/2014
12/2014
1/2015
0
5
10
15
20
25
30

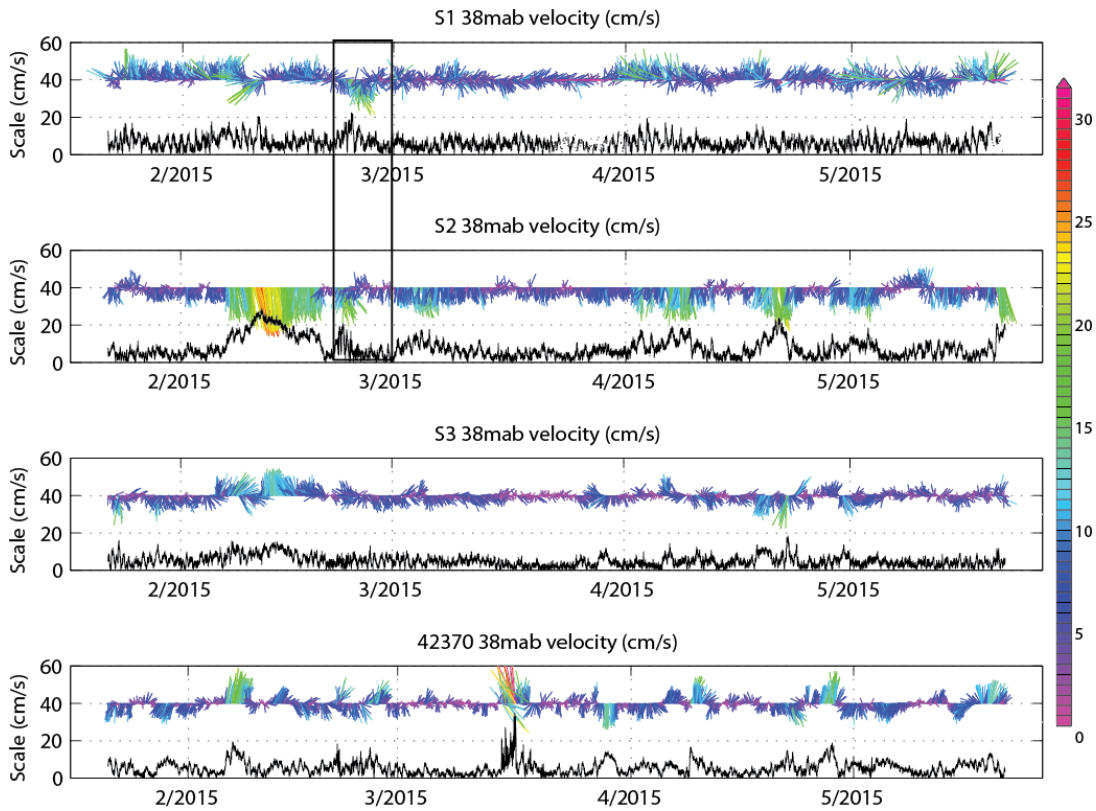

Figure 3.4 38mab velocity time series from S1, S2, S3, and 42370 ADCP observations. Vectors are colored based on magnitude (cm/s), and magnitude is also indicated by the black time series. North is toward the top of the plots. The time periods indicated by the black rectangles (parts of December 2014 and March 2015) are those selected for later analysis below.

The 38mab flow at mooring S2 is strongly southward (Figure 3.4), with infrequent reversals as expected from the mean and standard deviation analysis (Figure 3.3). Maximum current speeds reached 27 cm/s on 20 September 2014 and 29 cm/s on 11 February 2015. Currents at S3 were generally weak with a dominant southward component, though not as strongly unidirectional as at S2. The maximum recorded speed at 38mab at S3 was 22 cm/s on 31 October 2014, and speeds remained otherwise below 20 cm/s throughout the observational record. Currents at 42370 varied dominantly in the north-south direction with frequent reversals, though analysis indicates a 1.8 cm/s mean flow toward the southeast (Figure 3.3). Like the S3 location, current speeds remained below 20 cm/s except for an energetic event in mid-March, 2015, during which the 38mab current speed reached 35 cm/s on 16 March.

Variability near the local inertial time period (26.0 hours) is not as pronounced at S2, as it is at S1, nor does variability at this periodicity have large amplitude at S3 or 42370 compared to S1. There is no obvious coherence between the currents at S2 and S1 (and indeed calculations reveal no statistically significant coherence), though some individual strong current events do seem to coincide with strong events at S1 (e.g., late September 2014, early December 2014, late January 2015, mid-February 2015). No coherence is evident in the near-bottom currents at any of these mooring sites, despite their close proximity (3.4km to 6.3km between adjacent sites) indicating either the short spatial scales of currents at 1326 – 1386m (depth

range of the S2, S3 and 42370 moorings), or perhaps strong vertical shear between the shallower S1 mooring (1072m) and depths of the other moorings.

The vertical structure of the near-bottom currents at mooring locations S1 - S3 is examined from the Deployment 3 observations, as they have the most consistent data return near the sea floor. The mean velocity vector at different heights above the bottom shows clockwise turning with height above the bottom, consistent with a bottom Ekman spiral, at S1 (Figure 3.5). Such a classic turning of the current vector with depth is not clearly evident at S2 and S3, though a decay of the mean vector toward the bottom is suggestive of a logarithmic-type boundary layer at S2. S1 and S3 do not clearly show the decay of the current toward the bottom but this may be due to the much smaller speeds at these locations, and Ekman turning may be confined closer to the seabed than observations extend. No such analysis can be performed at 42370 because of the large bin spacing of the ADCP observations.

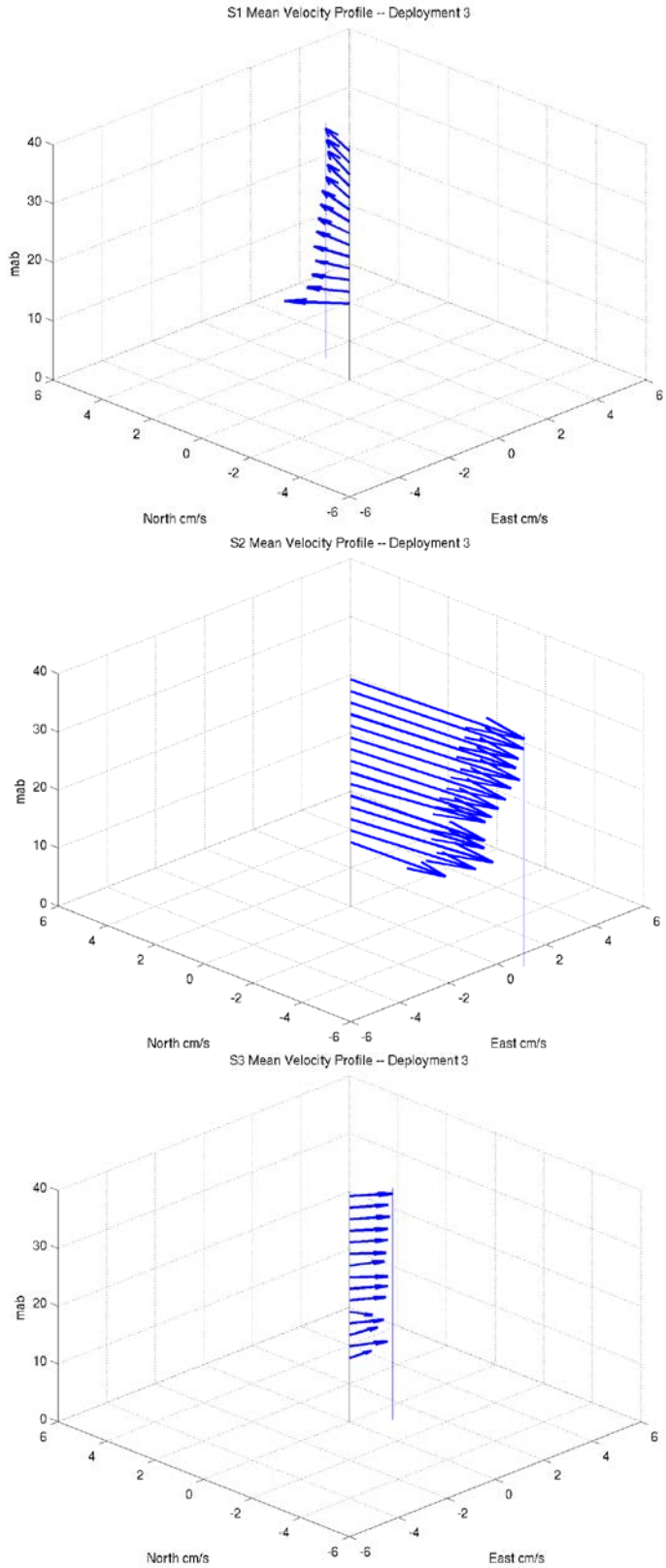

Figure 3.5 Profile of mean vectors for each ADCP bin from the third mooring deployment time period. The mean is computed over the portion of the observational record that had good data retrievals at all heights. A vertical line projects the mean vector of the topmost bin to the bottom for comparison with the other vectors.

Inspection of the vertical structure of near-bottom currents at S2 and S1 during time periods of energetic currents suggests very different characteristics at these two locations (Figure 3.6). During an extended period of strong near-bottom currents at S2 from 10 - 18 February 2015, the velocity at 13mab has reduced magnitude from the velocity at 39mab, again characteristic of a bottom boundary layer. In contrast, during a time period of strong quasi-inertial oscillations at S1, enhanced velocity magnitude is evident at 18mab compared to 36mab (this time period was during the second deployment and 18mab was the closest level to the bottom with good data return). Thus, not only do the currents at the shallower S1 location near the top of a pinnacle-like bathymetric feature exhibit different characteristic variability than at the other mooring locations, but it also exhibits a distinctly different vertical structure of currents with near-bottom enhancement of the currents during strong events.

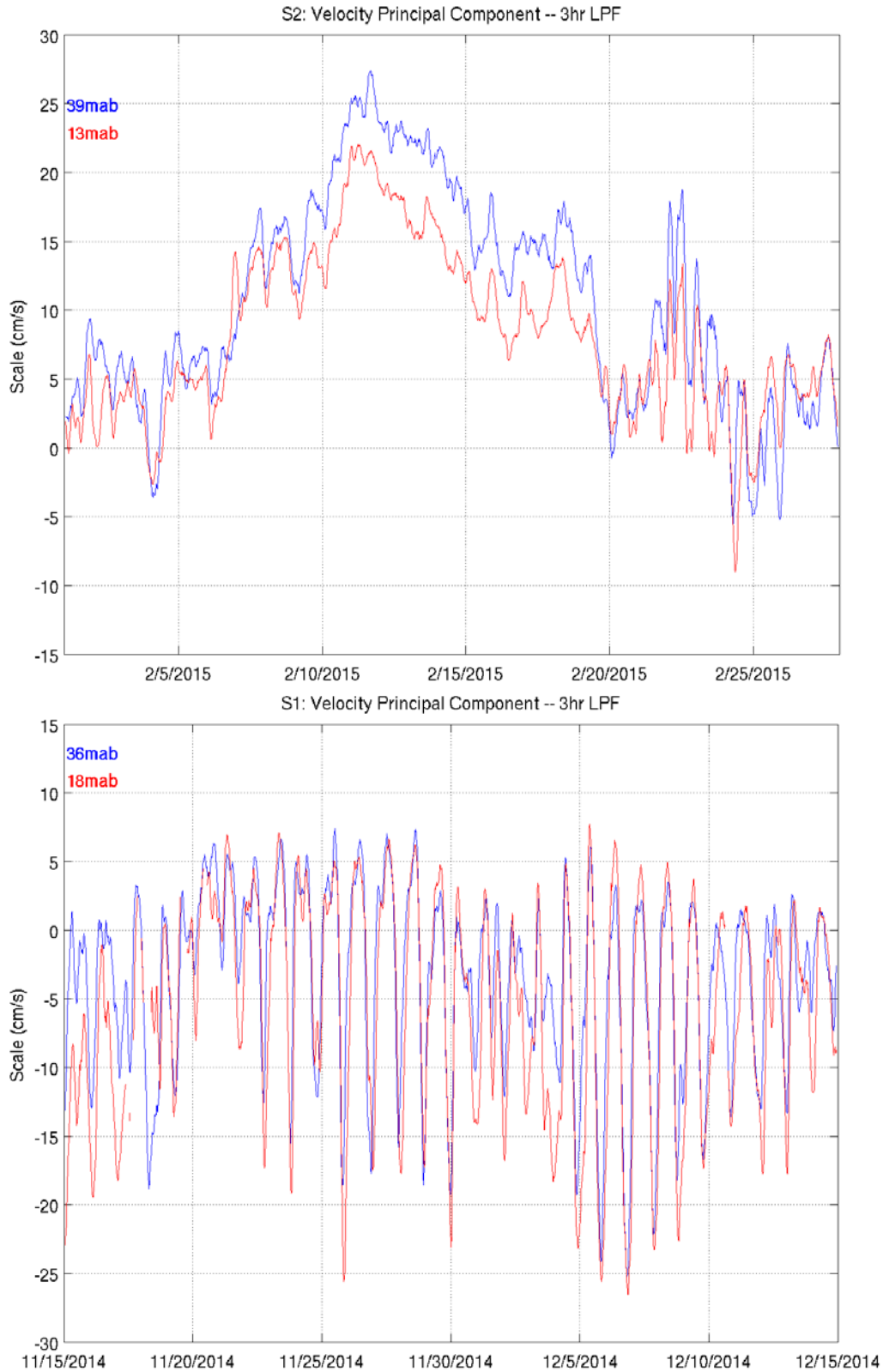

Figure 3.6 Top: Velocity projected onto the major principal axis computed over the time period 1-28 Feb 2015 at S2 at 39mab (blue) and 13mab (red). Bottom: Velocity projected onto the major principal axis computed over the time period 15 Nov – 15 Dec 2014 at S1 at 36mab (blue) and 18mab (red).

3.3 Modeled Near-Bottom Currents

Time series of velocity extracted from the model output are compared with the observations to establish aspects of the simulation that can be used with some confidence to interpret the dynamics governing the variability of the deep currents in this region. The simulated velocity time series at 38mab at the mooring locations share some important similarities with the observations. Mean model near-bottom velocities are directed generally toward the south (Figure 3.7), with enhancement at S2 along the steep bathymetry. However, there is a high bias of the mean velocity magnitude at all locations compared to the observations (Figure 3.3), with S2, S3 and 42370 mean velocity 5.3 - 5.5 cm/s greater in the model, but in similar directions. The model mean 38mab velocity at S1 is 4.7 cm/s directed toward the southeast compared to the very small mean from the observations. Standard deviation ellipses from model currents show remarkable agreement with observations, though slightly larger in magnitude. As in the observations, variability is strongly in the along-isobath direction at S2 and 42370 and more isotropic at S1 and S3.

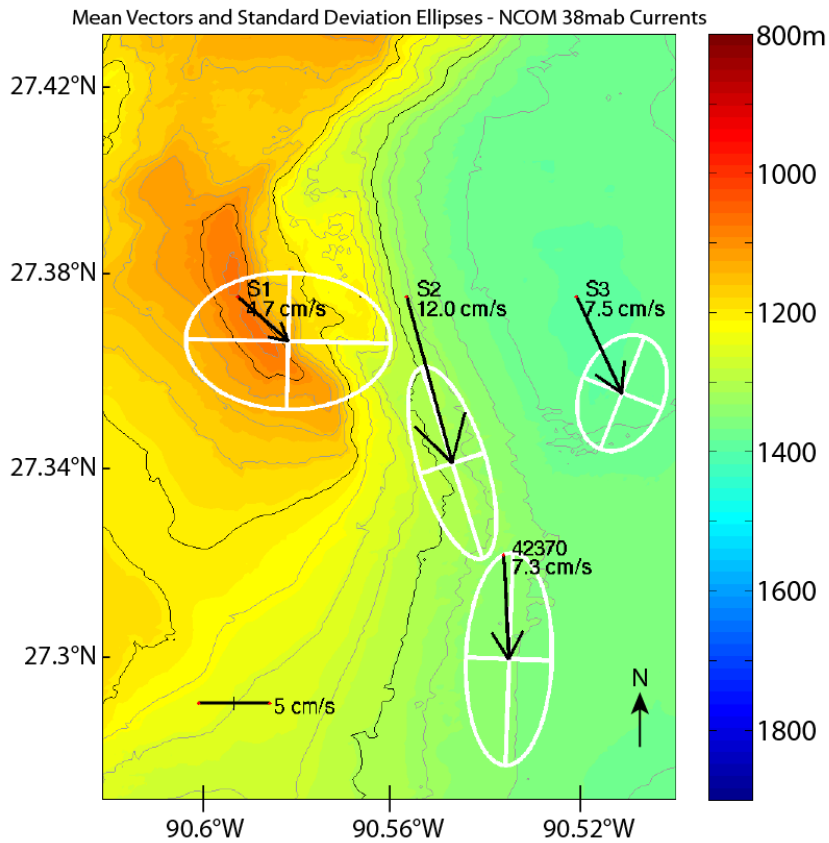

Figure 3.7 Mean vectors and standard deviation ellipses for the velocity vector time series simulated by the NCOM at 38mab at mooring locations S1-S3 and 42370. The tails of the vectors are at the mooring locations. The semi-major and semi-minor axes indicate the standard deviation of the velocity principal components (directions of greatest and least variability).

The high bias of the near-bottom mean current magnitude compared to observations may be due to the model's tendency to develop weak (on the order of several cm/s) mean flows along steep bathymetry. This

is consistent with the results of Dukhovskoy et al. (2009), which showed that even though use of the VQS vertical grid reduced spurious velocities to approximately one-third the magnitude of those formed when using fully terrain-following vertical coordinates, velocities of several cm/s still appear close to steep bathymetry. Further modeling of regions with such complex bathymetry likely warrants application of an unstructured mesh model in the future to allow grid refinement over these steep slopes, hopefully further reducing the numerical errors associated with computing horizontal gradients that spawn the spurious currents.

Time series of currents at the mooring locations show clearly the impact of the biased mean currents. However, removal of the bias (by subtracting the long term mean from the model and adding the long term mean from the observational time series) reveals variability in the model currents sharing many characteristics with the observational time series (Figure 3.8). In particular, S1 has pronounced near-inertial variability compared to the other mooring locations. Direction of variability (largely isotropic for S1 and S3, and more rectilinear at S2 and 42370). closely mimics the observations, and is consistent with inferences from the standard deviation ellipses (Figure 3.7). As in the observations, there is no significant coherence in currents between the different mooring locations.

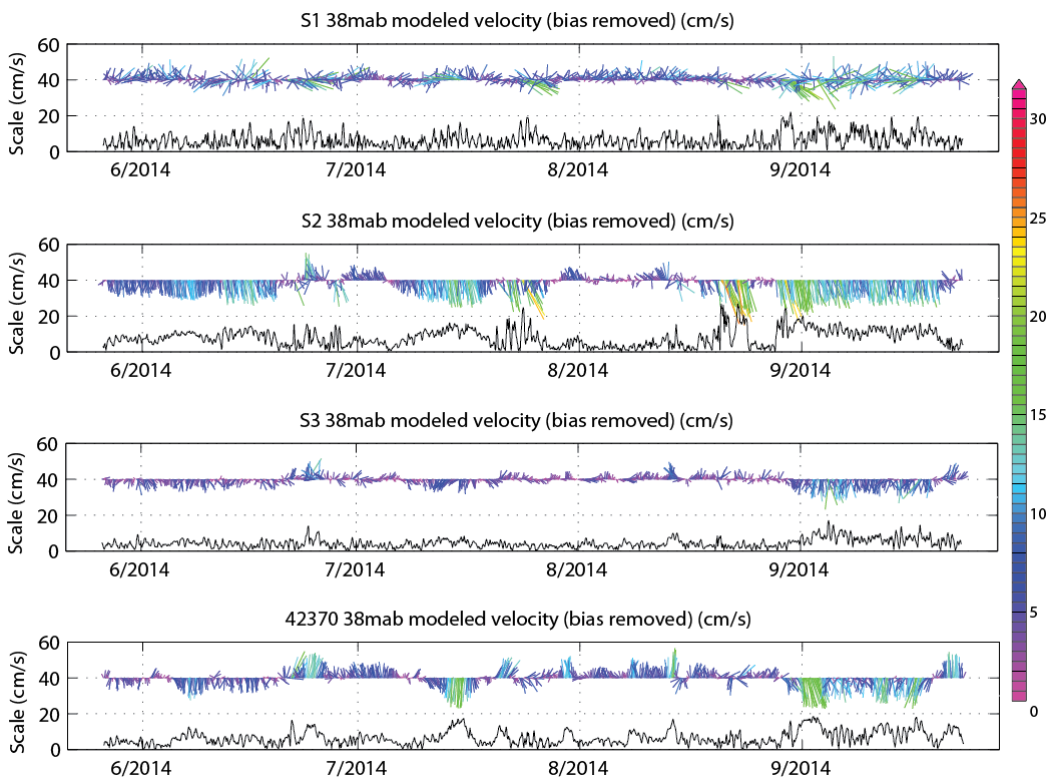

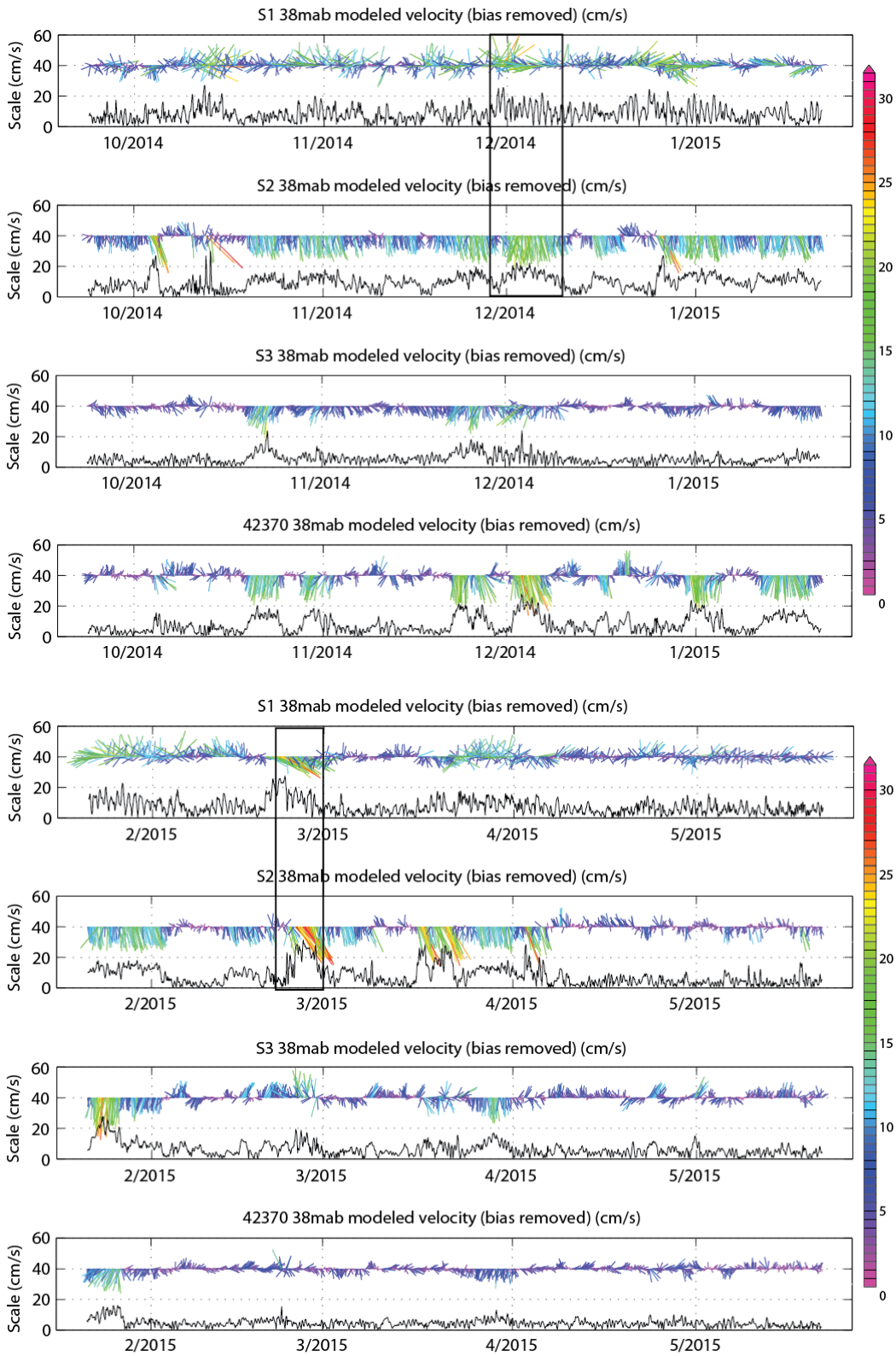

Figure 3.8 38mab velocity time series simulated by the NCOM at the S1, S2, S3, and 42370 mooring locations. Vectors are colored based on magnitude (cm/s), and magnitude is also indicated by the black time series. North is toward the top of the plots. The time periods indicated by the black rectangles (parts of December 2014 and March 2015) are those selected for later analysis below.

With few exceptions, there is no noticeable relation in timing of current fluctuations between the observations and the simulation. It has been established that the length scales of the near-bottom currents are likely small (due to the lack of coherence between currents at the closely spaced mooring locations). It is highly unlikely that any data assimilation methodology will achieve constraint in timing and location of such small scale features, particularly at depth, given the paucity of data available for assimilation. No observations exist which would resolve such small scales, particularly at subthermocline depths (nearly all data available for assimilation comes from satellite observations of the sea surface, and the most dynamically important variable, sea surface height, is sampled very coarsely in space and time by altimeters). State-of-the-art data assimilation capabilities for ocean models seek to constrain the large upper ocean mesoscale (typically 100km or greater) circulation features. Nevertheless, agreement in characteristic variability between the model and observations show the success of the methodology employed here – application of a model with realistic dynamics in a realistically fine-scale resolution simulation with accurate bathymetry – in providing greater understanding of the characteristics and dynamics of the near-bottom currents over this region with complex bathymetry.

3.4 Spectral Characteristics of Measured and Modeled Currents

A key focus of this research is the vertical structure of near-bottom currents, particularly at near-inertial frequencies. Cooper (2011) suggested from analysis of the limited observations extending below 100mab to within 20mab that currents with near-inertial fluctuations may be amplified near the seabed compared to at 100mab. Inspection of observed currents at S1 reveals evidence supporting this hypothesis (Figure 3.6). Identification and characterization of variability near the local inertial period is accomplished here through use of wavelet and rotary current spectra analysis.

The (Morlet) wavelet power spectra are computed for the 38mab velocity projected onto the principal axis at each mooring location, both from the ADCP (Figure 3.9) and model (Figure 3.10) time series. The results show the power (scaled by the total variance) at different periods evolving in time throughout the one-year record. There is substantial variability throughout the record in power associated with low frequency motions at all stations, with a pronounced increase in power near the inertial period, particularly at S1. Similar results are obtained from wavelet analysis of the observations and the model (the apparent overall reduction in normalized power seen in the model is likely due to the model having greater total variance).

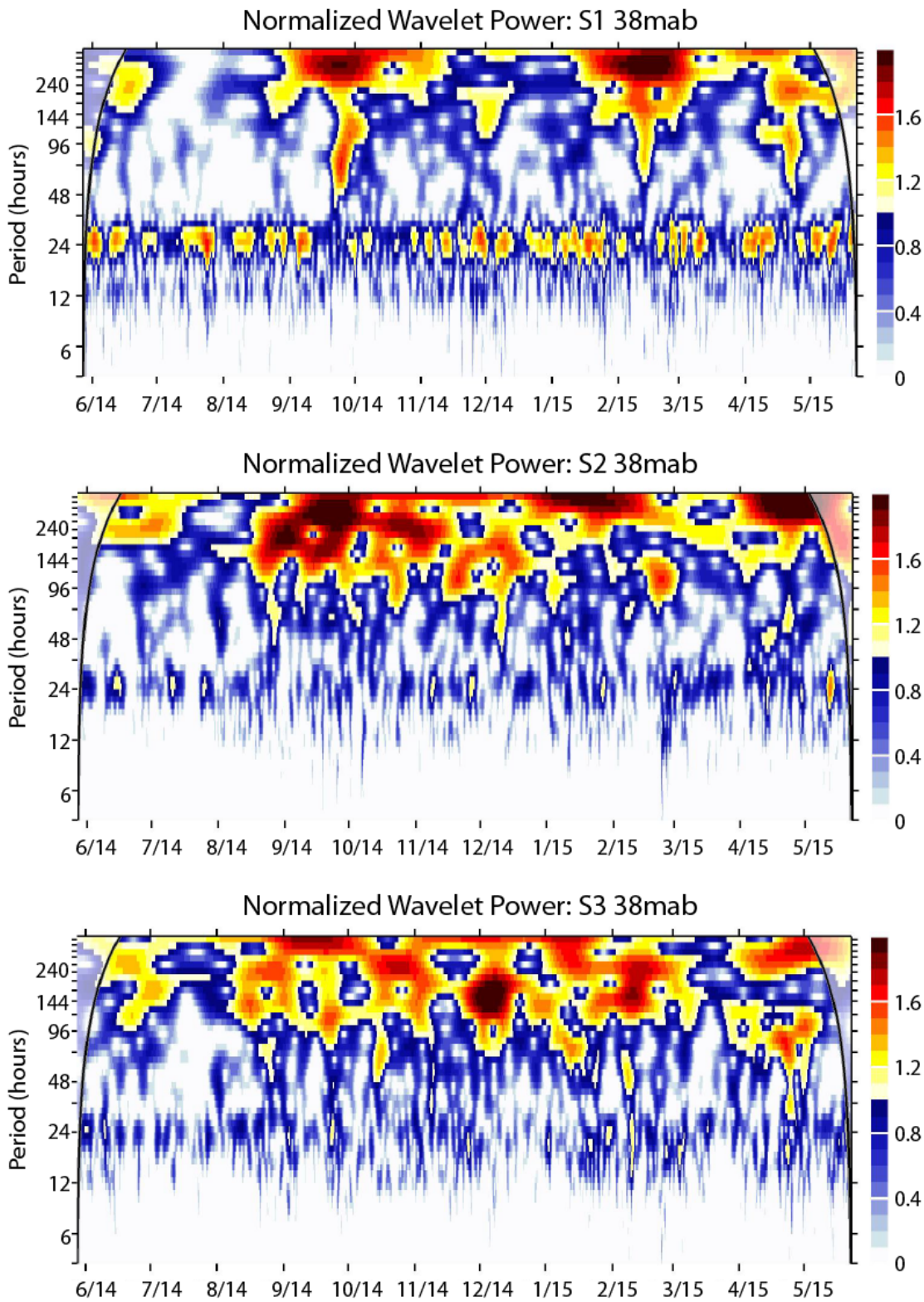

Figure 3.9 Normalized wavelet power spectra for the 38mab principal component velocity time series measured by the ADCPs. The color indicates the power normalized by the total variance. The horizontal axis is time (month/year) and the vertical axis is period (wavelet scale). The shaded regions in the upper corners indicate contamination by the record end points yielding less than 90% confidence.

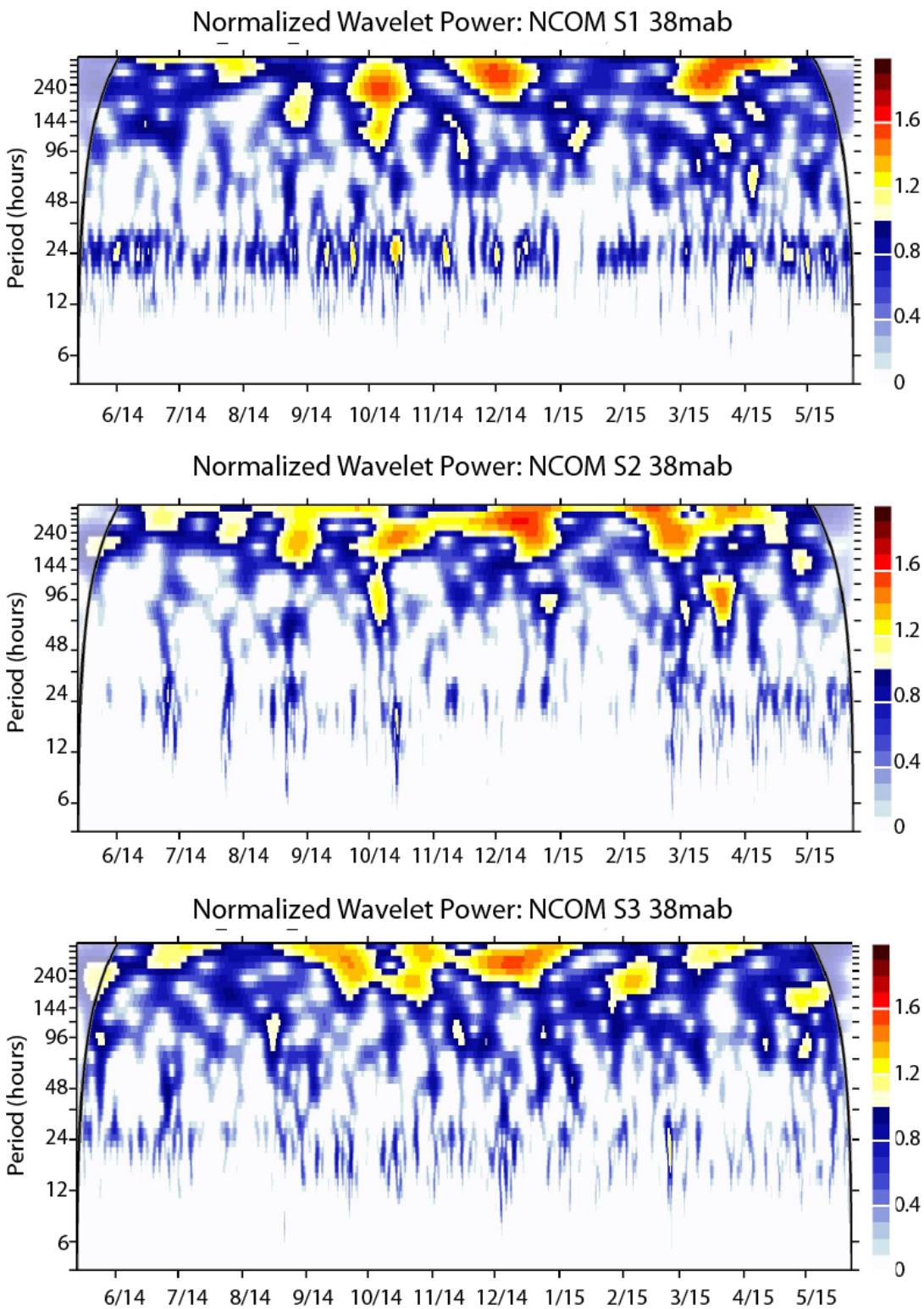

Figure 3.10 Normalized wavelet power spectra for the 38mab principal component velocity time series simulated by the NCOM at the mooring locations. The color indicates the power normalized by the total variance. The horizontal axis is time (month/year) and the vertical axis is period (wavelet scale). The shaded regions in the upper corners indicate contamination by the record end points yielding less than 90% confidence.

Rotary spectral analysis is a useful tool for analyzing near-inertial currents, as it is able to isolate the variance associated with the rotation of the local current vector at different frequencies, and this rotation is characteristic of inertial motions. There is a clear dominance of clockwise rotation (S-, the red curve) at S1 (Figure 3.11 and Figure 3.12) near the inertial period (which also happens to be very close to the diurnal tidal period at this latitude). A secondary peak in rotary power spectral density at the semidiurnal band is also evident. Currents at S2, S3, and 42370 also exhibit peaks near the diurnal and semi-diurnal periods, but smaller in amplitude than at S1. Importantly, the dominance of clockwise rotation over anti-clockwise rotation for the near-inertial fluctuations is not evident at these other mooring locations.

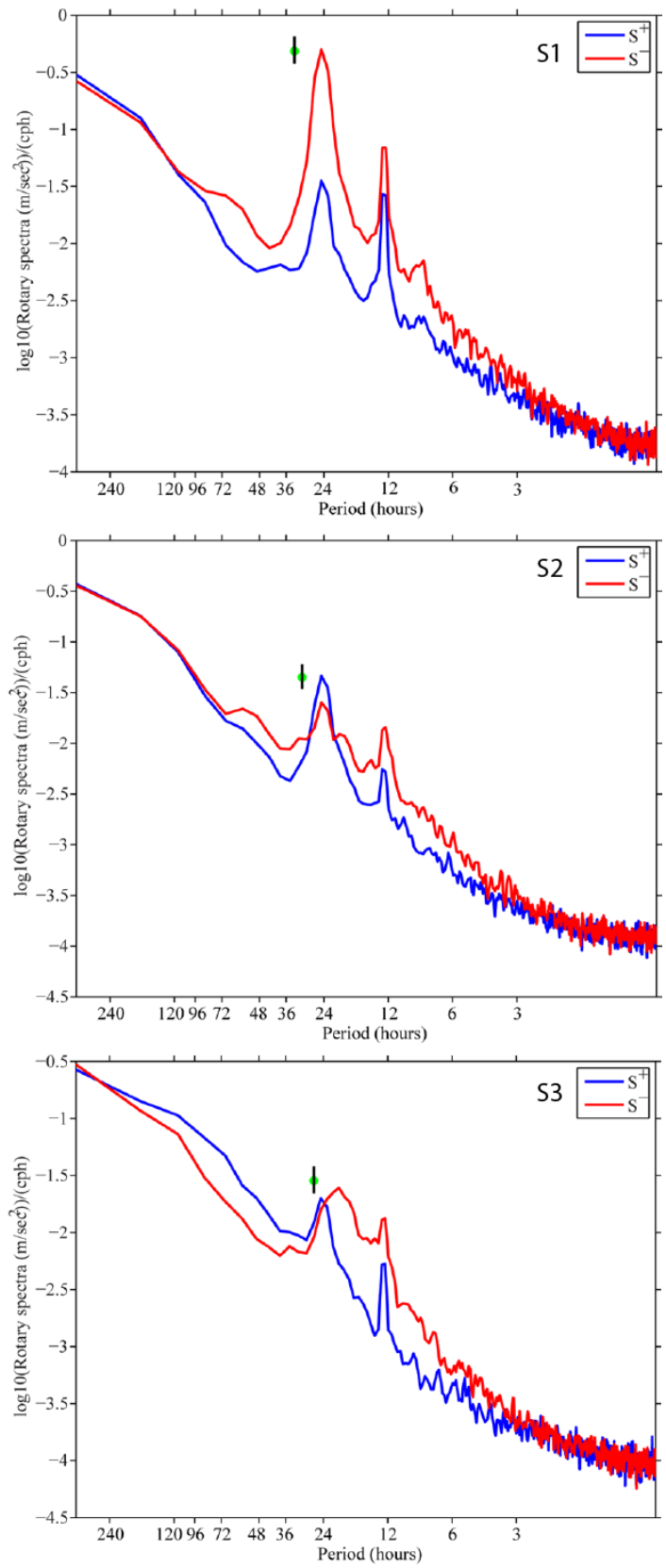

Figure 3.11 Rotary power spectra for the 38mab velocity time series measured by the ADCPs. The red curves (S-) indicate clockwise rotating currents and the blue curves (S+) indicate the power associated with anticlockwise rotating currents. The black line/green dot indicates 95% confidence interval.

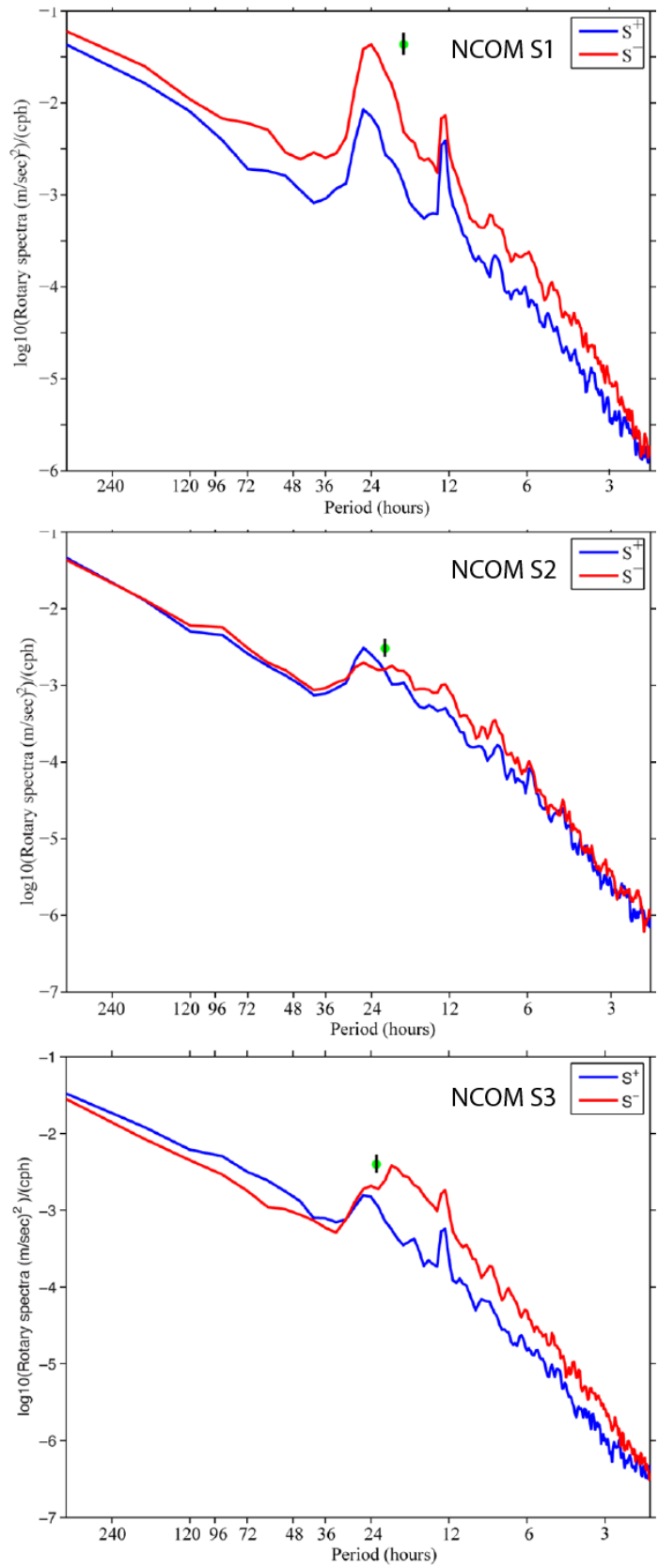

Figure 3.12 Rotary power spectra for the 38mab velocity time series simulated by the NCOM. The red curves (S-) indicate clockwise rotating currents and the blue curves (S+) indicate the power associated with anticlockwise rotating currents. The black line/green dot indicates 95% confidence interval.

It should be noted that harmonic analysis has also been performed to estimate the amplitudes associated with the dominant tidal constituents at each mooring location. Tidal current amplitudes are approximately 1 – 2 cm/s for the dominant diurnal constituents O1 and K1, and less than 1 cm/s for the semidiurnal M2 tidal constituent, or substantially smaller than the near-inertial oscillations of 10 - 20 cm/s observed at S1 (Figure 2.5.6). Additionally, currents associated with tidal motions may rotate in either the clockwise or the anti-clockwise direction, but inertial currents always rotate in the clockwise direction in the northern hemisphere.

The rotary coefficient, a scaling of the positive and negative rotary power spectral density, is an indicator of the dominance of clockwise or anticlockwise rotation for each frequency. To gain an understanding of the vertical dependence of inertial energy, the negative (clockwise) rotary power spectral density and rotary coefficient are computed as functions of depth at the frequency of the near-inertial peak at each mooring location from the year-long simulation (Figure 3.13). Inertial motions at each location are most energetic within the surface mixed layer, nearly uniform throughout the subsurface waters from 200 – 1000m, and generally decaying below this main thermocline depth. The exception is at S1, which exhibits a near doubling of rotary power spectral density at the inertial period near the bottom (and subsequently decaying just near the seabed due to friction) (black curve in Figure 3.13, left panel). The rotary coefficient shows that motions at this frequency are very strongly clockwise (rotary coefficient -> -1 indicates circular clockwise rotation of the current vector) throughout most of the water column. The dominance of clockwise motion is reduced below 1000 - 1100m for all mooring locations except S1. Rotary coefficients computed from the observations (x symbols in Figure 3.13, right panel) agree very well with the model results at 38mab, providing evidence of the veracity of these results from the model.

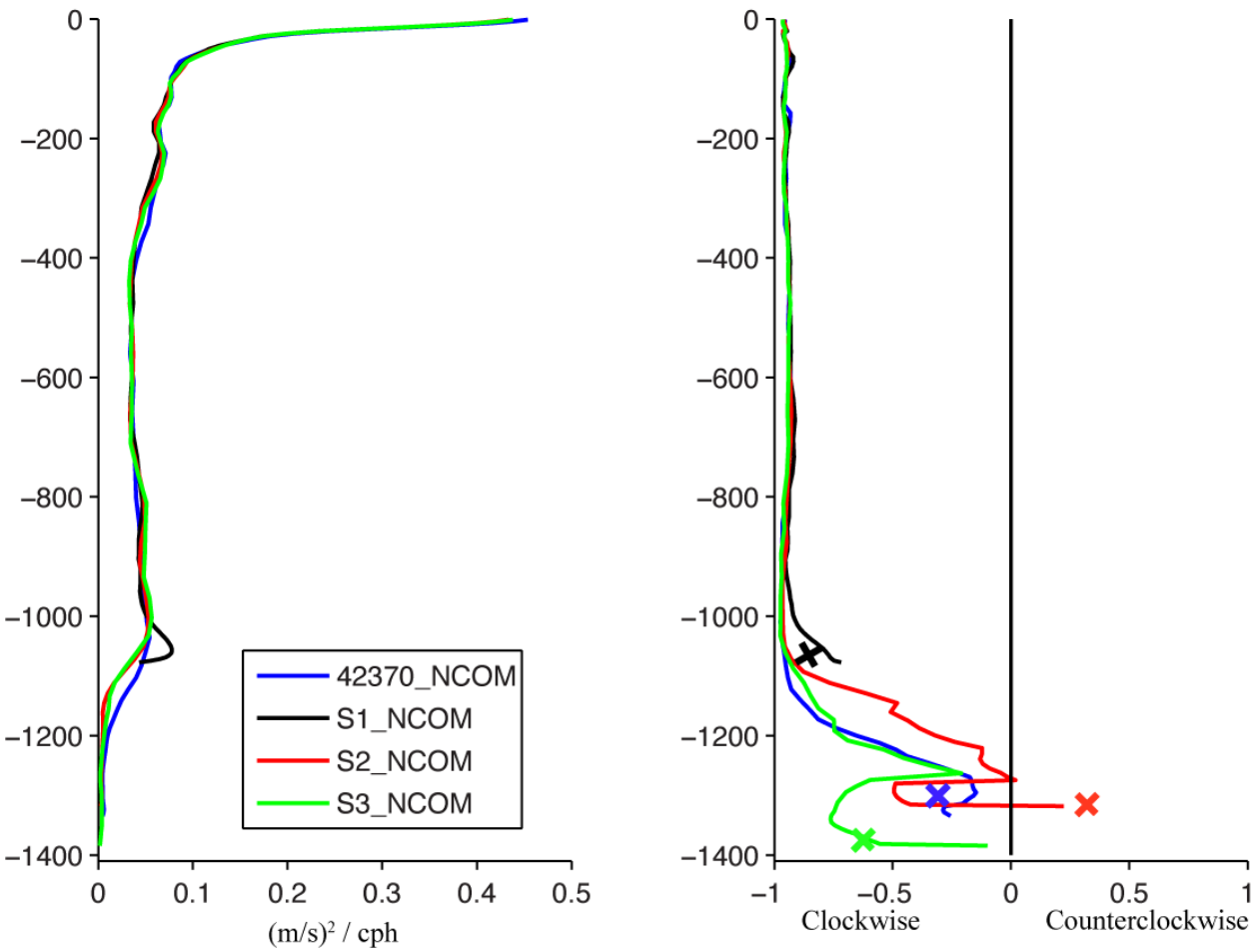

Figure 3.13 Left: Depth profile (m) of negative rotary power spectral density at the near-inertial peak for velocity simulated by NCOM at the four mooring locations. Right: Rotary coefficient computed from the near-inertial peak rotary power spectra density versus depth. Rotary coefficients computed from the ADCP measurements at 38mab are shown by the colored x symbols.

It is clear from this analysis that the deep inertial currents at the S1 mooring location exhibit distinctly different behavior than those at the other mooring locations. Inertial motions at S1 is much more pronounced than at the other locations, as inferred from clockwise turning of the current vector at near-inertial periodicity,. Additionally, the strong departure from near circular clockwise rotation occurs several hundred meters above the local seafloor depth at these other locations, and only minimally departs from near-circular rotation at S1. Possibilities for these differences could include: S1 is much closer to the main thermocline depth and inertial motions are more pronounced within the stratified thermocline layer; or the other locations lie below the depth of topographic irregularities in the region compared to S1, which is located on a pinnacle-like feature with little topographic relief extending above its location in the vicinity.

To examine the potential consequences of regional topographic relief on the behavior of inertial motions, a similar rotary spectra analysis is performed on a time series of current profiles extracted from the model at a location over deeper water far from the complex bathymetry of the study area (Figure 3.14). The negative rotary power spectral density exhibits much more gradual decay below the main thermocline than

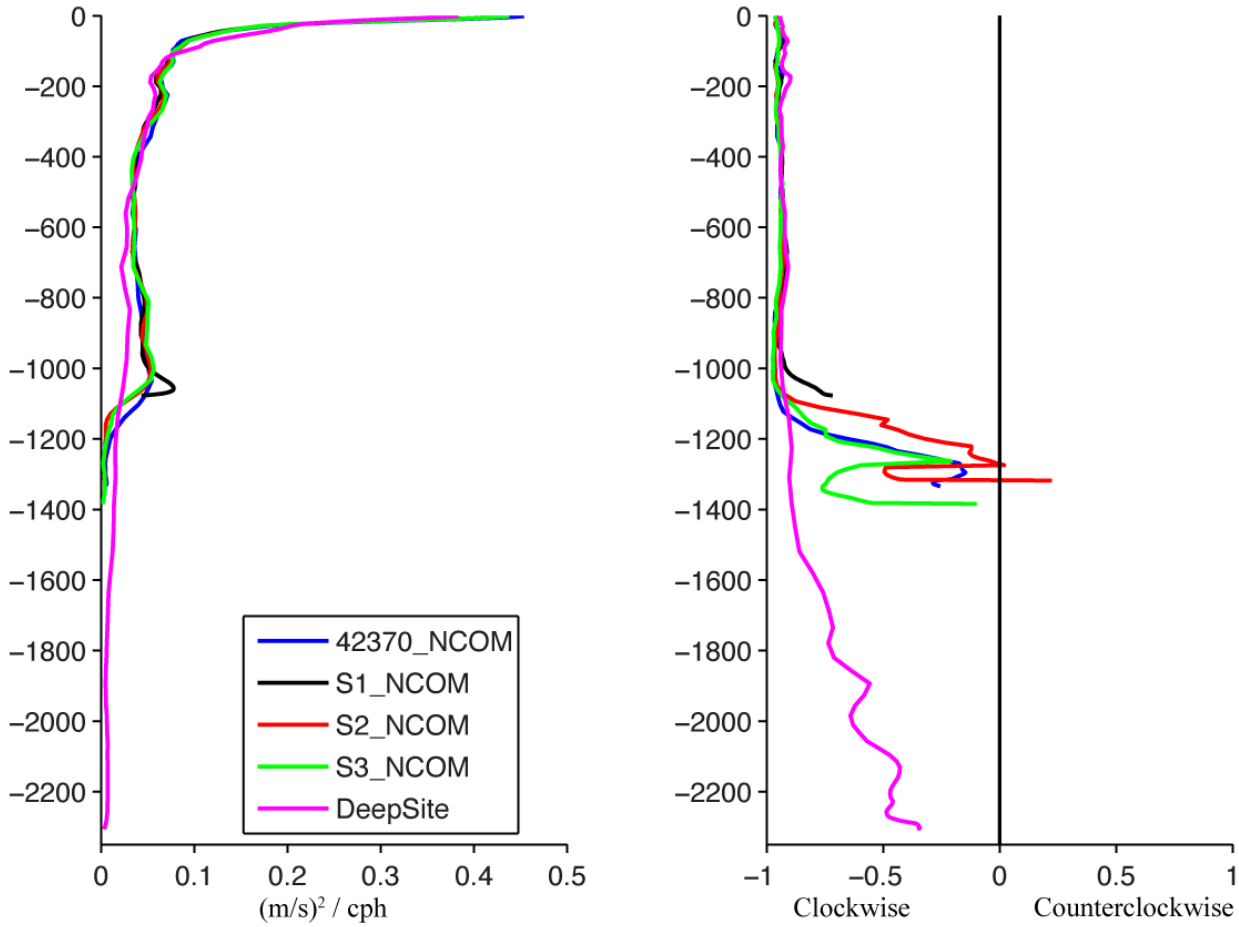

Figure 3.14 Same as Figure 2.5.13, but with the addition of a profile simulated at a deep water site (27.07°N, 90.17°W, 2308m) (pink curves).

at moorings S2 - S3 and 42370, and more gradual departure from near-circular clockwise motion (as shown by the rotary coefficient). Thus, it is apparent that the abrupt change in the characteristics of inertial motions at S2, S3, and 42370 arise not from their depth below the main thermocline, but rather the influence of surrounding topographic relief that extends several hundred meters above their local seafloor depths. The regional topography has a steering effect on the local currents beginning roughly at the top of the surrounding bathymetric features and influencing the area over length scales at least comparable to the bathymetric variations (O(10km)). is likely due to the model having greater total variance).

3.5 Analysis of Strong Near-Bottom Currents

Though in general there is little agreement between the highly variable currents from observations and the model, or between mooring locations, there are several time periods in which strong currents were both observed and simulated in the model at both S1 and S2 locations. Two particular time periods are late February 2015 early December 2014 (time periods indicated by black rectangles in Figure 3.4 and Figure 3.8). Inspection of model and observed winds during these time periods does not reveal any evidence that these currents were associated with any wind forcing event. However, due to the prevalence of the Loop

Current and eddies in this region during the study period, a link between these strong deep currents and the upper ocean forcing is investigated using the model.

In late February 2015, currents at 38mab at S1 showed strong (~25 cm/s) oscillations toward the south-southeast in the observations and toward the southeast in the model. Similarly, there were moderately strong southward directed currents at S2 in the observations, and a period of stronger southeastward currents in the model, although occurring several days after the observed peak. Inspection of the model sea surface height at this time reveals a meander of an anticyclone was situated just to the south of the moorings, such that the mooring locations experienced an eastward upper ocean flow (Figure 3.15 and Animation 5.2). This flow extended down to the depth of the pinnacle on which S1 was situated. Maps of model near-bottom velocity reveal enhancement of the flow as it separates around this pinnacle, and animations of the near-bottom flow reveal what appears to be a turbulent wake in the lee of the pinnacle with small-scale (1- 5km) vortices being entrained in the mean southward flow along the slope (Figure 3.15, bottom and Animation 5.2). These turbulent vortices move downslope and enhance the current associated with the mean cyclonic flow in the basin that impacts S2. These vortices cause pulses of enhanced currents in the region, which intermittently impact the S2 location. An area of reduced currents, or a “shadow” zone, appears to be immediately to the east of the pinnacle (Figure 2.5.15, bottom left). This shadowing effect can be seen to, at times, extend above the pinnacle (Animation 5.2).

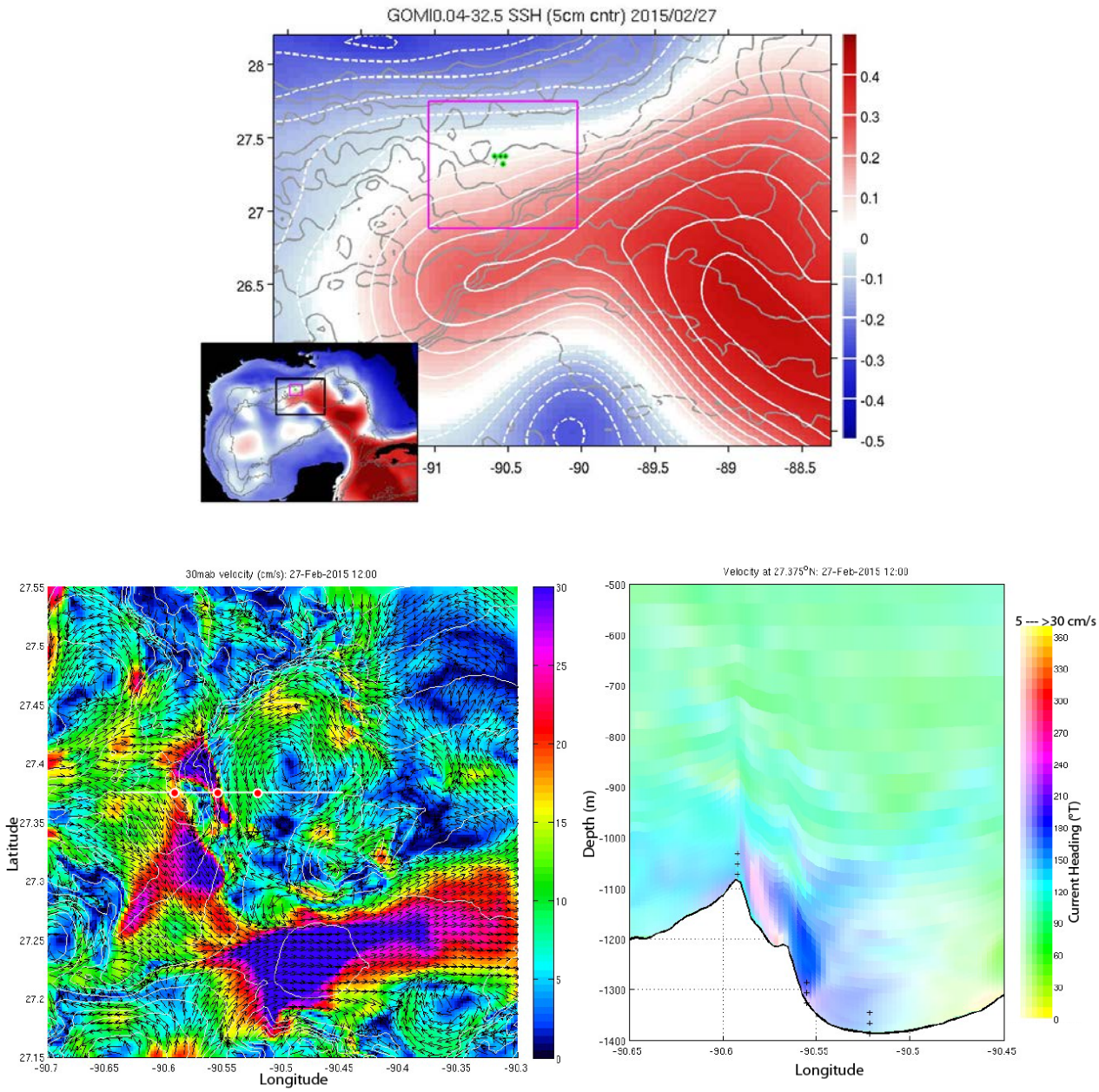

Figure 3.15 Top: Sea surface height from the HYCOM Nowcast/Forecast System on 27 February, 2015. The region in the large image is shown by the black rectangle in the small inset showing the entire Gulf region. Bottom Left: 30mab velocity vectors and speed (cm/s, colors) from the NCOM simulation on 27 February, 2015. Bottom right: Horizontal velocity shown by colors for a section crossing through the mooring array (27.375°N, white line in bottom left panel). Hue indicates direction and the color intensity indicates speed, as shown on the color bar. Mooring locations are shown by the red dots on the bottom left panel, and black dotted lines extending from the bottom in the bottom right panel. The bottom two panels are animated in Animation 5.2.

During early December 2014, a small cyclonic eddy was situated within the study area near its northwestern periphery, thus the upper ocean current over the study was generally westward or southwestward (Figure 3.16). A period of nearly westward currents with strong near-inertial oscillations occurred at S1 in both the

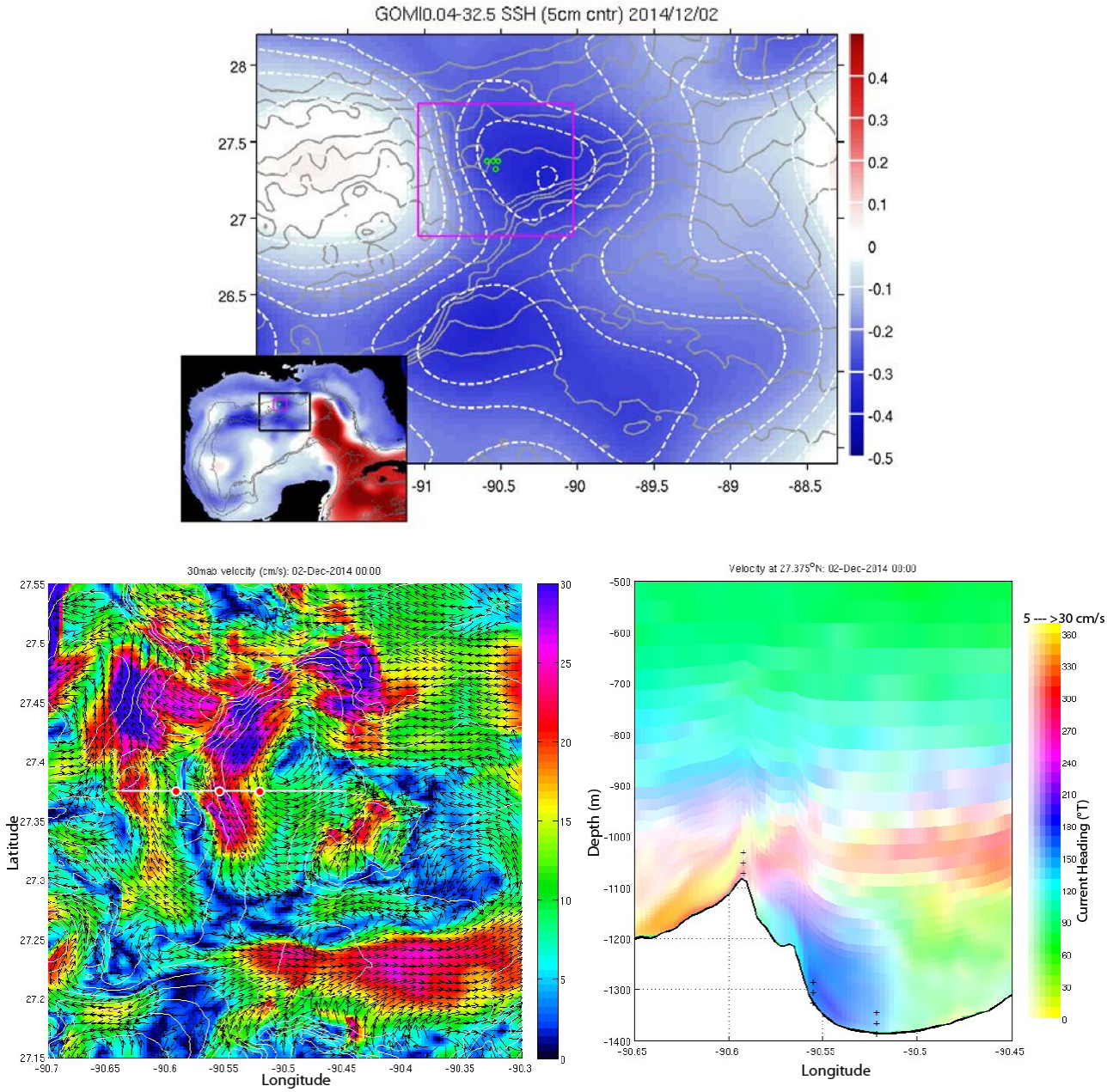

Figure 3.16 Top: Sea surface height from the HYCOM Nowcast/Forecast System on 2 December, 2014. The region in the large image is shown by the black rectangle in the small inset showing the entire Gulf region. Bottom Left: 30mab velocity vectors and speed (cm/s, colors) from the NCOM simulation on 2 December, 2014. Bottom right: Horizontal velocity shown by colors for a section crossing through the mooring array (27.375°N, white line in bottom left panel). Hue indicates direction and the color intensity indicates speed, as shown on the color bar. Mooring locations are shown by the red dots on the bottom left panel, and black dotted lines extending from the bottom in the bottom right panel. The bottom two panels are animated in Animation 5.3.

model and observations. S2 experienced several days of moderately strong southward currents, both observed and modeled. Inspection of maps and animations of near-bottom currents (Figure 3.16 and animations) shows this westward current impacting the eastern and northeastern rim of the basin containing

the mooring array, with pulses of energetic currents traversing the slope of the basin impacting the S2 location.

These events highlight the complexity of the near-bottom currents, their variability and short spatial scales within this region of high relief bathymetry. Though the mean flow is strongly topographically constrained and decoupled from the upper ocean flow, the intersection of the bathymetric features with the thermocline layer that mark the base of the upper ocean circulation features permits driving of energetic near-bottom currents at sub-thermocline depths by the overhead currents. Turbulent wakes spawn small-scale vortices and perturbations in the mean flow in the lee of the highest bathymetric features. These perturbations surprisingly seem to exert their influence several hundred meters downslope from their origins. Though cross-isobath propagation of energy is a characteristic of short topographic Rossby waves given certain wavelength and slope characteristics (Rhines, 1970), such cross-slope propagation of energy is somewhat surprising in this regime of strongly topographically constrained flows. This topic warrants further investigation.

3.6 Spatial Variability of Near-Bottom Currents

The bathymetric features in the region surrounding the study area generally extend from 1000m to 1500m depth, with relief of several hundred meters (Figure 2.5). The shallowest of the moorings is situated on a pinnacle with seafloor depth of 1072m, and the deepest lies in a basin at 1386m, representing well the depth variations of the region. The depth extent of the upper ocean circulation features varies, but generally extends down to the base of the main thermocline between 800 and 1200m. Analysis of full water column velocity time series in the Gulf of Mexico reveals an energy minimum at roughly 1000 - 1100m, with the circulation below this depth decoupled from the upper layer circulation. Thus, much of this region lies below the depth extent of the upper layer circulation, with some of the highest relief features being impacted by the base of this upper layer circulation. Examples of this were shown in the previous discussion of strong current events.

The mean current from the year-long simulation at 1050m, or just above most of the highest relief bathymetric features, shows a smoothly varying broad flow, generally west to east (Figure 3.17). The topographically constrained cyclonic circulation within the basin in the study region as inferred from the observations and seen in the model results extends upward to at least this depth. Following the seafloor at 30mab, the mean current exhibits much more spatial variability, with stronger currents generally along steeper topographic slopes and weaker currents within the small basins. A relative minimum in mean current speed can be seen very near the S1 mooring, and in a small region just to the east in both the 1050m and 30mab mean velocity maps. From these maps, it may be inferred that the pinnacle on which S1 was placed creates a “shadow” effect in its lee extending upward from the seafloor. The mean near-bottom current bifurcates at this pinnacle, and is asymmetrically enhanced to the north.

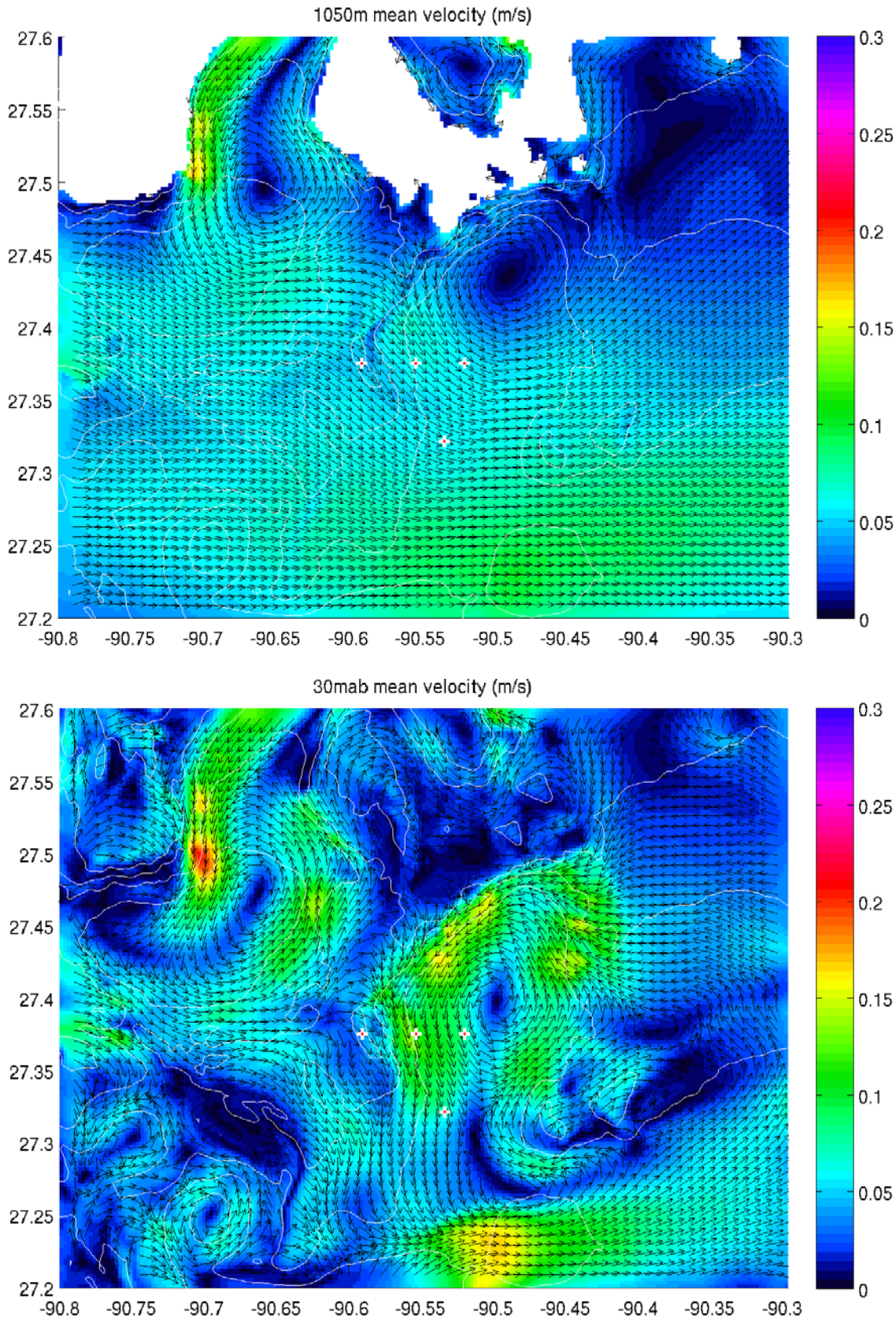

Figure 3.17 Mean velocity (speed in m/s indicated by colors) from the NCOM simulation at 1050m depth (top) and 30mab (bottom). The locations of the moorings are shown by the red dots.

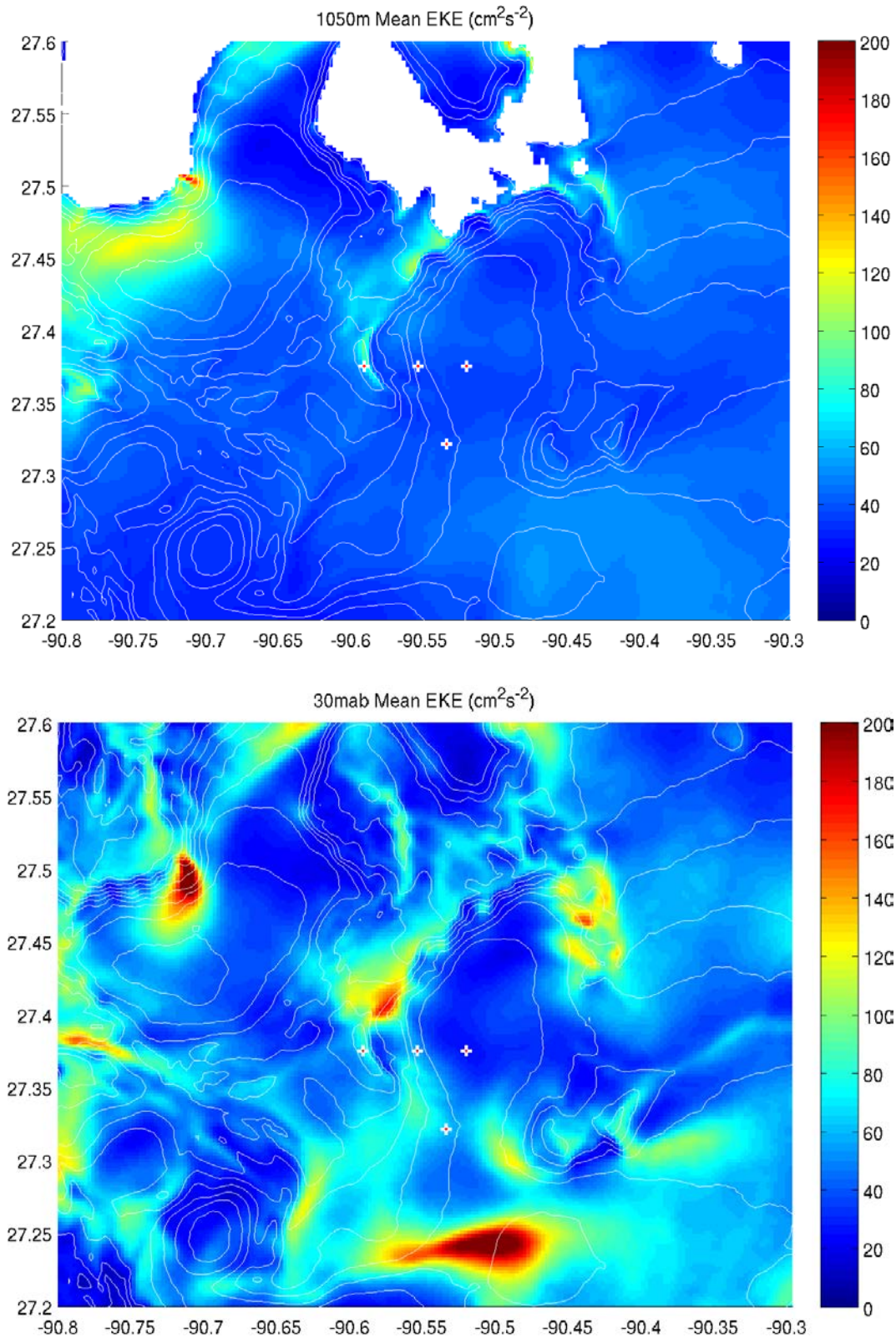

Figure 3.18 Mean eddy kinetic energy (cm2/s2) from the NCOM simulation at 1050m depth (left) and 30mab (right). EKE is computed here as the mean of the magnitude of the horizontal velocity anomalies from the mean over the entire simulation. The locations of the moorings are shown by the red dots.

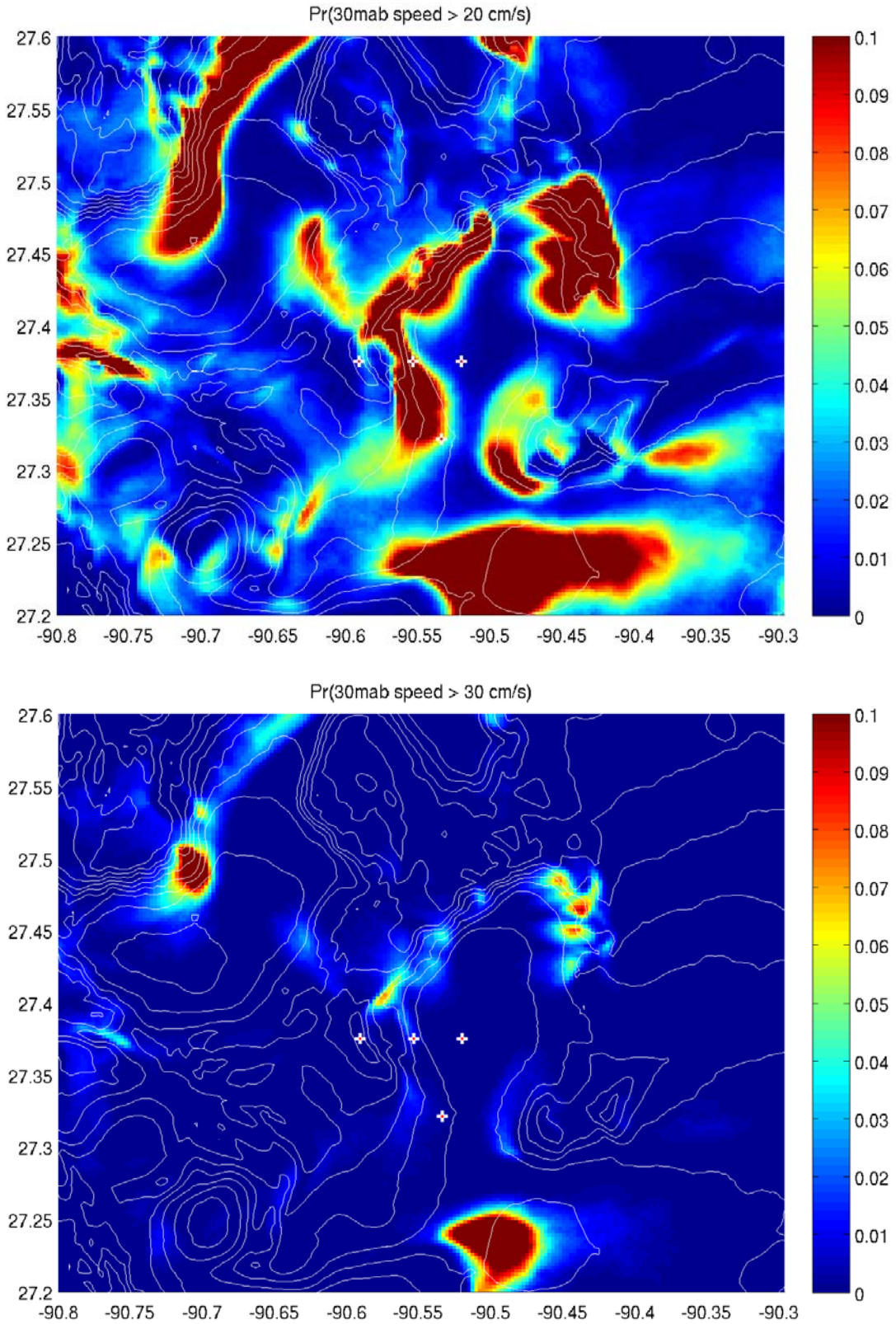

Figure 3.19 Probability of the instantaneous speed at 30mab exceeding 20 cm/s (left) and 30 cm/s (right) computed from the NCOM. The locations of the moorings are shown by the red dots**.**

The eddy kinetic energy (EKE), a measure of the variability of the current about its mean state, shows particularly strong current fluctuations along the slope of the basin immediately to the north of the mooring line (Figure 3.18). It is here that the vortices in the wake of the S1 pinnacle appear in animations to interact with the mean cyclonic flow around the basin, moving downslope and intermittently passing the S2 location giving rise to energetic current fluctuations there. A secondary "hot spot" for EKE in the 30mab currents appears to be the shallow northeastern rim of the basin, where strong currents were seen to have been spawned during the early December 2014 event under the generally westward upper ocean flow. The decay in EKE from the seafloor to just a few hundred meters above (1050m) is striking, suggesting the bottom intensified nature of the current variability.

Finally, a potentially useful product of this year-long high-resolution simulation is an estimate of the probability of high-speed currents at different locations around the region. The probability of currents exceeding 20 cm/s at any given time exceeds 10% over large areas of the model domain (Figure 3.19). In particular are the western and northeastern rims of the basin containing the mooring array, an especially steep region rising up to less than 1000m depth in the northwestern part of the model domain, and an area to the south, with interestingly low relief and greater depth. Along the mooring array, the region of high probability of 20 cm/s currents lies generally along the slope over the S2 mooring location, with S1 and S3 showing markedly smaller likelihood of strong currents. Raising the threshold to 30 cm/s, the spatial patterns of high probability of strong currents very much resembles the mean EKE map at 30mab (Figure 3.18). Analyses of this type could be considered when placing pipelines or other structures in the region.

4. IMPACT TO PRODUCERS

The results of Task 5 highlight the complexity of near-bottom currents and their variability within the outer continental shelf area of the northwestern Gulf of Mexico that is characterized by numerous bathymetric features such as salt domes, pinnacles, canyons and basins with length scales of roughly 10km. It is difficult to capture this variability over a region of even only a few kilometers in size with direct current observations. Thus, high-resolution numerical simulations should be considered, at least to complement moored observations, for projects in such regions. Additionally, for projects with large spatial footprints such as pipelines, it is especially important to consider the variability of characteristics of bottom currents throughout the region.

5. CONCLUSION

The overall goal of Task 5 was achieved in that it provided a one-year record of near-bottom currents recorded at three locations within a 10km region with complex bathymetry, and provided a one-year high-resolution model hindcast simulation of this region to complement analysis of the observational data. Observations of current profiles from within a few meters of the seabed to 100mab using a single ADCP proved technically challenging during this project. At these depths, the 200 kHz ADCP only had reliable data return out to about 30 meters from the instrument, likely due to lack of scattering particles in this relatively clean water. Through the use of three different mooring configurations, currents were recorded from approximately 70mab down to 10mab with a nearly complete time series at 38mab. Measuring a complete current profile with high vertical resolution would likely require multiple instruments on the same

mooring line. However, analysis of the model results suggest that missing measurements from the lower 10m of the water column would have likely recorded a frictional boundary layer.

The results of the Task 5 study highlight the complexity of the near-bottom currents and their variability in this region, the influence that high topographic relief extends over the region, and the interaction of upper ocean currents with the highest topographic features spawning energetic fluctuations in the near-bottom currents. To our knowledge, no such high-resolution (250m horizontal resolution and two – to –several meters vertical resolution) long simulation has been performed with such complex steep bathymetric features in deep waters. The results strikingly show the inadequacy of moored observations in capturing the complex dynamics and spatial variability in such a region. They also highlight dynamical processes, such as downslope energy propagation of turbulent vortices that can occur at these depths with potential impacts on structures located on the seabed. The utility of high-resolution numerical simulations should be considered for future projects in similar locations.

6. RECOMMENDATIONS

The work performed in Task 5 introduced a new paradigm for deep currents over complex bathymetry with energetic upper ocean circulation. Among the new ideas are: currents having very short length scales (less than 4km) and lack of coherence in variability over these short distances, influence of topographic relief on the variability (particularly at near-inertial frequencies) over a wider region, enhancement of inertial motions near the seabed over certain topographic features, and cross-slope energy propagation linked with turbulent vortices. Such high resolution numerical modeling over complex deepwater bathymetry is likely pushing the boundaries of the capabilities of numerical models with structured meshes. Further modeling to understand the dynamics of flow within this or a similar region would likely benefit from application of unstructured mesh models, like the Finite Volume Coastal Ocean Model (FVCOM), or the Semi-Implicit Eulerian-Lagrangian Finite Element (SELFE) model, which employs the VQS vertical grid system that shows much promise for these types of applications.

7. REFERENCES

Cooper, C.K. (2011), Bottom Current Extremes in the Deep Central Gulf, 2011 Offshore Technology Conference, Paper 21239-MS, Houston, TX.

Cummings, J.A., and O.M. Smedstad (2013). Variational data assimilation for the global ocean. Data Assimilation for Atmospheric, Oceanic and Hydrologic Applications, vol. II, Chapter 13, 303-343.

Dukhovskoy, D.S., S.L. Morey, J.J. O'Brien, P.J. Martin, and C. Cooper (2009). Application of a vanishing quasi-sigma vertical coordinate for simulation of high-speed deep currents over the Sigsbee Escarpment in the Gulf of Mexico, Ocean Modelling, doi:10.1016/j.ocemod.2009.02.009.

Dukhovskoy, D.S., R.R. Leben, E.P. Chassignet, C. Hall, S.L. Morey, and R. Nedbor-Gross (2015). Characterization of the uncertainty of Loop Current metrics using a multidecadal numerical simulation and altimeter observations, Deep Sea Res. Part 1, 100, 140-158.

Leben, R.R (2005). Altimeter-derived Loop Current metrics.In:Sturges,W., Lugo-Fernandez, A.(Eds.), Circulation in the Gulf of Mexico: Observations and Models. AGU, Washington, DC http://dx.doi.org/10.1029/161GM15.

Martin, P.J. (2000). A description of the Navy Coastal Ocean Model Version 1.0. NRL Report: NRL/FR/7322-009962, Naval Research Laboratory, Stennis Space Center, MS, 39 pp.

Morey, S.L., and D.S. Dukhovskoy (2013). A downscaling method for simulating deep current interactions with topography – Application to the Sigsbee Escarpment, Ocean Modelling, 69, 50-63, doi:10.1016/j.ocemod.2013.05.008.

Rhines, P.B. (1970). Edge-, bottom-, and Rossby waves in a rotating stratified fluid. Geophysical Fluid Dynamics 1, 273–302.

3. FINAL REPORT: CURRENTS DURING A JOINT TRS-LC OR LCE EVENT (TASK 6)

It is noted here that Task 6, "Currents During a Joint Tropical Revolving Storm-Loop Current or Loop Current Eddy Event", was not completed during the time period allotted for this subcontract as no candidate events presented during the three field seasons.

4. FINAL REPORT: REAL-TIME MEASUREMENT OF SURFACE CURRENTS (TASK 8)

Real-Time Measurement of Surface Currents– Final Report

RPSEA Document No. 11121.5801.01.Final3

Hi-Res Environmental Data for Enhanced UDW Operations Safety

RPSEA Project No. 11121-5801-01

September 30, 2016

Steven P. Anderson and Seth Zuckerman
Task 7-9 Principal Investigators
Areté Associates
1550 Crystal Drive, Suite 703
Arlington, VA 22202

LEGAL NOTICE

This report was prepared by *FUGRO GLOBAL ENVIRONMENTAL AND OCEAN SCIENCES, INC.* as an account of work sponsored by the Research Partnership to Secure Energy for America, RPSEA. Neither RPSEA, members of RPSEA, the National Energy Technology Laboratory, the U.S. Department of Energy, nor any person acting on behalf of any of the entities:

a. MAKES ANY WARRANTY OR REPRESENTATION, EXPRESS OR IMPLIED WITH RESPECT TO ACCURACY, COMPLETENESS, OR USEFULNESS OF THE INFORMATION CONTAINED IN THIS DOCUMENT, OR THAT THE USE OF ANY INFORMATION, APPARATUS, METHOD, OR PROCESS DISCLOSED IN THIS DOCUMENT MAY NOT INFRINGE PRIVATELY OWNED RIGHTS, OR

b. ASSUMES ANY LIABILITY WITH RESPECT TO THE USE OF, OR FOR ANY AND ALL DAMAGES RESULTING FROM THE USE OF, ANY INFORMATION, APPARATUS, METHOD, OR PROCESS DISCLOSED IN THIS DOCUMENT.

THIS IS AN INTERIM REPORT. THEREFORE, ANY DATA, CALCULATIONS, OR CONCLUSIONS REPORTED HEREIN SHOULD BE TREATED AS PRELIMINARY.

REFERENCE TO TRADE NAMES OR SPECIFIC COMMERCIAL PRODUCTS, COMMODITIES, OR SERVICES IN THIS REPORT DOES NOT REPRESENT OR CONSTIITUTE AND ENDORSEMENT, RECOMMENDATION, OR FAVORING BY RPSEA OR ITS CONTRACTORS OF THE SPECIFIC COMMERCIAL PRODUCT, COMMODITY, OR SERVICE.

ABSTRACT

This Final Report for Task 8 presents three conference papers that were prepared as technology transfer efforts during the execution of this portion of the defined effort. The objective of Task 8 was to develop, design, engineer, and test a technique to monitor surface current velocities in real-time over a range of at least 300 km per day, with a root mean square error for speed and direction not to exceed 10 percent or +/- 0.05 m/s over a horizontal bin of 1 km.

Existing research on ROCIS (Remote Ocean Current Imaging System), conducted by Areté and Fugro GEOS, was developed further during this program, moving ROCIS from a prototype system to a real-time service that was deployed commercially for 6 months in 2015. ROCIS is an airborne system that uses two high-resolution cameras (tied to an inertial navigation system (INS)) to derive surface current data (speed and direction vectors) along a flight path every 250m. In December 2014, Areté and Fugro flew a series of ROCIS capability demonstration flights over the Gulf of Mexico. From February to June 2015, the ROCIS prototype was deployed commercially in the Gulf of Mexico for a total of 137 flights, not only proving its capability, but also providing a unique and unprecedented view of the Loop Current and its evolution during this period.

The goal of this research was to produce an accurate real-time surface current measurement service. This goal was met and exceeded during this program. ROCIS is poised to support offshore oil and gas operations, assist with emergency oil spills, and support search and rescue in a way that is cost competitive with existing measurement technologies.

SIGNATURE AND DATE STAMP

FUGRO GLOBAL
ENVIRONMENTAL AND
OCEAN SCIENCES, INC.

By: _____
(Signature)

Name: **Grant A. Stuart**

Title: **Project Manager**

Date: 30 September 2016

THIS PAGE INTENTIONALLY LEFT BLANK

CONTENTS

1. EXECUTIVE SUMMARY

2. PAPER #1: REAL-TIME AIRBORNE OPTICAL REMOTE SENSING OF OCEAN CURRENTS

2.1 IEEE/OES 11th Current, Wave, & Turbulence Measurement Workshop, St. Petersburg, FL, March 2-6, 2015

3. PAPER #2: AIRBORNE OCEAN SURFACE CURRENT MEASUREMENT FOR OFFSHORE APPLICATIONS

3.1 Offshore Technology Conference, Houston, TX, May 4-7, 2015

4. PAPER #3: REAL-TIME OCEAN SURFACE CURRENT MEASUREMENTS IN THE GULF OF MEXICO

4.1 MTS/IEEE OCEANS ’15, Washington, DC, October 19-22, 2015

1	Final	Steven Anderson Task 7-9 PI – Areté Associates	Grant Stuart Systems Manager	Grant Stuart Systems Manager	30 September 2016
0	Draft version	Steven Anderson Task 7-9 PI – Areté Associates	Grant Stuart Systems Manager	Grant Stuart Systems Manager	30 August 2016
Rev	**Description**	**Prepared**	**Checked**	**Approved**	**Date**

1. EXECUTIVE SUMMARY

Strong surface currents affect a diverse set of marine activities in the Gulf of Mexico, including seismic surveys, exploration drilling, oil & gas development and production, search and rescue operations and oil spill mitigation. Synoptic, high resolution surface current measurements over a large area in ultra deep water are difficult and costly to achieve using present methods. Task 8 developed, designed, engineered, and tested a technique to monitor surface current velocities in real-time over a range of >300 km per day, with an RMS error for velocity <10% or +/-0.05 m/s over a horizontal bin of <1 km.

Existing research on ROCIS (Remote Ocean Current Imaging System), conducted by Areté and Fugro GEOS, was developed further during this program, moving ROCIS from a prototype system to a real-time service that was deployed commercially for 6 months in 2015. ROCIS is an airborne system that uses two high-resolution cameras (tied to an inertial navigation system (INS)) to derive surface current data (speed and direction vectors) along a flight path every 250m. ROCIS exploits space-time processing of ocean wave imagery to produce maps of surface currents in real-time. The currents measured by ROCIS have high spatial resolution over large areas and are collected in a matter of hours. Post-processing of the imagery data creates additional data sets with swaths of currents useful for investigating a variety of mesoscale features. The ROCIS system was made from commercial, off-the-shelf components and was designed to be quickly installed on any survey aircraft.

This Task 8 Final Report presents three conference papers that were prepared as technology transfer during the execution of this task. In December 2014, Areté and Fugro flew a series of ROCIS capability demonstration flights over the Gulf of Mexico. Paper 1 in this report was presented at the IEEE/OES 11th Current, Wave, & Turbulence Measurement Workshop in St. Petersburg, FL, March 2-6, 2015 and outlined details of the theory, design, and engineering of the real-time prototype and only preliminary results from the December 2014 capability demonstration. Paper 2 was presented at the Offshore Technology Conference in Houston, TX, May 4-7, 2015, and demonstrated the core technology and its ability to measure surface currents for offshore applications. From February to June 2015, the ROCIS prototype was deployed commercially in the Gulf of Mexico for a total of 137 flights, not only proving its capability, but also providing a unique and unprecedented view of the Loop Current and its evolution during that time period. The third paper included here was presented at the MTS/IEEE OCEANS ’15 Conference in Washington, DC, October 19-22, 2015 and focused on the commercial viability of the survey tool and 2015 commercial flights.

The goal of this research was to produce an accurate real-time surface current measurement service. This goal was met and exceeded during this program. Looking forward, ROCIS is well suited for operational missions to support offshore oil and gas operations, assist with emergency oil spills, and support search and rescue, where timely knowledge of surface currents is crucial.

As UAV technology improves, ROCIS technology will migrate to small fixed wing UAVs for cheaper and safer data collections. For now, ROCIS is currently and effective real-time system that is cost competitive with existing surface current measurement technologies.

2. PAPER #1: REAL-TIME AIRBORNE OPTICAL REMOTE SENSING OF OCEAN CURRENTS

2.1 IEEE/OES 11th Current, Wave, & Turbulence Measurement Workshop, St. Petersburg, FL, March 2-6, 2015

2.2

Real-Time Airborne Optical Remote Sensing of Ocean Currents

Steven P. Anderson
Seth Zuckerman
Environmental Intelligence Group
Areté Associates
1550 Crystal Dr., Suite 703
Arlington, VA 22202

Grant Stuart
Fugro GEOS
P O Box 740010
6100 Hillcroft (77081)
Houston, Texas 77274

***Abstract*— This paper reports on the implementation of real-time processing in the Remote Ocean Current Imaging System (ROCIS). ROCIS exploits time-space processing of airborne ocean wave imagery to produce maps of surface currents. ROCIS may enable new understanding of ocean processes and be employed to provide improved regional ocean forecasts.**

1. INTRODUCTION

The Remote Ocean Current Imaging System (ROCIS) exploits time-space processing of airborne ocean wave imagery to produce maps of surface currents (Figure 1). The system provides synoptic measurements of ocean surface currents over a broad area with a level of detail that allows small-scale circulation features to be identified.

ROCIS was first flown in October 2012 over the Gulf of Mexico [1,2] and demonstrated that the optical imaging technique has the potential to provide accurate (5 cm s^{-1}) surface current data over large areas both rapidly and cost effectively and complements traditional ocean survey approaches. This unique capability provides maps of current vectors on 250m x 250m (or finer) grids along the flight path. One limit of the original system was that current retrievals were calculated in post processing.

Real-time processing will provide the system operator with both visualization and recording of the ocean currents during the flight.

Real-time processing has several benefits:

- Data assurance is enhanced because of the real-time system performance feedback to the operator
- The operator can now redirect the aircraft in stride to focus on ocean features of interest
- Timely data distribution to end-users since post-processing is no longer required

Here we report on the next step in the system development: the implementation of real-time processing. The primary design specification was to have one current vector every 1 km along the flight track while maintaining an accuracy of 5 cm s^{-1} demonstrated in post processing.

Figure 1. ROCIS Imaging Payload. An aircraft is equipped with a pair of 8 megapixel panchromatic cameras to image the waves on the water surface and measure surface currents. Cameras are aimed fore and aft to assure at least one camera is clear of sun glint. The top picture shows the aft camera extending just below the fuselage of the King Air. The focal lengths and grazing angles are configured to support flight altitudes from 3,000 to 10,000 feet. The bottom picture is taken directly below the payload and shows both cameras, a launch tube for expendable buoys and a VHF receive antennae for receiving AXCP signals.

The Research Partnership to Secure Energy for America sponsored the ROCIS real-time development and demonstrations.

Section II reviews the passive remote sensing and original processing system. Section III describes the new real-time software and hardware configuration. Section IV shows the results of the field demonstration and conclusions are presented in Section V.

2. CURRENT RETRIEVAL PROCESSING

ROCIS builds on prior work that used airborne time-series imaging systems to remotely sense near-shore ocean currents [3, 4]. Passive optics view the ocean waves and currents are derived from detecting the Doppler shift of those waves. Adequate dwell (observation interval) to resolve the wave motion and the removal of aircraft motion are fundamental to accurate surface current retrievals.

The first step in the current retrieval process is mapping the images to the water surface in a geographic reference frame. This requires an Inertial Navigation System (INS) to determine absolute camera location and orientation and knowledge of the absolute water elevation.

Next, an image stack is created by extracting sub-images or "patches" (typically 250m x 250m) around a fixed geographic location on the water surface. This creates the space/time information of the surface waves for that location. A three dimensional Fourier transform of the image stack is performed and the power spectral density (3D-PSD) is calculated.

The wave dispersion equation is then fit to the observed 3D-PSD using least-squares fitting to derive both components of the current for that patch of water. In addition, the goodness-of-fit and signal-to-noise estimates are used to provide an error-metric, a quantitative estimate of uncertainty for the retrieval for the patch. Note the cameras image a broad band of ocean waves ((λ = 4m to 100m) which allows for quite precise current estimation under a large range of wind speeds and sea-states.

The post processing software combines the raw image files and navigation data (Figure 2). The current retrieval processing is conducted after the flight on a ground station computer (an Alienware gaming laptop). The disk drives and INS data are removed from the aircraft and connected to the ground station computer. The software is written in MATLAB and has been optimized for speed. *3.1*

These are the main processing steps:

- Read the navigation data and calculate center locations for each "patch"
- Read and apply camera calibration to each image sequentially
- Locate, extract and map the data to each patch in the field of view and append that to the stack for each patch.
- When a patch is no longer in the field of view or the required dwell is achieved for the stack; extract currents from each patch using the 3-D FFT processing
- Save currents and error metrics for each patch

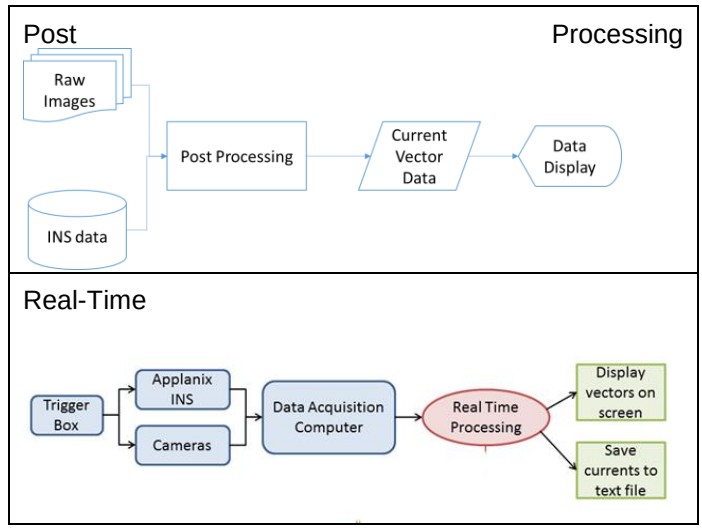

Figure 2. **Data Flow Diagram.** Data flow diagram from the original post processing and the new real-time processing.

We found that the time to run the post processing for a single row of current vectors was approximately equal to the time it took to collect the images. Specifically, extracting a current vector every 250m meters along the flight path for a four hour flight took approximately four hours of computational time. This gave us confidence that real-time processing was well within reach, however there were some challenges.

3. REAL-TIME PROCESSING

The original data acquisition computer cannot handle the data processing throughput required to produce real-time current measurements. In addition, the INS and image data had been collected separately (although synchronized by a trigger box). Thus, it was necessary to feed the INS data into the image acquisition system in real-time. Lastly, the patch location selection algorithm needed updating to anticipate the flight path. Updates to both the software and hardware were required for the acquisition system.

Real-time system hardware

Low equipment and operational costs were a system design goal. ROCIS is comprised of COTS cameras and image hardware components. ROCIS can be quickly installed into any survey aircraft with a photogrammetric hole so a dedicated aircraft is not required. Table 1 contains a list of the imaging hardware components for the real-time system. Figure 3 shows the hardware configuration diagram.

The cameras and computers draw a total of about 85W when it is collecting images and processing current retrievals. A separate laptop computer is used to control the acquisition system and to visualize the current retrievals. The computer, INS, trigger box and power supplies are packaged into a single 8U enclosure that is 18 inches high (Figure 4). The trigger box sends a pulse at 2 Hz to both cameras and the INS to synchronize image collection.

Table 1. ROCIS Real-Time DAQ Components	
Cameras	**Prosilica GX3300** 8 Megapixel CCD; 3296 x 2472 resolution 5.5 μm pitch *Kodak KAI-08050 sensor with 14 bit A/D*
Lens	**Zeiss Distagon T* 18mm f/3.5** 54° x 40° FOV
Trigger	**Areté custom built** 2 Hz trigger to sync camera and INS
Navigation System	**Applanix POS-AV 410** Fugro StarFix Augmentation
Acquisition Computer	**Intel Core i7 at 3.6 GHz** 8 Gbytes RAM and 4 Solid State Drives Windows 7
Control Computer	**Generic Laptop** Windows 7

3.2 Real-time system software

The new real-time software relies on the same code base for current estimates as used in the post processing software. This code has been well vetted and reusing the code assured similar performance and saved time by not having to refactor this part of the software. However, we needed to rewrite the image acquisition section of the software. The processing flow for the real-time implementation is shown in Figure 2.

The real-time image collection was implemented using MATLAB's Image Acquisition Toolbox and GigE Vision protocol. We developed image acquisition code to record the images from both cameras and configured the cameras for internal auto-exposure. In the process, we discovered that the MATLAB implementation of GigE failed to collect the changing exposure information from the cameras. MATLAB was very quick to respond to our inquiries and provided us with a patch to enable that functionality.

After the raw imagery and position information are written to disk, they are passed along to the current retrieval routines. The same processing steps described in the post processing are applied to each image in sequence, in real-time. The image acquisition, disk writing, and image processing takes less than 0.2 seconds so there is remaining computational overhead for the current retrieval calculation

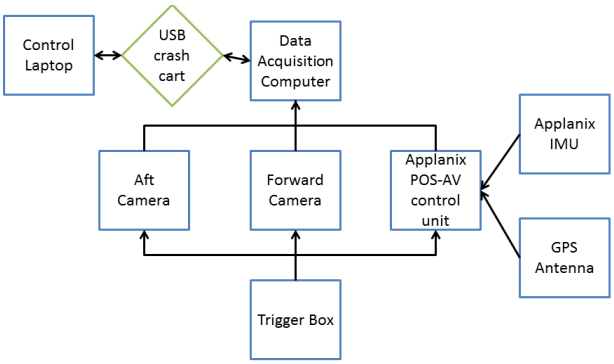

Figure 3. **ROCIS real-time hardware components**.

The 3-D PSD, dispersion calculation, and current extraction occur only when a "patch" has enough dwell (which is set to between 60 and 120 seconds). This processing takes longer than 0.5 second, so we use an image buffer to hold the images that accumulate while the current extraction is processing. Thus, the spacing of current vectors is limited by the processing bandwidth. In practice, we found that estimating currents every 9 seconds or longer was sustainable and stable. At typical flight speeds of 75 m s^{-1}, a patch processed every 9 seconds yields a current vector every 675 m.

The real-time display on the acquisition computer consists of diagnostics and a table of the current retrievals including time and location of each. There is not an interactive display on this computer because we found the unpredictability of the processing needed to respond to user interaction interfered with calculating current vectors. To maintain a stable acquisition system and optimal current spacing we decided to offload the display portion of the software to the control laptop.

A separate software code to visualize the current vector fields and diagnostic information runs on the control laptop (Figure 5). The DAQ serves up a copy of each current vector as it retrieved. Then the software on the laptop receives that data and updates the visual charts and graphs. The system operator can monitor and interact with the data from the laptop without impacting the DAQ performance.

4. RESULTS

4.1 Field Demonstration

In December 2014, Areté and Fugro flew a series of ROCIS capability demonstration flights over the Gulf of Mexico. The ROCIS imaging system was installed on a King Air at the Hagerstown, PA airport. A total of 12 ground targets (fiducials)

Figure 4. **ROCAS DAQ.** ROCIS real-time computer, INS, trigger box and INS mounted in the King Air.

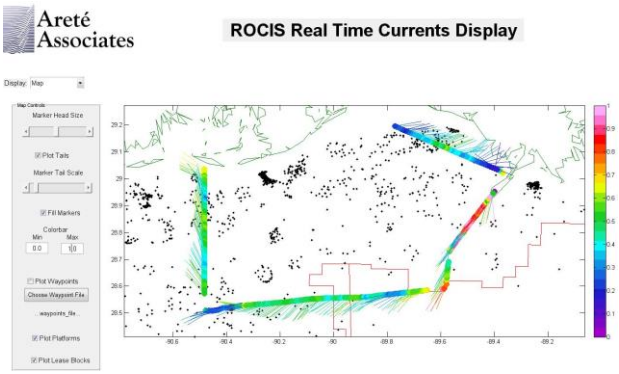

Figure 5. Real-Time Data Display. This is a screen capture of one of the data visualization windows showing the measured ocean currents. The chart shows a colored dot at each patch location indicating the current speed and the tail indicates the current direction. The user can pan and zoom the chart and it is automatically updated as additional data is collected.

were laid and surveyed next to the runway. We flew ROCIS over the targets and used them to boresight the cameras to the INS to assure optical alignment.

The flight operations were based at Houma–Terrebonne Airport during the week of December 1-7. Skies were foggy at the airport most the week. We encountered both scattered low clouds (~3000ft) on an inversion layer and high (>15,000 ft) clouds offshore. These clouds were visible in the NOAA Satellite imagery.

Only two people, a pilot and system operator, are required for the flight operations. They are provided with survey way points but also armed with knowledge of where the strongest current might be located. The flight crew did make some way point adjustments during the flight to avoid some cloudy areas.

4.2 Reciprocal lines and system performance

Accurate alignment of the camera to the navigation system ("boresight") is critical for measuring ocean currents since the aircraft is flying faster than 70 m/s and the ocean is moving so slowly. As is often done with boat mounted current meters, we conducted reciprocal survey lines to check system calibrations. It is assumed that the ocean currents change slowly in time so that any difference in observed current vectors is indicative of alignment errors.

On December 5, 2014, we flew a set of reciprocal flight lines at 7000 ft over Vermillion Bay. The total collection time between the lines was less than 30 minutes. Figure 6 shows the current vector data from the ROCIS Real Time system for the reciprocal lines. The standard deviation between lines was 5.8, 1.7 and 4.5 cm s^{-1} for along-track, across-track and current magnitude, respectively.

The largest differences are found in the along-track current component which is typical of previous results. This component is most sensitive to errors in mapping height and pitch. The errors in total current magnitude are approximately 5 cm/s. This is similar to previous results and thus we conclude the system is performing as expected.

True ground truth validation will require a dedicated boat on the water with coordinated simultaneous collections in a variety of environmental conditions. We have conducted such validations for airborne current retrievals in rivers in a separate program [5]. In that effort, we found airborne current errors below 10 cm/s when compared to ADCP observations. Similar validation of ROCIS is desirable but not within the scope of the program at this time.

4.3 Offshore Collections

The offshore collections were designed to sample regions that are operationally relevant to the deepwater operations in the Gulf of Mexico. Offshore flights were flown at an elevation of 7000 ft and typical speed of 72 m s^{-1}. These flights were each around 4.5 hours in duration and covered approximately 1000 km over the ocean.

The December 3 and 4 flights went out to the Loop Current which was located southeast of the Mississippi Delta. The December 6 flight was over a smaller area located near the Mississippi Canyon area. The currents measured during the December 3 flight are shown in Figure 7.

5. CONCLUSIONS

ROCIS exploits time-space processing of ocean wave imagery to produce maps of surface currents. These results demonstrate that the optical imaging technique has the potential to provide accurate surface current data over large areas both rapidly and cost effectively and complements traditional ocean survey approaches.

The real-time processing provides the system operator a visual display of ocean currents. This provides a situational awareness that was not available before. Route planning was conducted preflight to establish a flight pattern and waypoints over the region. The system operator had the ability and, in fact, did alter the route while underway based on observed currents and cloud conditions.

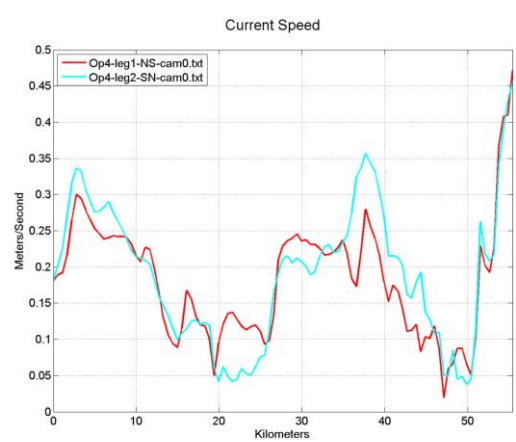

Figure 6. Real-Time Current Speeds from Reciprocal Flight Lines. Accurate alignment of the camera to the navigation system ("boresight") is critical for measuring ocean currents since the aircraft is flying faster than 70 m/s and the ocean is moving slowly. One way to assess this accuracy is to fly reciprocal lines, which can reveal alignment errors.

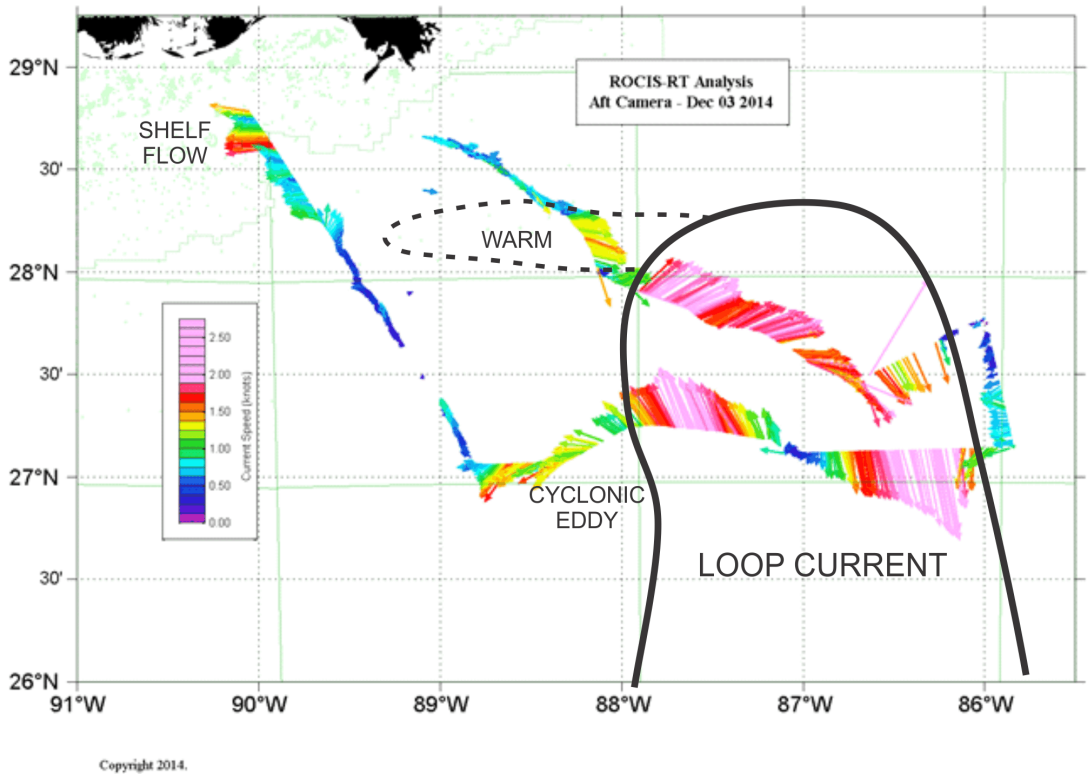

Figure 7. ROCIS Current Measurement from December 3, 2014. Currents were calculated on 250m x 250m patches along the flight path and then down averaged to every 1 km for plotting. The arrows indicate the flow direction and the color and length of the arrows indicate speed. A frontal analysis of mesoscale features identified in NOAA AVHRR SST images is overlaid on top of the current vectors.

Post processing will allow more densely spaced current vectors than the real-time data. ROCIS can provide vectors over a swath of up to 3 km across the flight track with spatial resolution less than 250m. Thus, post processing is still valuable for analysis of coherent features, statistical and Fourier analysis, estimation of convergence and vorticity, and assimilation into numerical models.

However, the real-time current vectors are as accurate as the post processed vectors. The timeliness of the real-time data will be particularly useful in operational situations. If additional reduction in latency is desired, it is straightforward to connect a satellite modem and telemeter the current vectors back to shore in real-time.

The compact size and low power of ROCIS makes it readily adaptable to different aircraft. It could also be integrated with multi-spectra and radar oil mapping systems on the same platform. The ability to mobilize the system promptly and concentrate data acquisition in specific areas would allow crucial surface current data to be acquired in support of search and rescue missions and oil spill response operations, leading to a significant improvement over current techniques, such as ocean drift prediction.

ACKNOWLEDGMENT

Mike Mastroianni, Tom Kraus, Matt Yi and Ken Vierra assisted with ROCIS system development and field operations. Derek Mintle expertly piloted the King Air. We especially thank John Dugan for his friendship and pioneering research on optical imaging of the marine environment.

6. REFERENCES

Anderson, S.P.; Zuckerman, S.; Shejun Fan; van Smirren, J., "Airborne optical remote sensing of ocean currents," Oceans - San Diego, 2013 , vol., no., pp.1,7, 23-27 Sept. 2013.

Zuckerman, S.; Anderson, S., "Advances in passive remote sensing of ocean currents and depths," Geoscience and Remote Sensing Symposium (IGARSS), 2014 IEEE International , vol., no., pp.3906,3909, 13-18 July 2014.

J.P. Dugan and C.C. Piotrowski, "Surface current measurements using airborne visible image time series," Rem. Sens. Environ., 84 (2): 309-319. 2003.

C.C. Piotrowski and J.P. Dugan, "Accuracy of bathymetry and current retrievals from airborne optical time series imaging of shoaling waves," IEEE Trans. Geoscience and Remote Sensing, vol. 40, pp. 2606-2618, 2002.

Dugan, J.P.; Anderson, S.P.; Piotrowski, C.C.; Zuckerman, S.B., "Airborne Infrared Remote Sensing of Riverine Currents," Geoscience and Remote Sensing, IEEE Transactions on , vol.52, no.7, pp.3895,3907, July 2014.

7. PAPER #2: AIRBORNE OCEAN SURFACE CURRENT MEASUREMENT FOR OFFSHORE APPLICATIONS

7.1 Offshore Technology Conference, Houston, TX, May 4-7, 2015

OTC-OTC-25956-MS

Airborne Ocean Surface Current Measurements for Offshore Applications

Steven P. Anderson, Areté Associates
Seth Zuckerman, Areté Associates
Jan Van Smirren, Fugro Global Environmental and Ocean Sciences, Inc.
Rob Smith, Fugro Global Environmental and Ocean Sciences, Inc.

Copyright 2015, Offshore Technology Conference

This paper was prepared for presentation at the Offshore Technology Conference held in Houston, Texas, USA, 4–7 May 2015.

This paper was selected for presentation by an OTC program committee following review of information contained in an abstract submitted by the author(s). Contents of the paper have not been reviewed by the Offshore Technology Conference and are subject to correction by the author(s). The material does not necessarily reflect any position of the Offshore Technology Conference, its officers, or members. Electronic reproduction, distribution, or storage of any part of this paper without the written consent of the Offshore Technology Conference is prohibited. Permission to reproduce in print is restricted to an abstract of not more than 300 words; illustrations may not be copied. The abstract must contain conspicuous acknowledgment of OTC copyright.

Abstract

Previous research programs have developed and demonstrated the capability to extract near-shore surface currents from airborne sequences of visual images of surface waves. This same technique can be used for remote sensing of the open ocean to retrieve surface currents over extensive areas in a relatively short period of time. Here, we demonstrate airborne current measurements over deepwater areas of the Gulf of Mexico. The system comprises a pair of digital cameras to image the surface waves, and inertial navigation system and software processing to retrieve the Doppler shift due to the ocean currents. The system measures currents in real-time along the flight path with an accuracy of 5 cm/s on 250 m x 250 m scales. A typical flight can cover 1000 km of linear flight lines in a 4 hour period. The survey data provide a synoptic scale view of Loop Current eddies and detailed measurements along oceanic fronts. This new technology can fulfill a need for rapidly acquiring real-time measurements of currents over a broad region in support of oil spill response; offshore surface current monitoring; and search and rescue operations.

Introduction

Ocean surface currents have a wide-ranging effect on various offshore applications and activities. Surface currents often change quickly in time and vary greatly over space due to shifting ocean patterns. Currents play a primary role in determining the movement and dispersion of oil during a spill. If unknown during spill response, surface currents can negatively impact planning, containment, monitoring, and recovery operations. Surface current monitoring is also a necessity in support of exploration and production activities, search and rescue operations, and seismic surveys.

Thus, there is a strong need to obtain accurate, detailed, and timely knowledge of ocean surface currents over large areas in a relatively short period of time. This paper reports on a new airborne technology capable of producing real-time surface current measurements over 1000km linear flight lines in 4 hours, with accuracies of 5 cm/s on 250 m scales. The Remote Ocean Current Imaging System (ROCIS) exploits space-time processing of airborne ocean wave imagery to produce maps of surface currents. ROCIS complements other ocean measurement systems that are currently in use such as satellites [1,2,3], drifting buoys [4], Acoustic Doppler Current Profilers (ADCP) [5] and HF radars [6]. While satellite and HF radar techniques provide large coverage areas, they are limited by resolution and, in the case of satellites, cloud cover. In situ measurement techniques typically cover limited areas. Drifting buoys are limited by Lagrangian current patterns and often drift out of the region of interest. Moored

ADCPs provide real-time current information but are limited to the location of observation. Similarly, shipboard ADCPs provide high spatial resolution but are limited to the speed of the vessel being used and cannot rapidly cover large areas of ocean.

ROCIS provides a cost effective rapid response solution for the provision of surface current surveys over large offshore regions. ROCIS produces currents in real-time by calculating one current vector along the flight path every kilometer. Higher spatial resolution is obtained by post-processing the image data after landing, yielding independent surface current estimates spaced 125 m apart.

This paper is divided into the following sections: the methodology used for measuring currents; an overview of the technology that comprises the acquisition system; presentation of results from a recent field demonstration in December 2014; and conclusions.

Methodology

ROCIS builds on prior work that used airborne time-series imaging systems to remotely sense near-shore ocean currents [7.8]. The fundamental approach employs passive optics to image the surface waves and retrieve the currents from the observed Doppler shift. Adequate dwell (observation interval) to resolve the wave motion and removal of aircraft motion are fundamental for accurate surface current retrievals.

The motion of deepwater surface waves is described by the linear dispersion relationship: $\omega = \sqrt{gk} + \vec{k} \cdot \vec{U}$, where ω is the angular frequency, k is the wavenumber and $\vec{U}$ is the mean surface current vector. Longer waves move faster than shorter waves and all the waves will feel a Doppler shift from the mean surface current. Note, the only free parameter in this formulation is the current vector $\vec{U}$ and it is this dispersion relationship that is exploited to retrieve the surface currents.

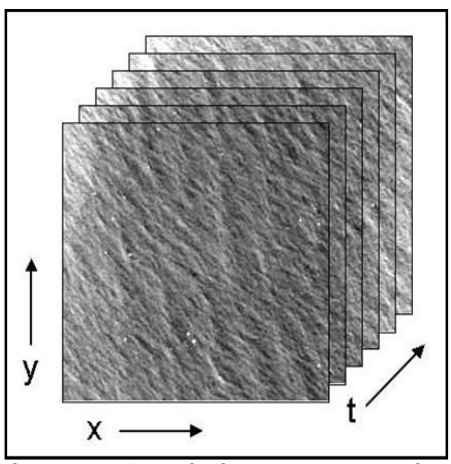

Figure 1. ROCIS collects time-series imagery at 2Hz. The images are mapped to geographic coordinates on the water surface using the INS information. The result is an image stack of the surface waves.

The first step in the current retrieval process is mapping the images to the water surface in a geographic reference frame. This requires an Inertial Navigation System (INS) to determine absolute camera location and orientation and knowledge of the absolute water elevation. Next, an image stack is created by extracting sub-images or "patches" (typically 250m x 250m) around a fixed geographic location on the water surface. This creates the space/time information of the surface waves for that location (Figure 1). A three dimensional Fourier transform of the image stack is performed and the power spectral density (3D-PSD) is calculated (Figure 2).

The wave dispersion equation is then fit to the observed 3D-PSD using least-squares fitting to derive both components of the current vector for that patch of water. In addition, the goodness-of-fit and the signal-to-noise estimates are used to provide an error-metric: a quantitative estimate of uncertainty for the retrieval for the patch. Note the cameras image a broad band of ocean waves (4m to 100m) which allows for quite precise current estimation under a large range of wind speeds and sea-states.

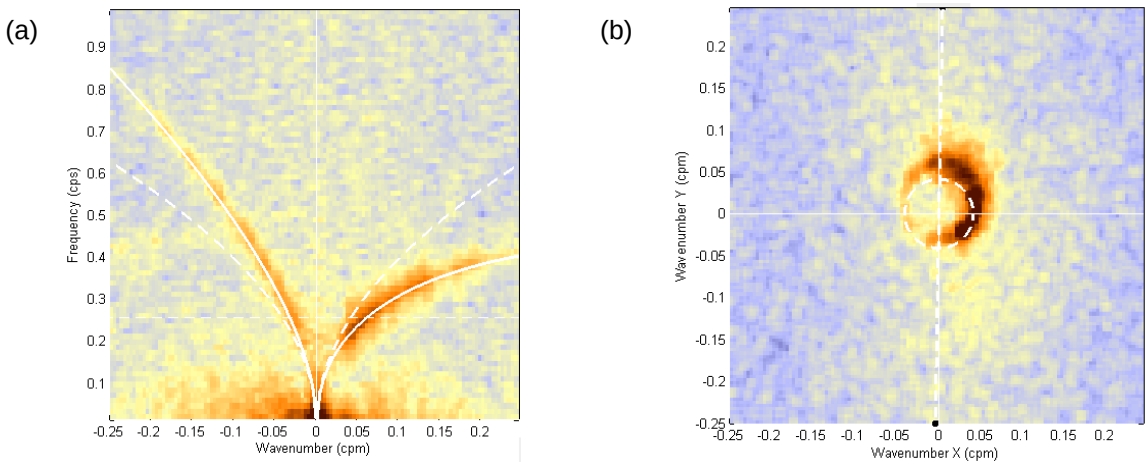

Figure 2. Power Spectral Density field from an image stack. This figure shows (a) a wavenumber slice in the direction of the current vector and (b) a frequency slice at 0.25Hz. Color shading indicates the energy level. The dashed line indicates the wave dispersion relation in the absence of currents. The dispersion surface is least-squares fit (solid line) to the observed PSD resulting in a current extraction (0.90 m s^{-1}.)

Technology

Low equipment and operational costs were a system design goal. ROCIS is comprised of COTS cameras and image hardware components. The system can be quickly installed into any survey aircraft with a photogrammetric hole, so a dedicated aircraft is not required. Figure 3 shows ROCIS installed on a Piper Navajo during our 2012 field demonstration.

ROCIS is made up of a pair of rigid-mounted cameras and an Applanix Inertial Navigation System (INS). Two 8-megapixel, panchromatic cameras are aimed down at an angle of 38° from the horizon. They look in opposite directions (one aft, one forward), image at 2 Hz, and are fitted with 18 mm lenses with red filters providing a large 54° x 40° field of view. The dual orientation ensures at least one camera will be free of sun glint regardless of sun orientation and aircraft heading. Nominal survey speeds of 75 m/s and flight altitudes of around 2,100 meters provide ~90 s of dwell over a swath of ~3000 m in the flight direction.

The Data Acquisition (DAQ) computer is an Intel Core i7 with 8 Gigabytes of RAM and four solid state data drives. The onboard software controls the cameras and collects the images and navigation data. After the raw imagery and position information are written to disk, they are passed along to the current retrieval routines. The 3-D PSD, dispersion calculation, and current extraction occur only when a "patch" has enough dwell (which is set to between 60 and 120 seconds). The spacing of current vectors is limited by the processing bandwidth. In practice, we found that estimating currents every 9 seconds is sustainable and stable. So as a result, real-time currents are extracted along the flight path only (not in swath.) At typical flight speeds of 75 m s^{-1}, a patch processed every 9 seconds yields a current vector every 675 meters along the flight path.

The real-time display on the acquisition computer consists of diagnostics and a table of the current retrievals including time and location of each. A separate software code to visualize the current vector fields and diagnostic information runs on the control laptop. The software on the laptop receives that data and updates the visual charts and graphs. The system operator can monitor and interact with the data from the laptop during data collection.

Accurate alignment of the camera to the navigation system ("boresight") is critical for measuring ocean currents since the aircraft is flying faster than 70 m/s and the ocean is moving so slowly. ROCIS uses an Applanix POS-AV 410 INS and Fugro Seastar to provide high accuracy real-time positioning. Boresighting of the INS to the individual cameras is accomplished by flying over and imaging fiducials (targets) with known locations, and determining offset angles through an iterative best fit process. This is sufficient to determine absolute current accuracy to better than 5 cm/s with the collection geometry.

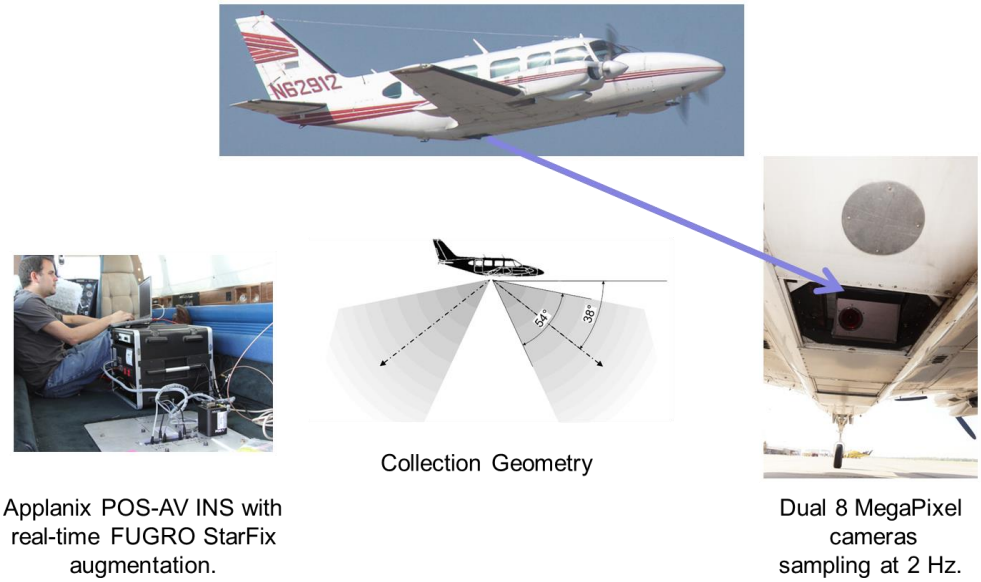

Figure 3. ROCIS imaging payload. An aircraft is equipped with a pair of 8 megapixel panchromatic cameras to image the waves on the water surface and measure surface currents. Cameras are aimed fore and aft to assure at least one camera is clear of sun glint. The focal lengths and grazing angles are configured to support flight altitudes from 3,000 to 10,000 feet.

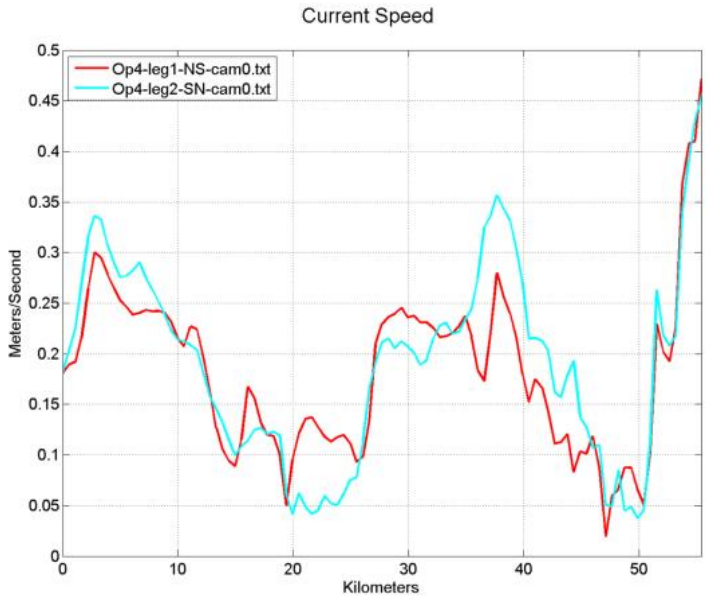

Figure 4. Real-Time Current Speeds from Reciprocal Flight Lines. Accurate alignment of the camera to the navigation system ("boresight") is critical for measuring ocean currents since the aircraft is flying faster than 70 m/s and the ocean is moving slowly. One way to assess this accuracy is to fly reciprocal lines, which can reveal alignment errors.

As is often done with boat mounted current meters, we conducted reciprocal survey lines to check system calibrations. It is assumed that the ocean currents change slowly in time so that any difference in observed current vectors is indicative of alignment errors. For example, on December 5, 2014, we flew a set of reciprocal flight lines at 7000 ft over Vermillion Bay. The total collection time between the lines was less than 30 minutes. Figure 4 shows the current speed data from the ROCIS Real Time system for the reciprocal lines. The standard deviation between lines was 5.8, 1.7 and 4.5 cm s^{-1} for along-track, across-track and current magnitude, respectively. The largest differences are found in the along-track current component which is typical of previous results [9]. This component is most sensitive to errors in mapping height and pitch. The errors in total current magnitude are approximately 5 cm/s.

There were few ground truth comparison opportunities offshore. In October 2012, we flew a series of three flights over the northern Gulf of Mexico. The flight path included flyovers of two Horizontal Acoustic Doppler Current Profiler installations: #42890 (Murphy Exploration & Production Co. drilling operations) and #42377 (Anadarko Petroleum Corporation), and one DCS Single Current Meter installed on the PAI (Petrobras America Inc) deepwater mooring. Measurement reporting depth for #42890, #42377 and PAI DCS are 15.2 m, 21.3 m and 1.5 m respectively. The ADCP and DCS data are 20 minute and 10 minute averages respectively which are compared to a ROCIS current from the nearest 250m x 250m patch.

Table 1. Measured currents comparison when ROCIS system passed the ADCPs and PAI DSC. Data collected in October 2012.

	Speed (m/s)	Direction (°T)
PAI DSC at 1.5m / ROCIS	0.48 / 0.47	156 / 170
ADCP #42890 at 15.2m / ROCIS	0.32 / 0.32	155 / 160
ADCP #42377 at 21.3m / ROCIS	0.30 / 0.41	143 / 103

True ground truth validation will require a dedicated boat on the water with coordinated simultaneous collections in a variety of environmental conditions. We have conducted such validations for airborne current retrievals in rivers in a separate program [10]. In that effort, we found airborne current errors below 10 cm/s when compared to ADCP observations. Similar validation of ROCIS is desirable but not within the scope of this program at this time.

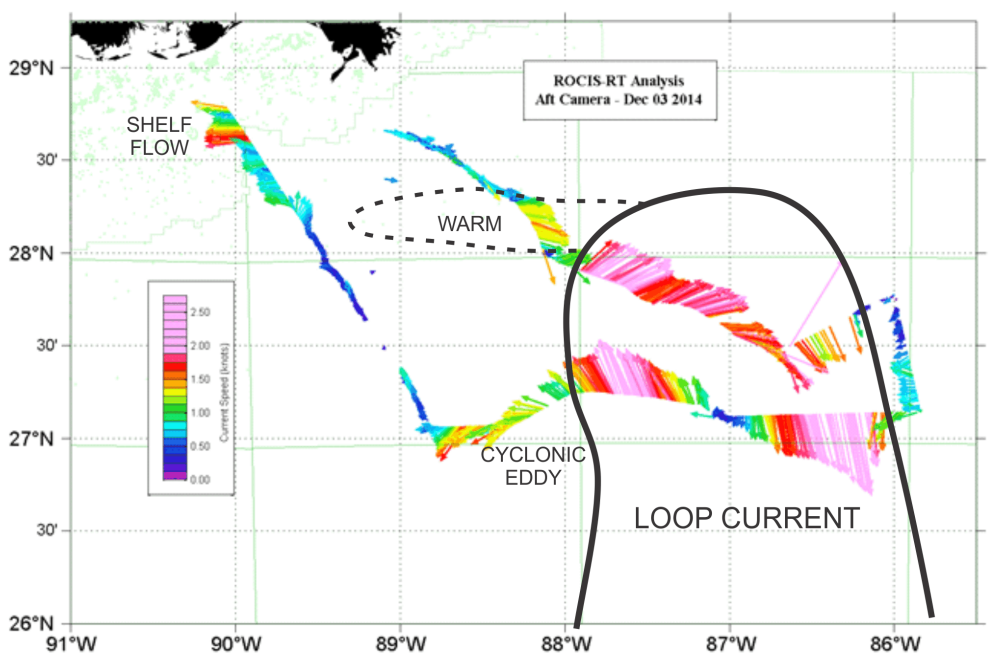

Figure 5. ROCIS Current Measurement from December 3, 2014. Currents were calculated on 250m x 250m patches along the flight path and then down averaged to every 1 km for plotting. The arrows indicate the flow direction and the color and length of the arrows indicate speed. A frontal analysis of mesoscale features identified in NOAA AVHRR SST images is overlaid on top of the current vectors.

Results

The first ROCIS capability demonstration was conducted in October 2012. This collection consisted of a series of three flights over a Loop Current Eddy in the northern Gulf of Mexico. Data processing for current retrievals happened after each flight on a ground station. This field collection demonstrated that during a single six-hour flight, a survey can cover 1,200 km over the region of interest, and yet still provide currents at high resolution and accuracy [9].

Here we report on the ROCIS real-time processing capability demonstration which occurred in December 2014. The offshore collections were designed to sample regions that are operationally relevant to the offshore operations in the Gulf of Mexico. The flights were flown at an elevation of 2100 meters and typical speed of 72 m s^{-1}. These flights were each around 4.5 hours in duration and covered approximately 1000 km over the ocean. The December 3 and 4 flights went out to the Loop Current (LC) which was located southeast of the Mississippi Delta. The December 5 flight was an engineering check out with reciprocal flight lines over Vermillion Bay. The December 6 flight was over the Mississippi Canyon area with a survey grid. The real-time currents measured during the December 3 flight are shown in Figure 5.

On December 3, 2014, the LC was located along eastern Gulf of Mexico and stretched north with the northern front located at to 28° 24' N in central Desoto Canyon based on National Oceanic and Atmospheric Administration (NOAA) Advanced Very High Resolution Radiometer (AVHRR) surface temperate satellite imagery. A cyclonic eddy is located along the western front centered near 27°N; 28°W. The survey cut directly across the cyclonic eddy and the northern lobe of the LC. The strongest currents observed reached 3.4 knots inside the eastern front of the LC and 2.5 knots inside the western front. The data show strong shelf flow to the west in Vermillion Bay with currents approaching 1.5 knots. There is also a region of eastward flow along southern Mississippi Canyon associated with a warm filament of water observed in the NOAA AVHRR imagery. Similar results were achieved on the December 4, 2014 flight.

Although ROCIS is optimized for robust current retrievals along the flight path, post-processing allows for extraction of a swath of current vectors along the flight track. We anticipate lower accuracy of current retrievals to either side of the flight line. This is due to the shorter dwell and image distortions encountered along the edges of the field of view. We have only just begun to explore the performance of off axis-current retrievals and do not have any quantitative assessment to provide at this time.

As an illustrative example of a swath of current retrievals, we post-processed imagery collected at the mouth of the Mississippi River near Southwest Pass (Figure 6). Current vectors were calculated at a resolution of 128m x 128m across a swath

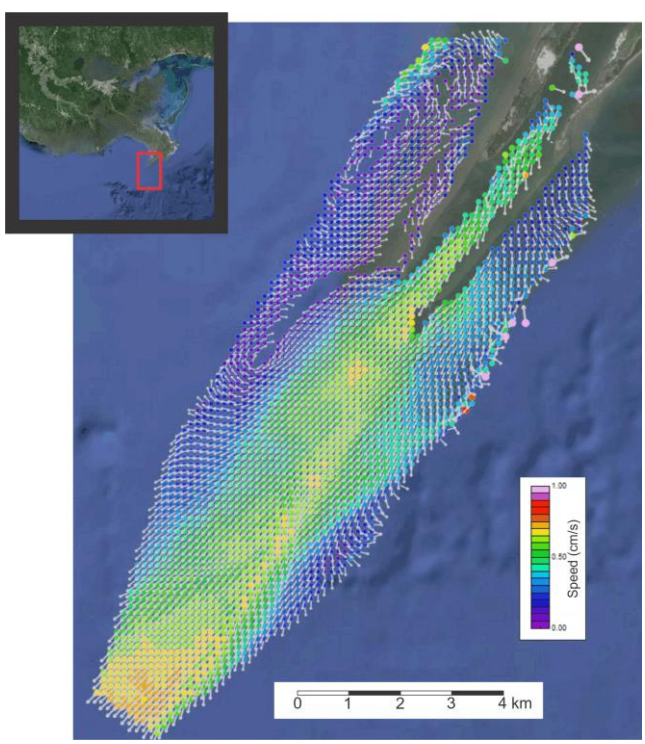

Figure 6. Swath of Current Vectors at Southwest Pass. Currents were calculated on 128m x 128m patches across a swath of 4 km and along the flight path. The arrows indicate the flow direction and the color and length of the arrows indicate speed.

of 4.0 km as the aircraft flew up the mouth of the river. The total collection time for the data shown in Figure 6 is about 5 minutes. The computational processing time for the current vectors in this figures was about 30 minutes. The data shows fine scale spatial structure in the jet of river water entering the Gulf of Mexico. Maximum current speeds reached 0.8 m s^{-1}. The jet spreads out and there is a recirculation seen on the northern side of the mouth.

Conclusion

ROCIS exploits time-space processing of ocean wave imagery to produce maps of surface currents. The results presented here demonstrate that the optical imaging technique has the potential to provide accurate surface current data over large areas both rapidly and cost effectively and complements traditional ocean survey approaches. The compact size and low power of ROCIS makes it readily adaptable to different aircraft. The large areal coverage is the clear advantage that ROCIS has over a ship-based current measurement system. However, ROCIS only provides a surface current, so it is not a complete solution to every application.

The real-time processing provides the system operator with a visual display of ocean currents. This provides a situational awareness that was not available before. ROCIS could also be integrated with multi-spectra and radar oil mapping systems on the same platform. The ability to mobilize the system promptly and concentrate data acquisition in specific areas would allow important surface current data to be acquired in support of search and rescue missions and oil spill response operations, potentially leading to a significant improvement over current techniques to predict ocean drift.

Acknowledgements

Mike Mastroianni, Tom Kraus, Matt Yi and Ken Vierra assisted with ROCIS system development and field operations. Derek Mintle expertly piloted the King Air. We especially thank Dr. John Dugan for his friendship and pioneering research on optical imaging of the marine environment. The Research Partnership to Secure Energy for America sponsored the ROCIS real-time demonstrations in 2014.

References

[1] Emery, W. J., A. C. Thomas, M. J. Collins, W. R. Crawford, and D. L. Mackas, “An objective method for computing advective surface velocities from sequential infrared satellite images,” J. Geophys. Res., vol. 91, no. C11, pp. 12 865–12 878, 198R.

[2] Walker, N., Leben, R., Anderson, S., Haag, A., & Pilley, C. (2009, October). High Frequency Satellite Surveillance of Gulf of Mexico Loop Current Frontal Eddy Cyclones. In OCEANS 2009, MTS/IEEE Biloxi-Marine Technology for Our Future: Global and Local Challenges (pp. 1-9). IEEE.

[3] Goldstein, R. M. and H. A. Zebker. "Interferometric Radar Measurement of Ocean Surface Currents." Nature, 328, 707-709., 1987.

[4] Anderson, S. P. and N. Sharma. "Satellite-Tracked Drifter Measurements of Inertial Currents in the Gulf of Mexico." Proceedings of the IEEE Ninth Working Conference on Current Measurement. March, 2008, Charleston, SC. IEEE #1-4244-1486-5/08.

[5] Anderson, S. P. and P. Matthews. "A Towed 75 kHz ADCP for Operational Deepwater Current Surveys." Proceedings of the IEEE Eighth Working Conference on Current Measurement. July, 2005, Southampton, UK. IEEE #07803-8989-1/05

[6] Barrick, D. , R. Long, C. Whelan, C. Cooper and J. Abadin. "Advance Warning of Loop Current from Single-Site SeaSonde on Genesis Oil Platform in the Gulf of Mexico." Proc. of the IEEE/OES Eighth Working Conference on Current Measurement Technology, Judith A. Rizoli, Ed., New York, 2005, IEEE.

[7] Dugan, J.P. and C.C. Piotrowski, “Surface current measurements using airborne visible image time series,” Rem. Sens. Environ., 84 (2): 309-319. 2003.

[8] Piotrowski, C.C. and J.P. Dugan, “Accuracy of bathymetry and current retrievals from airborne optical time series imaging of shoaling waves,” IEEE Trans. Geoscience and Remote Sensing, vol. 40, pp. 2606-2618, 2002.

[9] Anderson, S. P., Zuckerman, S.B., Fan, S., and J. van Smirren, Airborne optical remote sensing of ocean currents, Oceans 2013, (San Diego, CA), 1-7. 23-26 September, 2013.

[10] Dugan, J.P. and C.C. Piotrowski. "Estuarine Flows Measured from an Aircraft. IEEE 8th Current Measurements Technology Conference, Southampton, UK. 2005

8. PAPER #3: REAL-TIME OCEAN SURFACE CURRENT MEASUREMENTS IN THE GULF OF MEXICO

8.1 MTS/IEEE OCEANS ’15, Washington, DC, October 19-22, 2015

Real-time Ocean Surface Current Measurements in the Gulf of Mexico

Seth Zuckerman
Steven P. Anderson
Areté Associates
1550 Crystal Drive, Suite 703
Arlington, VA 22202
szuckerman@arete.com

Grant Stuart
Fugro GEOS
6100 Hillcroft
Houston, TX 77081

Cortis Cooper
Chevron
6001 Bollinger Canyon Road
San Ramon, CA 94583

***Abstract*—This paper reports on a series of airborne data collections we made in the Gulf of Mexico using the Remote Ocean Current Imaging System (ROCIS) to measure surface currents in real-time. ROCIS provides high spatial resolution over large areas of the ocean in a way not previously available with existing technologies. Such current measurements can be employed for improved regional ocean forecasting and a better understanding of mesoscale processes.**

I. INTRODUCTION

Accurate and timely knowledge of ocean surface currents is important for a variety of scientific and operational applications. Existing methodologies based on satellite feature tracking [1] and altimetry [2], high frequency (HF) radars [3], drifting buoys [4], and Acoustic Doppler Current Profilers [5]-[6] (ADCPs) are well established but not optimal for obtaining high spatial resolution measurements over broad areas. Satellite and HF radar techniques provide large coverage areas but have limited spatial resolution. In addition, satellite methods are limited by cloud cover and the performance of HF radars varies with environmental conditions. Drifting buoys only provide Lagrangian measurements and may drift out of the region of interest. Moored ADCPs only provide point measurements and shipboard ADCPs are limited by the speed of the vessel being used and have limited utility in high sea states.

The Remote Ocean Current Imaging System (ROCIS) was developed to provide high resolution maps of surface currents over large areas. ROCIS exploits space-time processing of airborne ocean wave imagery to produce maps of surface currents in real-time. Broad areas of the ocean can be covered during the duration of a single flight with measurements taken at a level of detail to allow small-scale circulation features to be identified.

ROCIS is an extension of previous airborne imaging systems developed to remotely sense near-shore ocean currents [7]-[8]. A previous version of the system was first flown in October 2012 over the Gulf of Mexico [9]-[10]. However, it was not real-time and required post-processing of image data to retrieve current measurements. This paper reports on our advances since then upgrading ROCIS to operate in real-time and on our multi-month deployment of the system to the Gulf of Mexico.

Section II provides an overview of the technology of the system. Section III reviews our field collections and results. Section IV discusses comparison of results to *in situ* data and the performance of ROCIS as a function of environmental parameters. Section V discusses sources of error, Section VI lessons learned, and Section VII provides a summary and conclusion.

II. TECHNOLOGY

A. Hardware

Low equipment and operational costs were a system design goal. ROCIS is made up of commercial-off-the-shelf (COTS) cameras and image hardware components. The system can quickly be installed into any survey aircraft with a photogrammetric hole. Fig. 1 shows the system installed on one of two King Air aircrafts used during our 2015 field collections.

ROCIS utilizes two cameras, one pointing forward and one backward, to mitigate the effect of sun glint contaminating the imagery from one direction. The cameras are 8-megapixel Prosilica panchromatic CCDs (3296 x 2472), with 18mm lenses and red filters. This yields a field of view of 54° by 40°, with the larger dimension oriented along the direction of flight to provide increased dwell.

The cameras image the water surface at 2 Hz, using a signal generated by a trigger box to synchronize both cameras with the inertial navigation system (INS). The INS is an Applanix POS-AV 410 with Fugro StarFix augmentation, which provides highly accurate real-time position and orientation information. Boresighting of the INS to the individual cameras is accomplished by flying over targets with known locations and determining offset angles through an iterative best fit process.

The data acquisition computer (DAQ) is an Intel core i7, 3.6 GHz, with 8 GB of RAM running Windows 7. Data are recorded onto 4 solid state drives (SSDs)—each camera is mirrored to its own pair of SSDs. This provides data redundancy and obviates the need to back up the data post-flight before further analysis can be started. The DAQ is controlled from a generic laptop via a remote desktop connection.

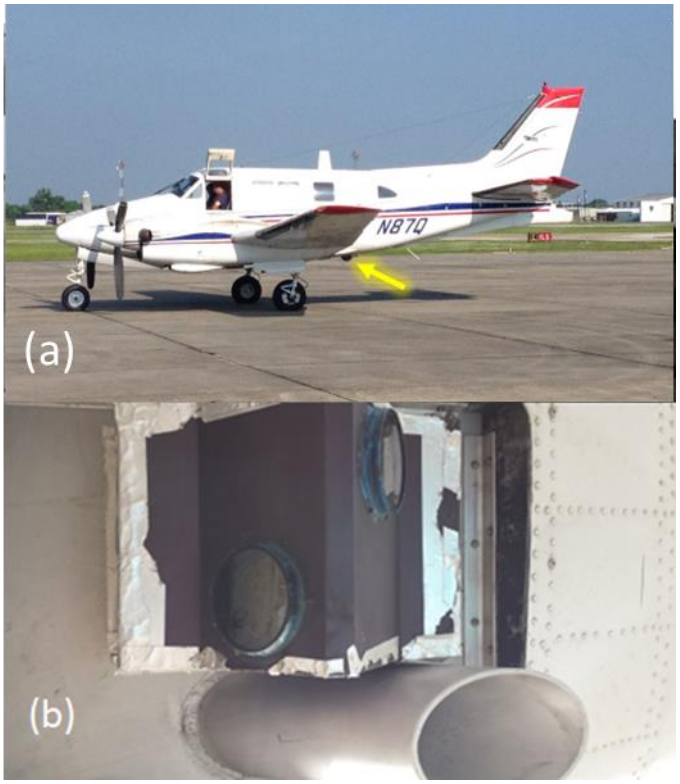

Fig. 1. (a) ROCIS installed on one of two King Air aircraft used during data collections. A yellow arrow points to the imaging payload located underneath the aircraft. (b) A view from under the aircraft showing the dual cameras pointing in opposite directions. Also visible is a tube for deploying airborne expendable bathythermographs (AXBTs) or airborne expendable current profilers (AXCPs).

B. Software

The real-time data acquisition and processing software is written in MATLAB using the Image Acquisition Toolbox and GigE vision protocol. Once initialized, very little operator interaction is necessary to collect images and calculate currents. The software controls the integration time for the cameras through separate auto-exposure loops. As images are received from the cameras, the software records them to the SSDs. Concurrently, synchronized position and attitude information is received from the INS over a serial port. The software then passes the images and metadata to the current retrieval algorithm (described below).

The system is configured to provide the maximum real-time spatial resolution possible while guaranteeing no lost image data. This interplay is dependent upon the underlying computer resources of the DAQ. As currently configured, the system calculates one current retrieval every 12 seconds. Given nominal flight speeds around 145 kts, this yields a retrieval every 850-1000 m along the flight path.

To minimize the processing load on the DAQ, all display and visualization of the real-time measurements is done on the control laptop. As each current retrieval is completed, it is sent to the laptop over the remote desktop connection. A graphical user interface (GUI) running on the laptop receives this information and updates the visual charts and graphs. The operator is able to view a live map of the results as well as several plots of diagnostic information to check data integrity.

C. Current Retrieval Algorithm

The current retrieval algorithm in ROCIS builds on prior work done using similar passive sensors [7]-[8]. The fundamental approach is to image the surface gravity waves and retrieve the currents from the observed Doppler shift. In deepwater, the motion of surface waves is described by the linear dispersion relation

$$\omega = \sqrt{gk} + \vec{k} \cdot \vec{U} \tag{1}$$

where ω is the frequency, k is the vector wavenumber and U is the mean surface current vector. By observing the Doppler shift of the waves via the collection of frequency values for the given wavenumbers present in the scene, we can fit for the free parameter U to retrieve the current.

The first step in the retrieval process is to georeference the images to the water surface. The high accuracy of the Applanix INS is crucial for this step. Next, an image stack is built up by extracting a square patch centered at each retrieval location (typically 256 x 256 m). Adequate dwell is necessary for a good retrieval, typically between 30-120 s depending on flight speed and altitude. Once an image stack is complete, the algorithm performs a three dimensional Fourier transform and calculates the power spectral density (3D-PSD).

The wave energy in the 3D-PSD lies along the two dimensional surface described by (1). A nonlinear least squares fit is performed to derive the current vector U. In addition, a goodness of fit value is estimated, which can later be used as an error metric to filter out wild points.

III. DATA COLLECTIONS

We flew ROCIS in the Gulf of Mexico from February to June 2015 for a total of 137 flights. Typical flights covered around 1000 km in 4 hours at altitudes ranging from 900 m to 2100 m. Fig. 2 shows the real-time current measurements from March 29, 2015. The coastline of southern Louisiana is shown at the top of the map. The cyclonic flow of the Loop Current in this region is visible in detail. We flew near daily and sometimes twice daily flights, providing a unique and unprecedented view of the Loop Current in this region and its evolution during this time span. Throughout the course of our data collections we observed the Loop Current migrate several hundreds of kilometers, as well as saw a large eddy break free and later reattach to the main flow.

Flight altitude is dependent on the cloud cover in the region of operation. The optimal altitude for flying ROCIS is 2100 m. At flight speeds of around 145 kts, this provides 120 s of dwell for each patch. However, during many of our data collections cloud cover below 2100 m forced the aircraft to fly lower (as low as 900 m) to operate below the cloud deck, decreasing the dwell. Longer dwells yield more accurate current retrievals since the frequency of the waves is better sampled. A more detailed discussion of the effect of clouds on the current retrievals is presented in Section V.

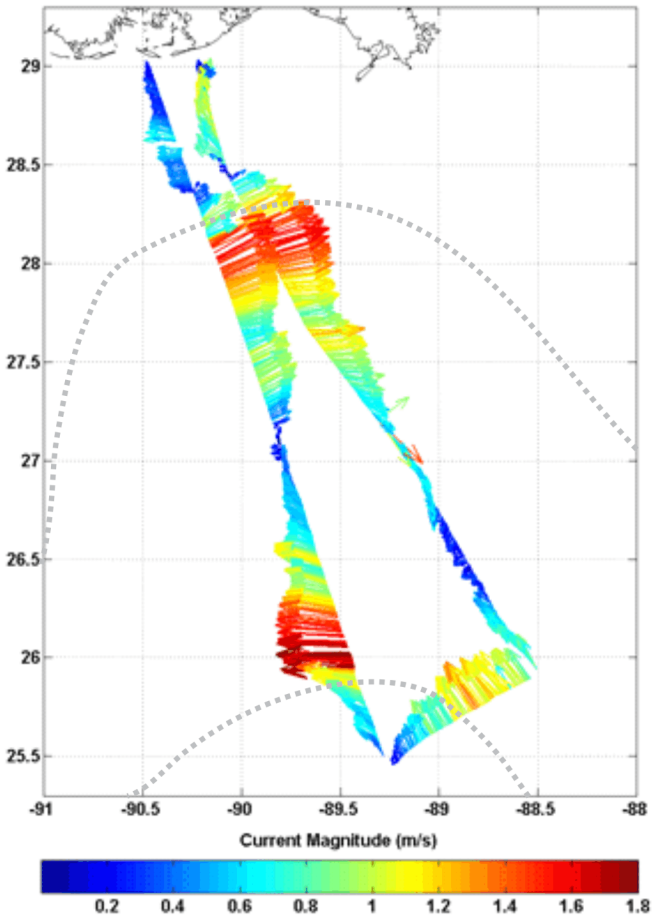

Fig. 2. ROCIS real-time current measurements from March 29, 2015. The detailed structure of the Loop Current is visible, with currents reaching 1.8 m/s at maximum. Dashed lines indicate the location of surface temperture fronts.

In an operational setting, the real-time current measurements are the most important data product ROCIS provides. However, since all of the image data are recorded to disk, several more advanced analyses can be undertaken using post-processing software. Currents can be retrieved at higher spatial resolutions than in real-time, either in a single line or grid. During the course of system development and testing we used such analyses to carry out sensitivity studies to determine the optimal algorithm parameters for use in real-time collections.

Additionally, the swaths of currents that post-processing provides are useful for the investigation of mesoscale ocean features. Fig. 3 shows one example of swath current retrievals at Southwest Pass, where the detailed structure of the Mississippi outflow is visible. ROCIS can provide vectors over a swath up to 4 km across the flight track with spatial resolution of 250 m or less depending on flight altitude. Such swath data is valuable for the analysis of coherent features, statistical and Fourier analysis, estimation of convergence and vorticity, and assimilation into numerical models.

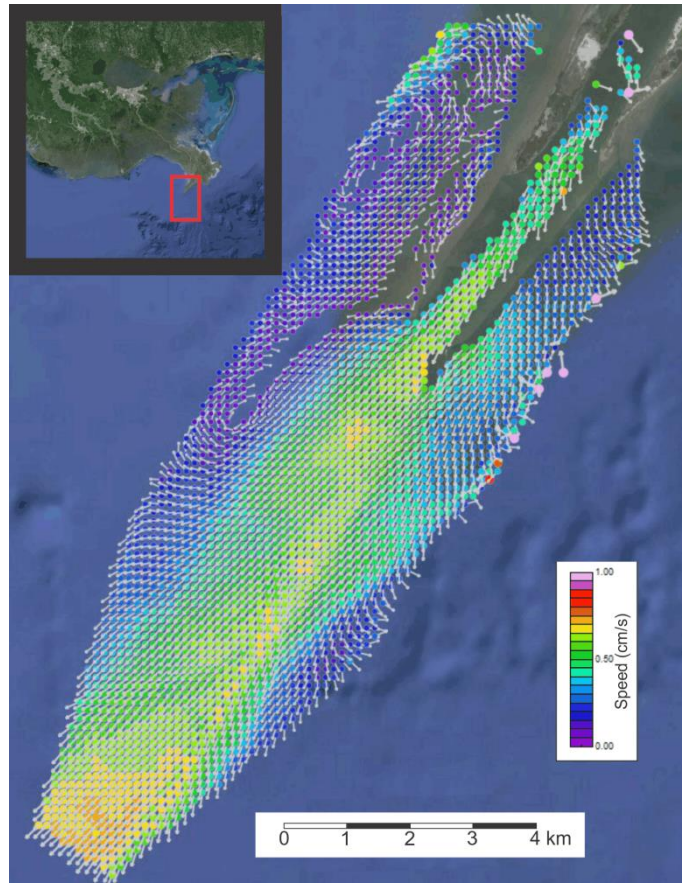

Fig. 3. ROCIS post-processed currents over the Mississippi River outflow at Southwest Pass. Currents were calculated on a grid of 128 x 128 m non-overlapping tiles. Current retrievals span a swath of 4 km across-track.

IV. SYSTEM PERFORMANCE

On several occasions during the course of our field collections ROCIS flew close to an ocean and atmospheric monitoring buoy located at N26.6698°, W90.4698°. This provided an opportunity for an *in situ* comparison and environmental characterization.

The current monitoring instrument on this buoy is an Aanderaa Doppler Current Sensor (DCS). It provides a point measurement at a depth of 1.5 m. ROCIS flew within 5 km of the DCS on 53 separate flights. For each flight, the closest real-time current measurement to the buoy was chosen as a comparison point. The scatter plot comparison is shown in Fig. 4. We found excellent agreement between the DCS and ROCIS real-time data. RMS errors were 0.16 m/s in magnitude and 15.9° in direction. The bias values were 0.08 m/s in magnitude and -2.5° in direction.

Data from the buoy also provided knowledge of the environmental conditions present while ROCIS was operating. Using the same 53 time periods as above, wind speeds ranged from 1 m/s to 14 m/s and significant wave heights ranged from 0.16 m to 3.2 m. Thus, ROCIS was able to successfully retrieve ocean currents in a wide range of wind and sea conditions.

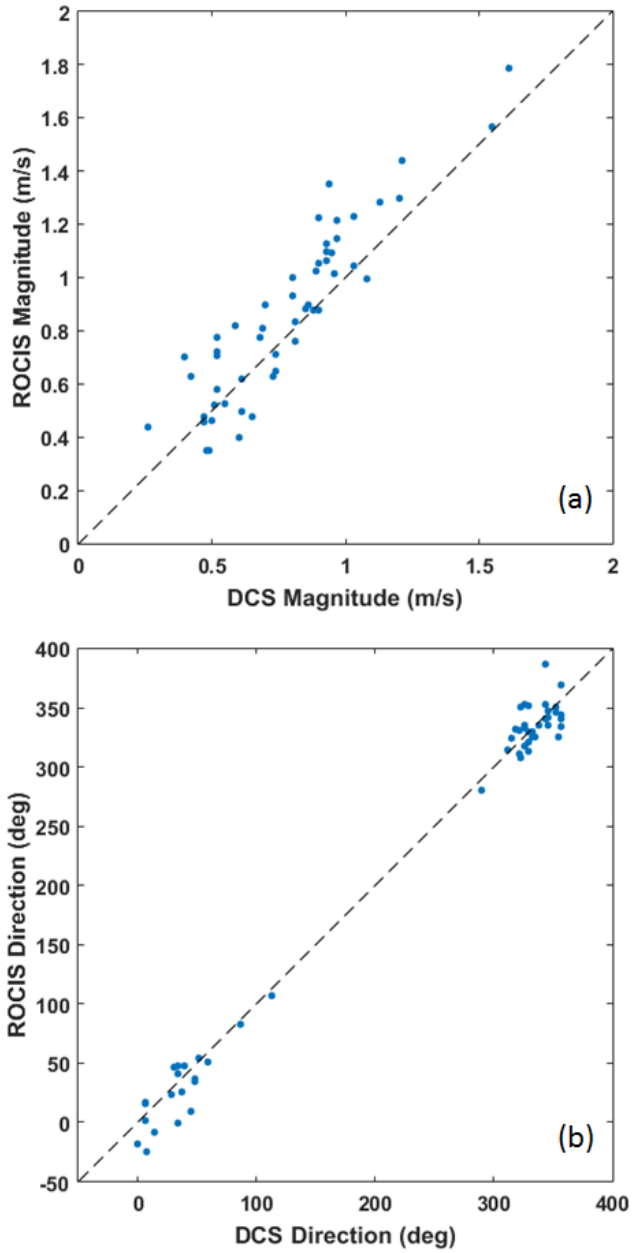

Fig. 4. *In situ* comparison: ROCIS real-time currents vs. DCS current measurements. ROCIS flew within 5 km of the DCS 53 times during our data collections. Panel (a) shows the magnitude comparison, with a RMS error of 0.16 m/s and bias of 0.08 m/s. Panel (b) shows the direction comparison, with a RMS error of 15.9° and a bias of -2.5°.

V. SOURCES OF ERROR

A. Clouds

Scattered clouds below the aircraft up to 50% still allow for excellent retrievals. Since the plane is moving quickly relative to the clouds, each individual cloud only fills up a few frames of data, saturating the majority of the pixels. In between these saturated frames, the rest of the frames in the image stack are still of high quality. The 3D-PSD is computed as normal, and energy due to the presence of clouds lies along a vertical stack at the origin, spanning all frequencies near zero wavenumber.

The current fitting algorithm only looks for wave energy described by the model in (1) and effectively ignores any additional energy in the 3D-PSD due to the clouds. However, beyond approximately 50% cloud cover there are not enough good images of the ocean waves and the SNR of wave energy along the dispersion surface rapidly deteriorates. Since the model in (1) no longer fits the observed data in the 3D-PSD this leads to wild points—retrievals with high goodness of fit values that are easily discarded.

Thus, clouds are not a significant limitation for successful current measurements with ROCIS. For all missions, the aircraft approached the survey region expecting to fly at the optimal altitude of 2100 m. Upon reaching the survey region, the operator and pilots assessed the cloud cover in the area and determined if a change of altitude was necessary.

B. Nonlinear Fit

A small amount of error is introduced into the current measurement due to the necessity of performing a nonlinear least squared fit. When a broad band of waves are present, as is almost always the case in the open ocean, it is common to have 1000-2000 data points in the nonlinear fit, yielding a small error due to the fit process itself on the order of 1-2 cm/s.

The fit error increases for two reasons: short dwell and low wave SNR. Shorter dwell, between 30-40 s, causes the frequency resolution of the 3D-PSD to greatly decrease. The frequency of the waves used in the fit is known less precisely, and the resulting fit error of the velocity increases slightly. By artificially shortening the dwell of an image stack with full dwell, we have shown this additional increase in fit error to be on the order of 3-5 cm/s.

If the wave SNR is prohibitively low (usually below 12 dB) due to the presence of excess cloud cover, sun glint, white caps, or a sufficiently narrow banded wave field, the fit error will increase greatly. As above, this is due to the observed data in the 3D-PSD not fitting the model described by (1). In such cases, the fit error can be quite large, though such wild points are easily flagged and discarded. determined if a change of altitude was necessary.

C. Georeferencing

Georeferencing errors include errors in the absolute measurement of the camera's attitude and position, errors in the boresight offsets between the cameras and inertial measurement unit (IMU), and error due to using an incorrect water surface height. Georeferencing errors cause frame-to-frame drift in the image stack and bias the resulting current measurement in the direction of the drift.

Errors in the absolute estimation of the camera's attitude and position are always present. However, using a high-performance INS system such as the Applanix POS-AV 410 minimizes these errors. In addition, we operated with Fugro StarFix augmentation for further GPS accuracy over the ocean. As such, we found these errors to have a negligible effect on the resulting current measurements.

After installing the system, a calibration flight over the airport is flown to image targets (runway lights), whose locations have previously been measured with survey GPS equipment. Using this data, the offset angles between the

cameras and IMU are estimated through an iterative best fit process. In our experience, these offset angles must be known to an accuracy of ±0.05° or drift will appear in the image stacks. We verified the accuracy of the calculated offsets by creating movies of georeferenced images either over the airport itself or over the beach the aircraft passed over on its way out to the survey region. In both instances, the surface height of the land was known from prior GPS measurements. In this way, any drift in the movie is solely due to errors in the offset angles. If excessive drift is present, then a recalculation of the offset angles is needed. Thus, through this iterative process errors due to inexact knowledge of the offset angles are reduced and made negligible.

Currently, imprecise knowledge of the water surface height is a large contributing factor to retrieved current error. The water surface height used in the algorithm is extracted from the geopotential Earth Gravitational Model 1996 (EGM96). This is a static ocean surface model, but the open ocean topography is modulated by tides and mesoscale variability which are not accounted for at this time.

A surface height error causes a drift in the image stack in the along-track direction, either toward or away from the direction of flight depending on whether the surface height is over- or under-valued. This drift vector is an additive error to the underlying current vector, and is inversely proportional to flight altitude. Theoretical calculations suggest that a 1 m height error produces a 1.7 cm/s along-track current error at 2100 m but a 4.0 cm/s error at 900 m. Qualitatively, we have observed higher point-to-point noise in the retrieved currents from flights at lower altitudes than higher altitudes. Ongoing efforts are underway to better quantify this result.

VI. LESSONS LEARNED

A. Real-time Measurements

Though more complicated analyses will always require post-processing of image data, we found several important benefits to having real-time processing and visualization. First, data quality checks can happen in real-time instead of waiting until after landing. The operator is able to visualize the current vectors as they are calculated. If several vectors in a row are erroneous, this may be an indication that an algorithm parameter needs adjustment. Additionally, the operator can redirect the aircraft in stride to focus on particular ocean features of interest. Lastly, and most importantly, real-time processing provides rapid data distribution to end-users. Immediately upon landing, a text file with measurements can be uploaded to a data server for timely regional ocean forecasting.

B. Aircraft Operations

Five months of near daily flights required intensive manpower from both operators and pilots. Crews were regularly switched out after 2-4 weeks in the field. In addition, FAA aircraft regulations required maintenance to be performed after 100 hours of flight which occurred approximately once a month. To accommodate this requirement while not losing 7-10 days of collections, two aircraft were used and the imaging payload was moved back and forth. Each move required a recalibration of the cameras as we found that the boresight offset angles changed by more than 0.05° with each reinstallation.

ROCIS from an unmanned aerial vehicle (UAV) is a long-term option. UAV flight speeds are much slower than the King Air, which will allow for much lower flight altitudes to achieve similar dwells. The UAV could be launched directly from a boat or other offshore platform. Since the UAV would already be in the survey region, data coverage would be approximately equal to that of a manned aircraft, which requires extensive transit distances.

UAVs can be used for near-shore wave imaging where land in the scene is used for image registration [11]. For offshore applications, the limiting technology is the class of INS available on such UAVs, which are not accurate enough for direct current measurements. However, we believe that within five years the technology will exist to operate ROCIS from a UAV.

VII. CONCLUSIONS

ROCIS exploits space-time processing of ocean wave imagery to produce maps of surface currents in real-time. Real-time currents have high spatial resolution over large areas and are collected in a matter of hours. Post-processing of the imagery data creates additional data sets with swaths of currents useful for investigating a variety of mesoscale features. The system is made from COTS components and is designed to be quickly installed on any survey aircraft.

From February to June 2015, we flew near daily flights over the Loop Current in the Gulf of Mexico. On several occasions we flew over an *in situ* buoy. A current comparison with a DCS yielded good agreement, and environmental data showed the range of wind and wave conditions that ROCIS is able to successfully operate under.

ROCIS is well suited to operational missions such as search and rescue and oil spill response, where timely knowledge of surface currents is crucial. As UAV technology improves, ROCIS technology will migrate to small fixed wing UAVs for cheaper and safer data collections.

8.1.1.1.1 ACKNOWLEDGMENT

At Areté Associates, we thank all our colleagues who have helped with various parts of system development, testing, and field collections. At Fugro GEOS, we thank all of the very capable system operators who admirably handled several months of continuous data collections. We thank all of the pilots at Dynamic Aviation who expertly flew daily, and often twice-daily, missions. For *in situ* buoy data, we thank Petrobras America, Inc. Lastly, we especially thank John Dugan for his friendship and pioneering research on optical imaging of the marine environment.

8.1.1.1.2 REFERENCES

[1] W. J. Emery, A. C. Thomas, M. J. Collins, W. R. Crawford and D. L. Mackas, "An objective method for computing advective surface velocities from sequential infrared satellite images," *J. Geophysical Research*, vol. 91, pp 12 865-12 878, November 1986.

[2] R. Leben, G. Born and B. Engegreth, "Operational altimeter data processing for mesoscale monitoring," *Marine Geodesy*, vol. 25, pp. 3-18, February 2002.

[3] J. D. Paduan and L. K. Rosenfeld, “Remotely sensed surface currents in Monterey Bay from shore-based HF radar (Coastal Ocean Dynamics Application Radar),” *J. Geophysical Research Atmosphere*, vol. 101, pp. 20 669-20 686, September 1996.

[4] S. P. Anderson and N. Sharma, “Satellite-tracked drifter measurements of inertial currents in the Gulf of Mexico,” *Current Measurement Technology*, Charleston, SC, 2008, pp. 285-288.

[5] S. P. Anderson, C. K. Cooper, D. B. Driver and J. van Smirren, “EddyNet: a measurement program for collecting real-time current profiles from the Gulf of Mexico,” *Current Measurement Technology*, San Diego, CA, 2003, pp. 277-281.

[6] S. P. Anderson and P. Matthews, “A towed 75 KHz ADCP for operational deepwater current surveys,” *Current Measurement Technology*, Southampton, UK, 2005, pp. 46-49.

[7] J. P. Dugan and C. C. Piotrowski, “Surface current measurements using airborne visible image time series,” *Remote Sens. Environ.*, vol. 84, pp. 309-319, February 2003.

[8] J. P. Dugan and C. C. Piotrowski, “Accuracy of bathymetry and current retrievals from airborne optical time series imaging of shoaling waves,” *IEEE Trans. Geosci. Remote Sens.*, vol. 40, pp. 2606-2618, December 2002.

[9] S. P. Anderson, S. Zuckerman, S. Fan, and J. van Smirren, “Airborne optical remote sensing of ocean currents,” *Oceans*, San Diego, CA, 2013, pp. 1-7.

[10] S. Zuckerman and S. P. Anderson, “Advances in passive remote sensing of ocean currents and depths,” *IEEE Int. Geoscience and Remote Sensing Symp.*, Quebec City, Quebec, Canada, 2014, pp. 3906-3909.

[11] R. A. Holman, K. T. Holland, D. M. Lalejini, and S. D. Spansel, “Surf zone characterization from unmanned aerial vehicle imagery,” *Ocean Dynamics*, vol. 61, pp. 1927-1935, June 2011.

5. REMOTE OCEAN CURRENT IMAGING SYSTEM COMMERCIALIZATION REPORT (TASK 9)

ROCIS Commercialization Plan

RPSEA Document No. 11121.5801.01.09

Hi-Res Environmental Data for Enhanced UDW Operations Safety

RPSEA Project No. 11121-5801-01

October 3, 2016

Steven P. Anderson
Principal Investigator, Tasks 7-9
Areté Associates
1550 Crystal Drive, Suite 703
Arlington, VA 22202

Grant A. Stuart
Project Manager
Fugro
6100 Hillcroft
Houston, TX 77081

LEGAL NOTICE

This report was prepared by *FUGRO GLOBAL ENVIRONMENTAL AND OCEAN SCIENCES, INC.*as an account of work sponsored by the Research Partnership to Secure Energy for America, RPSEA. Neither RPSEA, members of RPSEA, the National Energy Technology Laboratory, the U.S. Department of Energy, nor any person acting on behalf of any of the entities:

a. MAKES ANY WARRANTY OR REPRESENTATION, EXPRESS OR IMPLIED WITH RESPECT TO ACCURACY, COMPLETENESS, OR USEFULNESS OF THE INFORMATION CONTAINED IN THIS DOCUMENT, OR THAT THE USE OF ANY INFORMATION, APPARATUS, METHOD, OR PROCESS DISCLOSED IN THIS DOCUMENT MAY NOT INFRINGE PRIVATELY OWNED RIGHTS, OR

b. ASSUMES ANY LIABILITY WITH RESPECT TO THE USE OF, OR FOR ANY AND ALL DAMAGES RESULTING FROM THE USE OF, ANY INFORMATION, APPARATUS, METHOD, OR PROCESS DISCLOSED IN THIS DOCUMENT.

THIS IS AN INTERIM REPORT. THEREFORE, ANY DATA, CALCULATIONS, OR CONCLUSIONS REPORTED HEREIN SHOULD BE TREATED AS PRELIMINARY.

REFERENCE TO TRADE NAMES OR SPECIFIC COMMERCIAL PRODUCTS, COMMODITIES, OR SERVICES IN THIS REPORT DOES NOT REPRESENT OR CONSTIITUTE AND ENDORSEMENT, RECOMMENDATION, OR FAVORING BY RPSEA OR ITS CONTRACTORS OF THE SPECIFIC COMMERCIAL PRODUCT, COMMODITY, OR SERVICE.

ABSTRACT

This Commercialization Plan for the Remote Ocean Current Imaging System (ROCIS) outlines the overall strategy the prime subcontractor, Fugro Global Environmental and Ocean Sciences (GEOS), Inc., together with technology partner, Areté Associates, will develop a business model for an operational ROCIS-RT survey service. This document will consist of reviewing the market opportunities and developing a business execution plan. The goal will be to have a field-ready package and operational service available following completion of this task.

SIGNATURE AND DATE STAMP

FUGRO GLOBAL ENVIRONMENTAL AND OCEAN SCIENCES, INC.

By: _____
(Signature)

Name: **Grant A. Stuart**

Title: **Project Manager**

Date: **3 October 2016**

THIS PAGE INTENTIONALLY LEFT BLANK

CONTENTS

		Page
1.	**INTRODUCTION**	**1**
1.1	Transition to an operational airborne current measurement service	1
2.	**COMPANY DESCRIPTION**	**2**
2.1	Teaming Arrangement	2
2.2	Technology Partner: Areté Associates	2
2.3	Service Provider: Fugro Companies	2
3.	**REMOTE OCEAN CURRENT IMAGING SYSTEM (ROCIS)**	**4**
3.1	Description of Technology Innovation	4
4.	**COMMERCIAL APPLICATIONS**	**5**
4.1	Surface Current Monitoring	5
	4.1.1 Manned Fixed-Wing Airborne Surface Current Survey	5
	4.1.2 Surface currents from helicopters	5
	4.1.3 Surface currents from unmanned airborne vehicles	5
4.2	Emergency Response	5
4.3	Littoral bathymetry	5
4.4	Surface object detection	5
4.5	Ice detection and tracking	5
4.6	Science Applications	5
5.	**POTENTIAL MARKET SECTORS**	**7**
5.1	Seismic surveys	7
5.2	Exploration drilling	7
5.3	Oil & gas development and production	7
5.4	Search and rescue operations	7
5.5	Oil spill mitigation	7
6.	**COMPETITIVE TECHNIQUES**	**8**
6.1	Satellite Remote Sensing	8
6.2	Drifters	8
6.3	Acoustic Doppler Current Profilers (ADCP) from platforms	8
6.4	High-Frequency Radar	8
6.5	Vessel-mounted ADCP current surveys	8
7.	**BUSINESS MODEL**	**10**
7.1	Inaugural commercial project (Chevron, Feb-June 2015)	10
7.2	Single client, single location	11
7.3	Multiple clients, multiple locations	11
7.4	Fee-based subscription	11

7.5 Purchase of two production grade ROCIS systems 11

8. MARKETING 12

8.1 International Traffic in Arms Regulation (ITAR) 12

8.2 Business development activities 12

8.3 Fugro marketing 12

APPENDICES

A. APPENDIX A – ROCIS DRAWINGS & PHOTOS

1	Final	Grant Stuart, Fugro	Rob Smith, Fugro Managing Director	Rob Smith, Fugro Managing Director	3 October 2016
0	Draft	Steven P. Anderson, Areté Grant Stuart, Fugro	Rob Smith, Fugro Managing Director	Rob Smith, Fugro Managing Director	30 September 2016
Rev	**Description**	**Prepared**	**Checked**	**Approved**	**Date**

ABBREVIATIONS

GEOS	Global Environmental and Ocean Sciences Inc.
GoM	Gulf of Mexico
Hi-Res	High Resolution
HRD	Hurricane Research Division
HSEQ	Health, Safety, Environment, and Quality
IMS	Integrated Management System
INS	Inertial Navigation System
LC	Loop Current
LCE	Loop Current Eddy
NMEA	National Marine Electronics Association
NOAA	National Oceanic and Atmospheric Administration
NM	nautical mile
OCS	Outer Continental Shelf
PI	Principal Investigator
QA	Quality Assurance
QC	Quality Control
RPSEA	Research Partnership to secure Energy for America
ROCIS	Remote Ocean Current Imaging System
ROCIS-RT	ROCIS Real-time
UDW	Ultra Deep Water

1. INTRODUCTION

Strong ocean currents can disrupt various deepwater activities, cause downtime for oil and gas exploration and production activities, and transport spilled oil long distances. Thus, accurate and timely observations of ocean currents significantly help with planning and assuring safe operations. The ocean varies on a broad range of temporal and spatial scales and it is important to use the type of measurement system best suited to a specific application.

This development program leveraged recent advances in remote sensing to demonstrate, and rapidly transition to operations, an airborne current measurement capability: the Remote Ocean Current Imaging System (ROCIS). ROCIS provides a cost effective and rapid response solution for the provision of surface current surveys over large offshore regions.

1.1 Transition to an operational airborne current measurement service

The ultimate goal of this effort was to have an operational airborne current service that is responsive to various needs of the offshore industry. To this end, Fugro Global Environmental and Ocean Sciences (GEOS), Inc. is the service provider. Areté Associates has licensed the technology to Fugro, provided them with robust data collection systems, and provide technical support as needed. Fugro will work directly with clients to carry out all aspects of surveys.

ROCIS flight demonstrations were completed in December 2014, and ocean current measurements from the demonstrations were distributed to RPSEA and industry representatives in near-realtime. The demonstration was so convincing that Fugro was contracted in January 2015 to collect ROCIS data over the Loop Current in support of operations. During 2015, we conducted 135 flights, surveyed 65,000 miles and collected over 5 million images of the ocean surface.

Thus, ROCIS is now a commercial service and the final project goal was successfully achieved.

This Commercialization Plan lists the commercial applications, recognizes potential markets, reviews competition, identifies transition challenges, and proposes business models.

2. COMPANY DESCRIPTION

2.1 Teaming Arrangement

The task of commercializing ROCIS as an operational current survey service will bring together Fugro, as prime subcontractor and service provider, and Areté Associates, as subcontractor and technology partner, as the team engages potential clients in the marine survey market. Under a general teaming agreement umbrella, the two have also executed a License Agreement whereby Areté has licensed its ROCIS software algorithm for image processing, current retrieval, visualization code, and output data formats exclusively to Fugro for use globally on manned aircraft in the commercial oil and gas sector. Furthermore, Fugro has purchased two complete ROCIS payloads in 2016 to utilize this exclusive license.

2.2 Technology Partner: Areté Associates

Areté Associates developed the core technology algorithms at the heart of the ROCIS innovation. Areté Associates is a unique enterprise contributing to national security through the performance of advanced science and engineering research and development, as well as military and intelligence studies and analysis. Areté has positioned itself to undertake production of high-end systems that have evolved from our science and engineering base and exploit our intellectual property.

2.3 Service Provider: Fugro Companies

The Fugro group of companies deliver earth and engineering data services, from project preparation through to data acquisition, processing, analysis and interpretation, reporting and consulting.

Fugro Global Environmental & Ocean Sciences, Inc. (Fugro GEOS) is the world's leading supplier of meteorological and oceanographic (metocean) services for offshore and coastal engineering applications. With over 30 years' experience in a diversity of projects worldwide, we are well placed to respond to the metocean needs of our clients. We offer metocean solutions through cost-effective, high quality and technically advanced measurement, consultancy, information systems, ocean observing systems, forecasting services, and platform and riser response monitoring. The expertise, experience and skills of our staff, enable us to bridge the gap between the scientific and engineering disciplines and to understand and fulfil your engineering requirements.

The broad spectrum of metocean services and systems we offer includes:

- Metocean measurement services
- Metocean criteria, desk studies and numerical modelling
- Real-time environmental monitoring systems
- Integrated real-time buoy monitoring systems
- Meteorological & oceanographic forecasting services
- Data analysis and data management

Fugro Geospatial, Inc. provides the airborne collection platform. Fugro Geospatial transforms photogrammetric data from a wide range of aerial sensors into spatially accurate map products and GIS

datasets. Our aerial mapping capabilities serve a wide range of areas such as natural resources management, urban planning, economic development, emergency response, environmental, and engineering activities.

Fugro's highly automated processing systems deliver projects in half the time compared to traditional photogrammetric methods. Our wholly owned assets and large production facilities across the globe enable flexible scheduling to meet customer needs. All of Fugro's digital imaging acquisition and processing procedures are International Standards Organization (ISO) Certified with accuracy capabilities that meet or exceed industry standards.

3. REMOTE OCEAN CURRENT IMAGING SYSTEM (ROCIS)

3.1 Description of Technology Innovation

The Remote Ocean Current Imaging System (ROCIS) exploits time-space processing of airborne ocean wave imagery to produce maps of surface currents. The system provides synoptic measurements of ocean surface currents over a broad area with a level of detail that allows small-scale circulation features to be identified.

This program has demonstrated that the optical imaging technique provides accurate (5 cm s-1) surface current data over large areas both rapidly and cost effectively and complements traditional ocean survey approaches. This unique capability provides maps of current vectors on 250m x 250m (or finer) grids along the flight path. Real-time processing provides the system operator with both visualization and recording of the ocean currents during the flight.

Real-time processing has several benefits:

- Data assurance is enhanced because of the real-time system performance feedback to the operator
- The operator can now redirect the aircraft in stride to focus on ocean features of interest
- Timely data distribution to end-users since post-processing is no longer required

The compact size and low power of ROCIS makes it readily adaptable to different aircraft. It can also be integrated with multi-spectra and radar oil mapping systems on the same platform. The ability to mobilize the system promptly and concentrate data acquisition in specific areas allows crucial surface current data to be acquired in support of search and rescue missions and oil spill response operations, leading to a significant improvement over current techniques, such as ocean drift prediction.

4. COMMERCIAL APPLICATIONS

The following are potential commercial, civil, and military applications for the Remote Ocean Current Imaging System (ROCIS).

4.1 Surface Current Monitoring

4.1.1 Manned Fixed-Wing Airborne Surface Current Survey

This is the original program mission to collected ocean currents from fixed wing aircraft in support of operational ocean monitoring and forecasting.

4.1.2 Surface currents from helicopters

This application is suitable to collected data in locations hard to reach with a fixed wing aircraft. The ROCIS can readily adapted to rotary wind aircraft.

4.1.3 Surface currents from unmanned airborne vehicles

UAV operations create a new “organic” data collection capabilities. UAV’s will be deployed from ships and platforms at sea to survey surrounding waters. The main challenges for UAV operations are finding a small inertial navigation system suitable and accurate enough for ROCIS and UAV flight regulations.

4.2 Emergency Response

The ability to mobilize the system promptly and concentrate data acquisition in specific areas allows crucial surface current data to be acquired in support of search and rescue missions and oil spill response operations, leading to a significant improvement over current techniques, such as ocean drift prediction.

4.3 Littoral bathymetry

The 3-D PSD algorithm that is used to derive surface currents can also be used measure shoaling waves to estimate bathymetry. This provides an additional product for clients.

4.4 Surface object detection

Objects on the ocean surface are sometimes hard to detect in a single image with cutter from waves and whitecaps. Time-stacking ocean imagery is a proven way to reduce the wave clutter to improve detection and tracking of objects on the water. A software update will enable ROCIS to detect objects like small boats, buoys, and other hazards to navigation. Search and rescue and marine mammal tracking are examples of potential applications.

4.5 Ice detection and tracking

ROCIS images can be used to detect ice margins and icebergs. Time-space processing will allow for the determination of drift speed and heading. This may be useful for monitoring and forecasting ice development and movement in support of a range high latitude operations.

4.6 Science Applications

ROCIS can provide vectors over a swath of up to 3 km across the flight track with spatial resolution of less than 250m. Thus, post processing is valuable for scientific analysis of coherent features, statistical and

Fourier analysis, estimation of convergence and vorticity, and assimilation into numerical models. ROCIS is available to support many diverse scientific process studies.

5. POTENTIAL MARKET SECTORS

5.1 Seismic surveys

As seismic surveys are often one of the first operations in a prospective exploration area, knowledge of the surface current conditions in an unknown region during survey operations is useful.

5.2 Exploration drilling

During exploration drilling, ROCIS can assist both in providing asset protection by measuring the surface currents upstream from the drilling platform, as well as feed real measurements into model forecasts to give the operator time to unlatch from a well if currents are predicted to exceed predetermined operating thresholds.

5.3 Oil & gas development and production

Similar to exploration drilling, oil and gas development and production requires accurate information on the surface currents. Currents become critical when positioning assets in the field and supporting construction of the platform. ROCIS data can provide both asset protection and support operational ocean current forecasts.

5.4 Search and rescue operations

Satellite data and predictive current models often provide the initial guidance for search teams when first determining a search area. The large area synoptic measurements obtained using ROCIS are uniquely suited to improve the search and rescue (SAR) effort by providing direct measurements of the search area in high resolution.

5.5 Oil spill mitigation

As in search and rescue, ROCIS measurements will increase the accuracy of the models and assist stakeholders when determining zones at risk to hydrocarbon exposure. By improving oil spill models, response commanders can deploy their assets more efficiently and effectively.

6. COMPETITIVE TECHNIQUES

Various measurement systems are presently employed monitor surface currents in the ocean. The below summarizes a few of the primary approaches that compete to provide data similar to what ROCIS measures.

6.1 Satellite Remote Sensing

Satellite remote sensing provides estimates of ocean currents using feature tracking algorithms or satellite altimetry. Satellites provide a view of the largest scale features but cannot be relied on to provide timely and precise observations of the sea surface due to cloud cover or limited coverage coupled with sensor resolution.

6.2 Drifters

Drifting buoys have proven to be a cost effective means of collecting ocean current observations; however, this Lagrangian technique, observing currents moving with the flow as opposed to from a fixed location, does not provide a means of actively targeting and monitoring a specific site or area.

6.3 Acoustic Doppler Current Profilers (ADCP) from platforms

Acoustic Doppler Current Profilers (ADCP) mounted on moorings and platforms can provide real-time current information but are not always optimally located, since they are fixed or mounted at a certain location, to aid with ocean prediction.

6.4 High-Frequency Radar

High-frequency (H/F) Radar systems deployed along the coast or from offshore structures have shown some operational utility to the deepwater industry but only provide radial current information (unless deployed in pairs) and have limited resolution and range.

6.5 Vessel-mounted ADCP current surveys

Shipboard ADCPs collect ocean current profiles while underway, providing surveys of synoptic ocean features associated with ocean currents. These systems have traditionally been hull mounted on research vessels, mounted on poles placed over the side, or towed behind vessels of opportunity. The ships can operate both day and night, but real-time data collection is limited primarily by weather and sea-state. Shipboard ADCP surveys are routinely used to supplement other measurement systems during critical offshore operations, and several commercial service providers offer this capability.

ADCP technology, at over 40 years old, is mature. However, surveying by ship is not always an ideal solution. First, mobilization and transit times can create a lag of several days (or more) before data collection begins. Second, ship speed is limited to 4 - 8 knots (depending on sea-state and installation details), thus limiting the coverage area and preventing multiple areas of interest to be mapped due to transit times between them, unless more than one vessel is used. The vessel's speed also prevents a synoptic assessment of the extent of the LC or eddy to be determined; this sparseness of data coverage limits its suitability for initializing numerical models. Finally, in addition to the lost time and cost associated

with vessel mobilization, the necessity for refuelling, resupplying, and crew changes further reduces efficiency.

The table below summarizes various current survey techniques and the benefits and limitations of each measurement approach.

Service / Technique	Provides	Features	Limitations
Measurements from rigs and platforms	Current profile to 1000m	Persistent, real time	Stationary, no surface measurement
Drifters	Lagrangian tracks	Persistent, real time, cost effective,	Uncontrollable, limited information
Wave Gliders	Surface current, profile to 100m	Persistent, real-time, mobile	Very slow (1 knot)
HF Radar	Radial currents	Regional coverage Persistent	Complex installation, must have two for vector
VM-ADCP	Current profiles to 300m	Mobile, Persistent (weather)	Slow (4 knots) over the side. Weather down time.
Satellite	Large scale surface current, sea surface height/temperature	Persistent, view of the largest scale features	cloud cover, limited coverage, lower resolution, not direct measurement of current

7. BUSINESS MODEL

7.1 Inaugural commercial project (Chevron, Feb-June 2015)

Much of the business model to commercially execute ROCIS surveys was defined for us when the team was given the opportunity to take measurements for Chevron for five months in 2015. We flew ROCIS in the Gulf of Mexico from February to June 2015, for a total of 137 flights. Typical flights covered around 1000 km in 4 hours at altitudes ranging from 900m to 2100m. The figure below shows the real-time

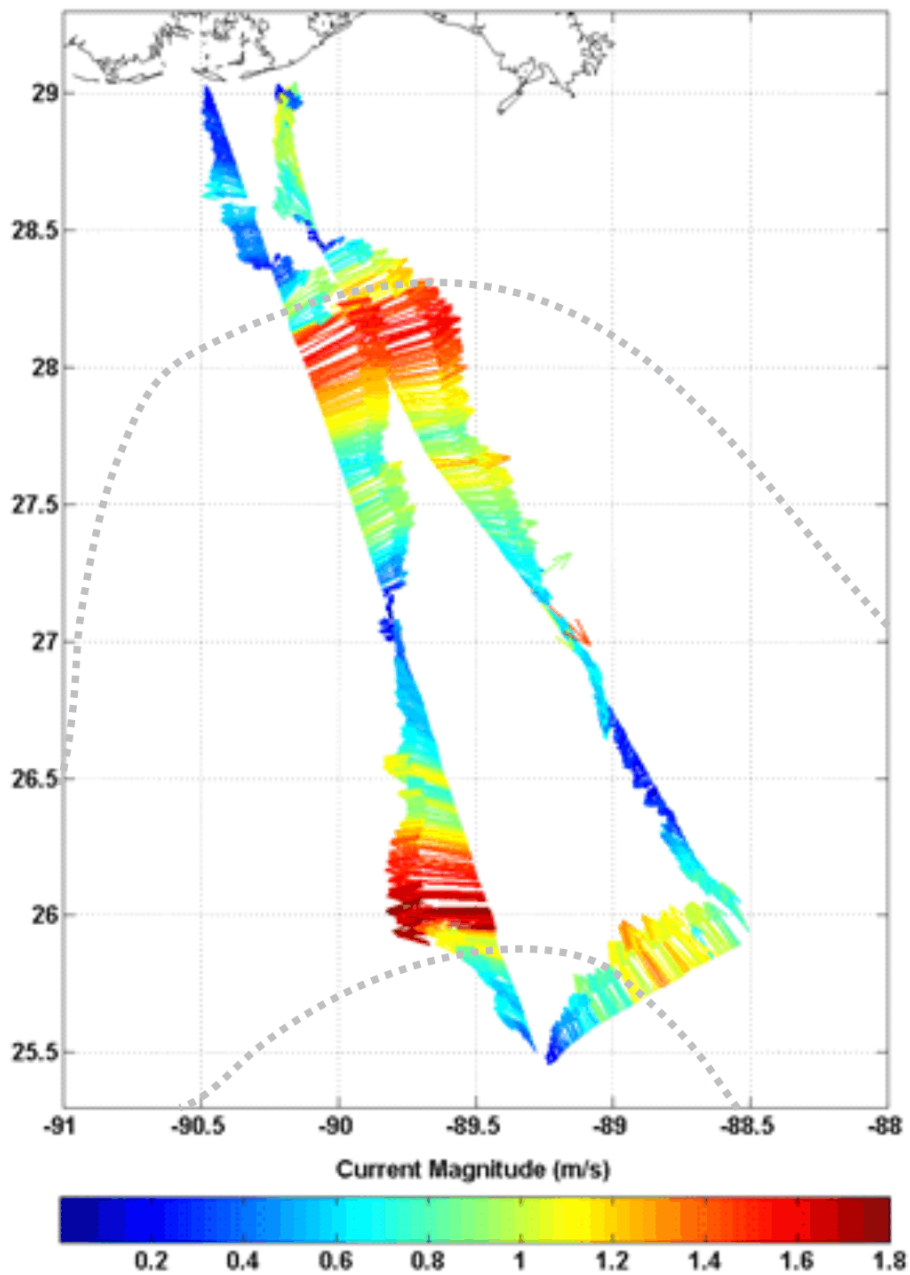

current measurements from March 29, 2015. The coastline of southern Louisiana is shown at the top of the map. The cyclonic flow of the Loop Current in this region is visible in detail. We flew near daily and

sometimes twice daily flights, providing a unique and unprecedented view of the Loop Current in this region and its evolution during this time span. Throughout the course of our data collections we observed the Loop Current migrate several hundreds of kilometers, as well as saw a large eddy break free and later reattach to the main flow.

7.2 Single client, single location

The first commercial use of ROCIS was based on a single client, single location basis. A mobilization fee was charged in order to get the aircraft, crew, and survey technicians to the airfield base of operations. The cost to return the aircraft to its home airfield was also included in this upfront cost. The lead time for response from initial callout to the first day of survey operations was approximately one week. Once on site, the service was provided on a per flight basis on operational days and a standby rate on days that ROCIS surveys were not flown. In addition to the per flight charge, a license fee was applied on a per nautical mile surveyed.

7.3 Multiple clients, multiple locations

Instead of a single client for a single location, ROCIS surveys could be provided for a small group of stakeholders for multiple locations. This would spread the operating costs over multiple clients and keep ROCIS flying for longer than what the budget from a single client could support. Once on site, ROCIS could support multiple locations and provide data on a client by client basis; alternatively, the group could agree to the share the data. This arrangement could also support augmentation of a shared hydrographic model for the region or for individual locations.

7.4 Fee-based subscription

At this point, keeping ROCIS surveys operational requires a significant ongoing source of dedicated funding. Absent a contracted entity or group, providing ROCIS as a service in which surveys are conducted two to three times a week is cost prohibitive. In order to operate ROCIS on such a basis, a subscription service, requiring 30 - 40 subscribers, would be required to produce benefits for all parties. This business model is probably unlikely until operational costs decrease or demand grows for the service to support such a model.

7.5 Purchase of two production grade ROCIS systems

In April 2016, Fugro took delivery of two production grade ROCIS systems to support commercial implementation of ROCIS as an operational service. Areté Associates redesigned the system and upgraded various hardware components, including a combined trigger box/power supply, a built-in IMU mount, a ruggedized payload with ruggedized cable connections, and upgraded CPU on the data acquisition computer. Photos and drawings of the systems are included as Appendix A. This investment demonstrates Fugro's commitment to implementing ROCIS as a commercial service.

8. MARKETING

8.1 International Traffic in Arms Regulation (ITAR)

Areté Associates has completed an internal determination that the ROCIS system is not ITAR controlled. It should be noted that some inertial navigation systems are ITAR controlled. Fugro, however, has identified suitable non-iTAR controlled INS systems. Therefore, ROCIS can be operated on a global basis.

8.2 Business development activities

Fugro and Areté Associates have made concerted efforts to present the benefits of ROCIS to the ultra-deepwater marketplace and continue to do so.

As part of both the technology transfer requirements of the RPSEA subcontract as well as own efforts, ROCIS has been presented at multiple conferences and meetings to disseminate results from initial field collections. ROCIS has been presented to date at the following:

- OCEANS '13 MTS/IEEE San Diego, CA September 23-26, 2013.
- IGARSS 2014, Quebec, Canada, July 13-18, 2014.
- IEEE/OES 11th Current, Waves & Turbulence Measurement (CWTM), St. Petersburg, FL, March 2015
- Offshore Technology Conference, Houston, TX, May 2015.
- OCEANS '15 MTS/IEEE Washington, DC, October 19-22, 2015.
- AGU/ASO/TOS Ocean Sciences 2016, New Orleans, LA February 21-26, 2016.
- Offshore Technology Conference, Houston, TX, May 2016.

Fugro and Areté Associates continued to execute ROCIS surveys in 2015 and generated a lot of buzz surrounding the results of the operational service. The team has and will continue to approach potential clients through meetings and provision of detailed proposals.

8.3 Fugro marketing

During 2016, Fugro has brought its commercial marketing resources to bear, updating its ROCIS services brochure, building a dedicated web presence for ROCIS, and issuing a press release. Efforts will continue to promote ROCIS as a useful metocean measurement tool. Below are examples of Fugro's marketing efforts:

Fugro press release:
Fugro issued a press release on February 8, 2016 announcing the success of the first commercial use of ROCIS in the field for a commercial client.
http://www.fugro.com/media-centre/press-releases/fulldetails/2016/02/08/fugro-delivers-surface-current-data-with-innovative-new-system

YouTube Spot:
https://youtu.be/aeWYgn3aLXE

Fugro website:

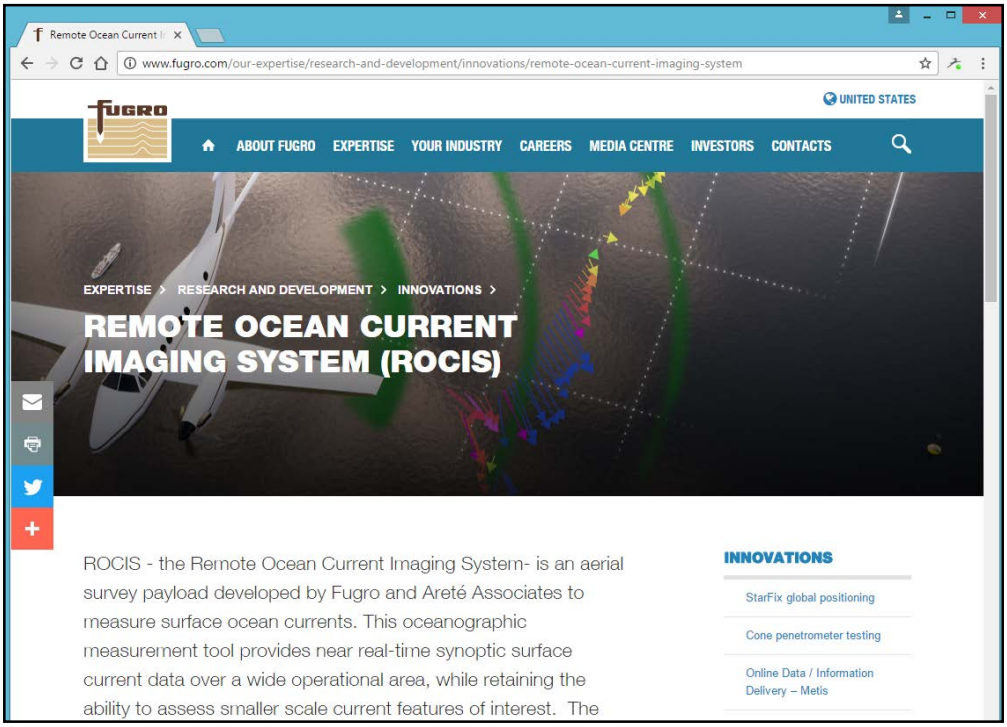

http://www.fugro.com/our-expertise/research-and-development/innovations/remote-ocean-current-imaging-system
http://www.fugro.com/ask/measuring-and-forecasting-strong-surface-currents

Fugro service flyer:

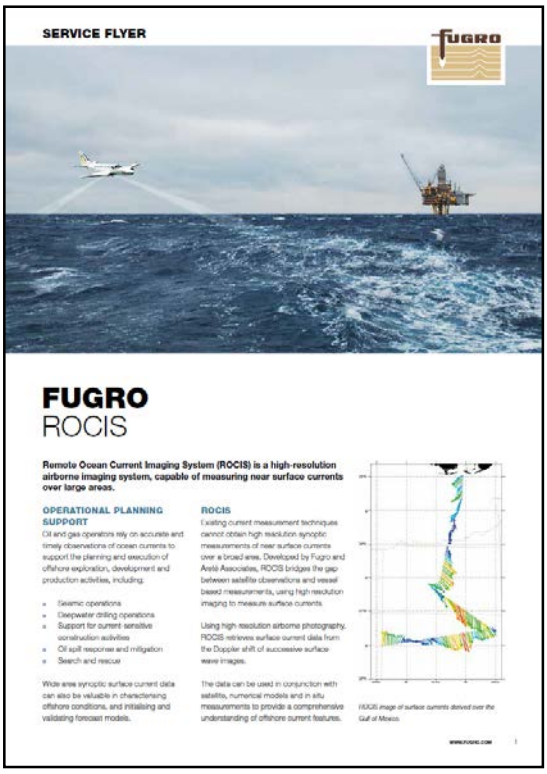
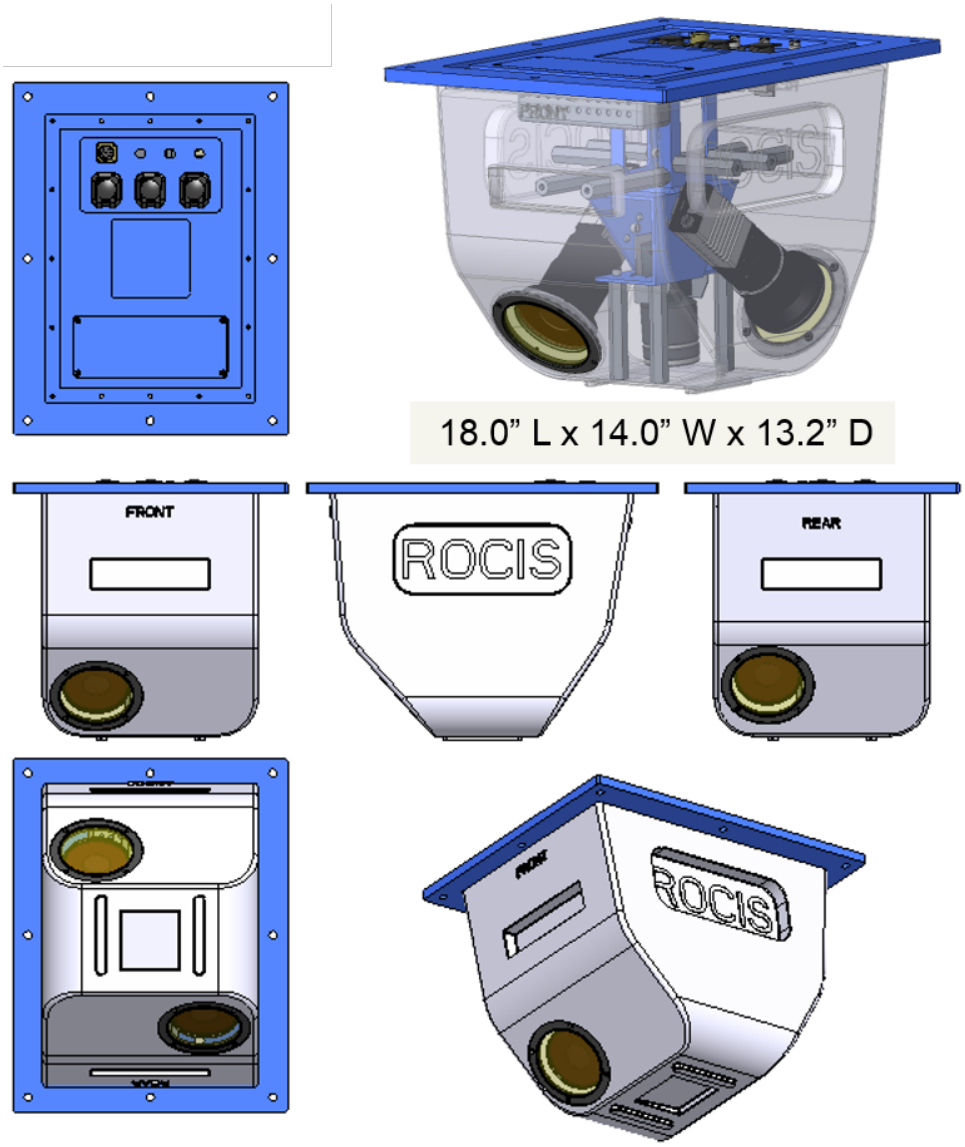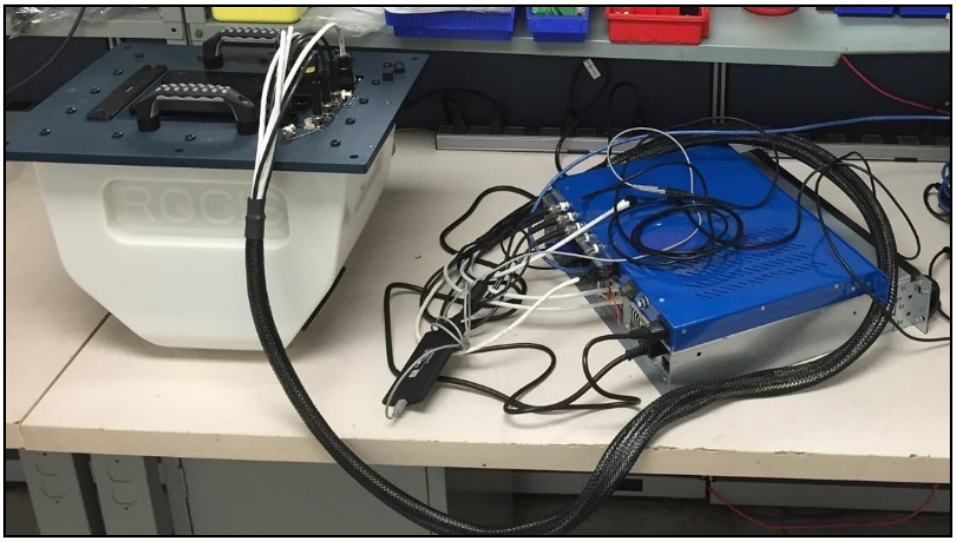
A. APPENDIX A – ROCIS DRAWINGS & PHOTOS